Fourth DELTA
User- meeting

Dortmund
26. November 2008

Dear reader,

The last Wednesday of November is DELTA User-Meeting's day. It is since 2005 and we will continue this short tradition in the next years.

DELTA is a unique combination: A synchrotron facility build on the campus of a university. This offers excellent conditions to educate young scientists. I think it was prudent to maintain and to reoccupy the position of a professor at DELTA. We appreciate the appointment of Prof. Dr. Shaukat Khan as the successor of Prof. Dr. Klaus Wille. I am convinced that Prof. Khan is a warrantor for the continuity in education and research at DELTA.

Furthermore, the ‚NRW Forschungsschule – *Forschung mit Synchrotronstrahlung*' coordinated by Prof. Tolan was approved in 2008 by the Land Nordrhein-Westfalen. The research school will start in the next months and will open new ways in research and education for graduated students.

The present annual report of the fourth DELTA User-Meeting is a clear answer to the efforts done by several institutions in 2007/2008 to improve the general situation of DELTA. This year we, the DELTA users, present 30 reports twelve more than in the annual reports of 2005, 2006 or 2007. A quite nice result which was only possible by big efforts, hard work, and services provided to maintain or even improve the performance and the operation of DELTA. Thanks to the crew.

Alex von Bohlen

Prof. Dr. Shaukat Khan

Beamline overview:

BL 0 in preparation

- Technische Universität Dortmund
- White beam at DELTA bending magnet, critical energy 2.2 keV
- Infrared

BL 1 in preparation

- Technische Universität Dortmund
- White beam at DELTA bending magnet, critical energy 2.2 keV
- Lithography

BL 2

- ISAS Dortmund
- White beam at DELTA bending magnet, critical energy 2.2 keV
- Energy and wavelength dispersive x-ray fluorescence spectroscopy

BL 3 and BL 4

- FEL

BL 5

- Forschungszentrum Jülich
- U250 electromagnetic undulator
- Energy range: 5 - 400 eV
- Photoemission, coincidence measurements, spectroscopy

BL 8

- Universität Wuppertal
- Superconducting asymmetric wiggler (SAW), critical energy 7.9 keV
- Energy range: 1 - 30 keV
- Focus on material science, EXAFS, QEXAFS, ReflEXAFS, XRD

BL 9

- Technische Universität Dortmund
- Superconducting asymmetric wiggler (SAW), critical energy 7.9 keV
- Energy range: 4 - 30 keV
- X-ray reflectivity, (surface) x-ray diffraction, SAXS, XSW, inelastic x-ray scattering

BL 10 in preparation

- Universität Siegen/Universität Wuppertal
- Superconducting asymmetric wiggler (SAW), critical energy 7.9 keV
- Energy range: 4.5 - 16 keV
- X-ray diffraction, absorption spectroscopy (EXAFS)

BL 11

- Technische Universität Dortmund
- U55 permanent magnet undulator
- Energy range: 55-1500 eV
- Photoemission spectroscopy, photoelectron diffraction

BL 12

- Technische Universität Dortmund
- White beam at DELTA bending magnet, critical energy 2.2 keV
- Energy range: 5 - 220 eV
- Photoemission spectroscopy

X-Ray Lithography at DELTA - Development of the New Beamline 1
D. Lietz, M. Paulus, C. Sternemann, U. Berges, J. Friedl, A. von Bohlen, B. Hippert, M. Tolan

Upgraded Endstation for Simultaneous Angle-Resolved and Spin-Polarized Photoemission
L. Plucinski, S. Cramm, B. Kuepper, F. Matthes and C.M. Schneider

In-situ surface sensitive X-ray investigations of thin bismuth films quench condensed on float-glass substrates
C. Markert, D. Lützenkirchen-Hecht, R. Wagner and R. Frahm

SAXS studies on Staphylococcal Nuclease
M. Schroer, C. Krywka, S. Schmacke, M. Paulus, C. Sternemann, R. Winter and M. Tolan

In-situ reflection mode XAS measurements of non equilibrium dissolution processes in aqueous electrolytes at beamline 8
M. Valtiner, P. Keil, V. Möllmann, R. Wagner, D. Lützenkirchen-Hecht, R. Frahm and G. Grundmeier

Structural properties of Ag@TiO_2 nanocomposites measured by means of reflection mode XAS measurements at beamline 8
V. Möllmann, P. Keil, M. Valtiner, R. Wagner, D. Lützenkirchen-Hecht, R. Frahm and G. Grundmeier

Investigation of iron-based alloys by fluorescence EXAFS
D. Lützenkirchen-Hecht, S. Cammelli, R. Wagner, C.A. Degueldre and R. Frahm

A XANES study of the aging of amorphous titania at room temperature
D. Lützenkirchen-Hecht, M. Wagemaker, W.J.H. Borghols, R. Wagner and R. Frahm

Report: EXAFS and XANES measurements of $Fe(phen)_2(NCS)_2$ spin crossover system
B. Arezki, U. Pietsch, Y. Bodenthin, D. Lützenkirchen-Hecht, R. Wagner and R. Frahm

Phase separation of bulk amorphous GeO
Ch.J. Sahle, C. Sternemann, A. Hohl, R. Wagner, D. Lützenkirchen-Hecht, A. Herdt, O. Feroughi, H. Conrad and M. Tolan

X-ray Diffraction characterization of Metal-Organic Frameworks (MOFs) thin films grown on Functionalized Organic Surfaces
O. Shekhah, H. Wang and C. Wöll

Nanocrystal formation in silicon and germanium monoxide
O. Feroughi, C. Sahle, C. Sternemann, A. Hohl and M. Tolan

Residual Stresses Analysis in Cobalt-Diamond Composites
H.-A. Crostack and U. Selvadurai-Laßl

X-ray investigation of CdSe/CdS and CdSe/CdS-ZnS core-shell nanorods
Ö. Kurtulus and U. Pietsch

Characterizing the Structure and Kinetics of Protein Adsorbates by X-Ray Reflectivity at DELTA beamline BL 9
F. Evers, K. Shokuie, M. Paulus, C. Sternemann, M. Tolan and C. Czeslik

Phase Behavior Characterization of Monomer-Clay Dispersions by X-ray Scattering Method
N. Javid, N. Bradley, J. Sefcik, J. Liggat and R. Perthrick

Structural properties of CoFeB/MgO multilayers
M. Vadalà, K. Zhernenkov, B.P. Toperverg, H. Zabel, H. Kubota and S. Yuasa

XSW measurements of Sulphur distribution in Polymer layers
M. Brücher, A. von Bohlen, R. Wagner, D. Lützenkirchen-Hecht and R. Hergenröder

2D-GISAXS investigation of crystal structure in thin polymer films
Y. Gu and A. Davydoc

The CO_2 and THF hydrate formation process
F. Lehmkühler, H. Conrad, C. Sternemann, M. Paulus, L. Böwer and M. Tolan

Investigating the molecular structure of polyethylene gas pipes
S. Schmacke, T. Theisen, D. Grahl, M. Paulus, C. Sterneman and M. Tolan

X-ray diffraction studies of thick Vs thin films of low and high molecular weight poly(3-hexylthiophene) P3HT fraction
S. Joshi, S. Grigorian, U. Pietsch, P. Pingel, D. Neher, M. Forster and U. Scherf

XRD Studies of different Metal-Organic-Frameworks
D.C.F. Wieland, O. Shekhah, M. Paulus, C. Sternemann, C. Wöll and M. Tolan

Current status and activities at the XAS/XRD Beamline 10
U. Pietsch, K. Istomin, S. Gorfman, C. Sternemann, R. Wagner, D. Lützenkirchen-Hecht, R. Frahm

Bonding configuration of cyclopentene and benzene on GaAs(001) surfaces
R. Paßmann, T. Bruhn, C. Friedrich, D. Weier, F. Schönbohm, C. Westphal, N. Esser, P. Vogt

Photoelectron spectroscopy (XPS) and photoelectron diffraction (XPD) studies on the local adsorption of benzene on Si(100)
D. Weier, A. Beimborn, T. Lühr, F. Schönbohm, S. Döring, U. Berges and C. Westphal

Photoelectron spectroscopy (XPS) studies on the system zirconium oxide on Si(100)
F. Schönbohm, D. Weier, U. Berges and C. Westphal

XPD-Measurement of the Si/SiO_2-interface on Si(110)
T. Lühr, D. Weier, F. Schönbohm, S. Döring, U. Berges and C. Westphal

Characterization of the TGM Beamline (Bl12) at DELTA
M. Schmidt, U. Berges and C. Westphal

Ultraviolet photoemission spectroscopy at DELTA - Development of the New Beamline 12
C. Taubitz, M. Räkers and M. Neumann

X-Ray Lithography at DELTA

Development of the New Beamline 1

D. Lietz[a], M. Paulus[a], C. Sternemann[a], U. Berges[a], J. Friedl[a], A. v.Bohlen[b], B. Hippert[a], M. Tolan[a]

[a] Fakultät Physik/DELTA, TU Dortmund, Maria-Goeppert-Mayer-Str. 2 , 44227 Dortmund, Germany
[b] ISAS, Bunsen-Kirchhoff -Str. 11, 44139 Dortmund
contact: daniela.lietz@tu-dortmund.de

1 Introduction

In the age of miniaturization the development of smallest technical components by deep X-ray lithography becomes more and more important. Especially synchrotron radiation is of great avail due to its special properties. With its small wavelengths in the order of ångstroms and the small divergence, yielding a parallel beam at the experiment, it is possible to produce components with a lateral resolution of sub-micrometers and a very high edge steepness. Due to the intensive radiation and the large penetration depth it is feasible to manufacture units with a height of some millimeters at a lateral structure of micrometers. Such structures are used e.g for midget hard disks in CF-cards, USB-sticks, navigation-systems, mobile phones etc.

2 Basic Principles

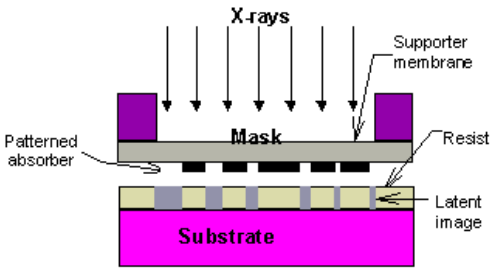

Fig. 1: Schematic setup of the mask and the coated wafer for X-Ray exposure.

The process for X-ray lithography is described in the following. As shown in fig.1 the radiation passes an X-ray mask and impacts a specially coated wafer. The mask contains the lateral structure of the components which shall be produced. For that an absorber material with a high atomic number is applied on a membrane with a low atomic number. The wafer behind the mask carries a photosensitive resist which is chemically affected by the radiation, which passes the non-absorbing regions of the membrane. Thereby the resist hardens in the radiated regions and in a subsequent chemical developing the unradiated parts can be removed. The result is a negative of the mask in the resist. Afterwards the components can be produced by galvanic precipitation. The advantage of using synchrotron radiation is the accessible depth and the high edge steepness of the structure and also the exposure of a large area at once. Due to the masks it is feasible to produce about several hundred components (e.g. small cogwheels for micro-drives) within one step which needs a few minutes.

3 First Experiments at BL 2

In December 2007 the first tests have been accomplished in order to find out if it is possible to realize a lithographic manufacturing process at DELTA. For that purpose an exposure setup has been built at the ISASline BL 2. Fig. 2(a) shows the flight path with the beryllium window and the chamber where the exposure of the wafer to the synchrotron light takes place. In the chamber the motorized carriage (so-called scanner) is located to move the wafer and the mask continuously across the 11 cm broad and 1 cm high beam. The scanner is shown in fig. 2(b). The resist had a thickness of about half a millimeter and the exposure proceeds at a bending magnet (1.5 T) with a white beam and a critical energy of 2.2 keV. This energy range is most appropriated for lithography processes.

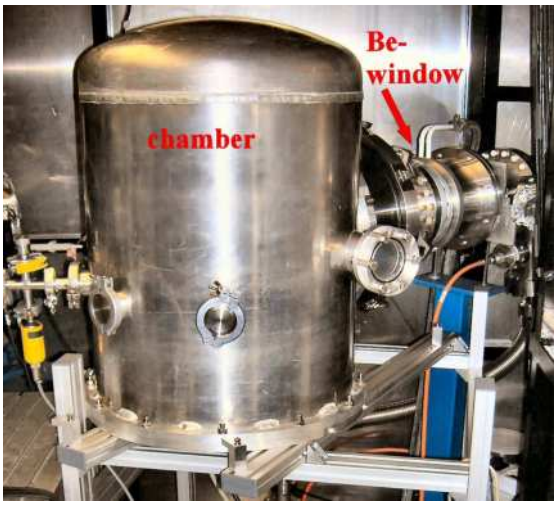

(a) Endstation at BL 2

(b) Scanner used to move the wafer and the mask across the beam

Fig. 2: (a): The endstation of BL 2 is shown with the flight path, the Be-window and the vacuum chamber. (b): Scanner with the device to fix the wafer and the mask.

After the exposure and the chemical developing SEM micrographs were taken at the ISAS in order to investigate the orthogonality and the edge steepness of the structures. These values are a measure for the quality of the process. During this testing phase it was demonstrated that it is possible to perform state of the art X-ray lithography at DELTA. In fig. 3 the high steepness and the perpendicular edges are clearly visible.

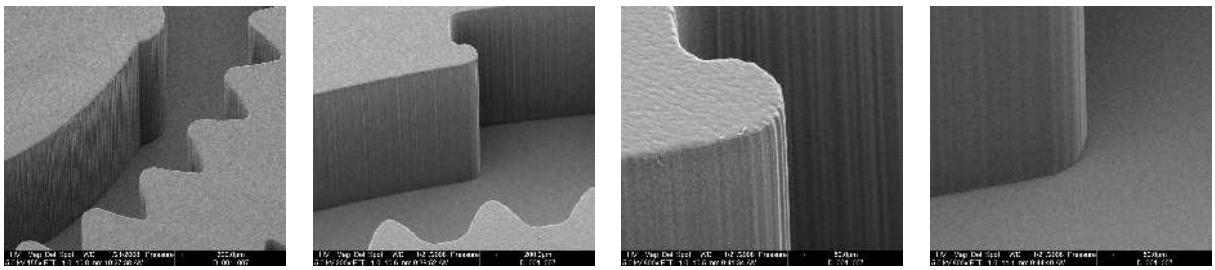

(a) 155-times magnified (b) 200-times magnified (c) 800-times magnified (d) 800-times magnified

Fig. 3: SEM micrographs of the exposed and developed resist. (a): Image section which shows a segment of the produced structure in the resist. (b): View on a structure detail, where the good steepness is shown. (c)+(d): Upper and lower edge of the structure in (b). The good orthogonality from surface and edge becomes clearly visible.

4 Development of a Lithography Beamline - BL 1

Due to the very good results in December 2007 it was decided to build a new beamline at DELTA dedicated for lithographic manufacturing purposes. Therefor the bending magnet of BL 1 was chosen. At first the layout has been planed. The outlet-chamber was already installed and during the last summer shutdown the pipe to transit the radiation protection wall was mounted. Further equipment like beamshutter, pumps, valves, etc. are already ordered. The setup will be finished in the first half of the year 2009 so that afterwards the lithography technique can be used to manufacture micro-structures.

We would like to thank the DELTA machine group for providing synchrotron radiation and technical support.

Report - U250 PGM
Beamline 5

"Upgraded Endstation for Simultaneous Angle-Resolved and Spin-Polarized Photoemission"

Participants:
Lukasz Plucinski, Stefan Cramm, Bernd Kuepper, Frank Matthes, and Claus M. Schneider

Institute of Solid State Research, IFF-9 "Electronic Properties"
Research Centre Jülich, 52425 Jülich, Germany

Contact: L.Plucinski@fz-juelich.de

Motivation

State-of-the-art photoemission investigation of modern materials requires combination of a high-resolution in both *k*- and energy with a two-dimensional (2D) detection system being a standard since over a decade. Adding spin-resolution to such a 2D system is an additional challenge and such devices are not yet available commercially. We have constructed an intermediate solution, combining high-resolution 2D spin-integrated ARPES detector with one-dimensional (1D) spin-polarized detector into one system. This new machine enables simultaneous detection of a 2D ARPES spectrum and 1D spin-resolved spectrum, which is a major step forward comparing to the previous machine at Beamline 5, and comparing to the other state-of-the-art spin-polarized spectrometer systems around the world, which may provide angular resolution but would not offer a simultaneous 2D detection.

In addition our machine allows all functionalities of the regular x-ray photoemission spectroscopy (XPS), and a motorized sample manipulation system, with software controlled movement, allows incorporation of advanced XPS techniques (e.g. photoelectron diffraction and x-ray standing wave on wedged samples).

Experimental Setup

An entirely new setup, mounted on a new, dedicated frame, has been installed at our experimental platform. The platform, build out of large concrete blocks, has been moved and adjusted to optimize the position of the new system. As of Fall 2008 the system contains:

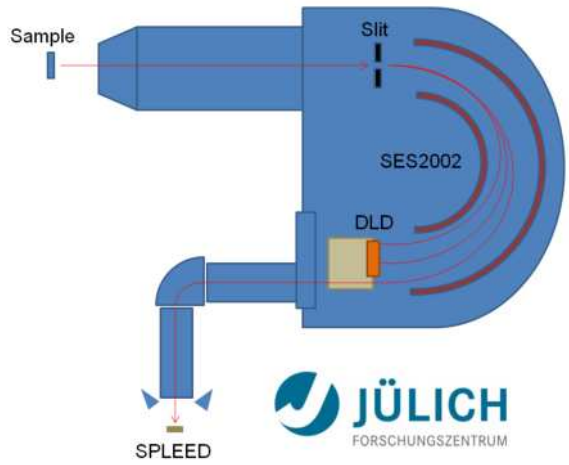

Fig 1. Schematic view of the new spectrometer system.

- Detector setup based on VG Scienta SES2002 spectrometer (details discussed below),
- UHV manipulator/goniometer which allows for all 3 degrees of freedom with software-controlled movement available and possibility of LHe cooling,
- Commercial LEED/Auger system,
- Sample preparation system which provides annealing up to 600 C, sputtering, and evaporation, connected to the spectrometer chamber via UHV transfer system,
- Load-lock system which enables loading up to 9 samples without interrupting the vacuum in the experimental chamber,
- Additional e-beam heater is currently being built and will be available later this year. It can be used to prepare single-crystal substrates of W, Re, or Mo.

Schematic view of the detector setup is presented in Fig. 1. It contains a delay-line-detector (DLD) from Surface Concept GmbH (used for 2D detection) and a SPLEED detector from Focus GmbH (used for spin-resolved detection). In Summer and Fall 2008 we have commissioned a brand new DLD detector which has a better stability and image quality, and its compactness allows incorporating a mini-lens electron optics to transfer part of the electrons to the SPLEED system. A new DLD system offers similar or better properties as the original 'phosphor' detector from VG Scienta, while in addition provides a time resolution of 500 ps or better. SPLEED

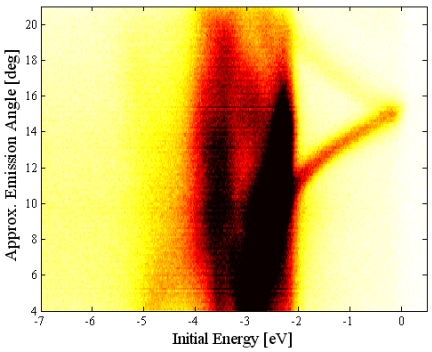

Fig 2. Angle resolved spectrum of a clean Cu(100) at hν= 147 eV. Total acquisition time 12 minutes.

system uses part of the electron beam which passes DLD, with angular resolution of approx. ±1.5 deg. There is an additional set of electron optics behind the DLD detector, with a 90-degree deflector which enables SPLEED to measure both in-plane and out-of-plane spin components simultaneously. At a typical photon energy range between 20 and 100 eV the best choice for pass energy is 20 or 50 eV -- scattering energy at the SPLEED detector is optimized at 104.5 eV, thus these pass energies provide close energy match (with slight acceleration) which is a convenient situation in electron optics.

All experiments are performed under UHV with pressure in the low E-10 mbar range of better. We have taken special care to build a fast and reliable pumping system -- currently the Endstation uses 5 turbomolecular pumps, 2 large ion pumps, and 3 titanium sublimation pumps which allow achieving base pressure in the E-11 mbar range on the regular basis.

Results

The new spectrometer system enables quick collection of high-resolution angle-resolved and spin-polarized data, and in this section we provide examples of typical data.

Fig. 2 presents 2D angular map from clean Cu(100) single crystal sample measured in the swept mode. Spectrum has been taken at a slightly off-normal emission angle to show strongly dispersing *sp*-band at binding energies between 0 and 2 eV. The quality of the image proves high spatial resolution of the DLD detector with negligible image irregularities. Spectrum has been taken at a relatively high photon energy to show that the beamline and spectrometer are not limited to the lower VUV region and in fact it is possible to measure ARPES spectrum up to at least 500 eV.

Fig. 3 presents a typical spin-polarized spectrum taken on well-known Co/Cu(100) system. At a total acquisition time of below 30 min we have obtained a spectrum where majority and minority features are clearly separated with a maximum polarization of 30% while using theoretical value 0.25 for Sherman function. SPLEED detector operates behind the complex electron optics system which in addition floats on top the Herzog plate potential of the SES2002. We believe that optimization of the voltages in this system will lead to a further increase of the countrate and decrease of acquisition time in SPLEED detector. In fact acquisition times are even shorter at photon energies 20-40 eV where the photoemission cross-section is higher and the beamline provides higher photon flux.

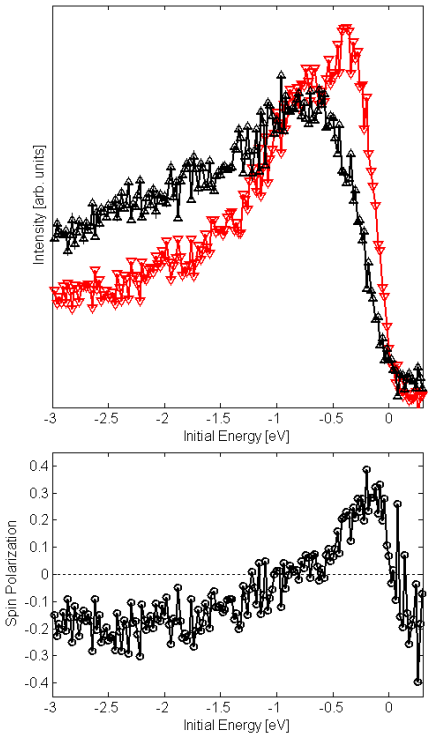

Fig 3. Spin-polarized and spin-polarization spectra of 12ML Co on Cu(100) at hν= 54.3 eV. Sherman (asymmetry) function 0.25. Total acquisition time 28 minutes.

Summary

The new endstation installed at the Beamline 5 has been commissioned. First results show that with the new system one is able to measure combined APRES and spin-resolved photoemission data quickly and conveniently at high energy and angular resolution.

The beamline provides high intensity over the wide energy range from VUV to the soft-x-rays. Combining this with our flexible analyzer system based on a modern SES2002 spectrometer allows variety of studies ranging from extremely high-resolution ARPES (e.g. on complex oxide systems) up to high angular resolution photoelectron diffraction in the soft-x-ray regime.

Acknowledgements

The detector system has been designed in close collaboration with A. Oelsner from Surface Concept GmbH. We acknowledge fruitful discussions with B. Wannberg from VG Scienta and M. Escher from Focus GmbH.

In-situ surface sensitive X-ray investigations of thin bismuth films quench condensed on float-glass substrates

C. Markert, D. Lützenkirchen-Hecht, R. Wagner and R. Frahm

Fachbereich C – Physik, Bergische Universität Wuppertal,
Gaußstraße 20 , 42097 Wuppertal, Germany

A combination of in-situ X-ray reflectometry, surface sensitive reflection mode X-ray absorption spectroscopy (XAFS) and simultaneous electrical resistivity measurements was used to investigate the surface and volume microstructure of thin quench condensed bismuth (Bi) films as a function of the deposition temperature, the film thickness and their changes induced by a subsequent annealing treatment. All experiments were performed in an ultra high vacuum evaporation chamber with a base pressure of less than 5 x 10^{-10} mbar. The film thickness as well as the deposition rate ($\leq 0.20 \pm 0.05$ nm/s) were controlled by a calibrated quartz crystal thickness monitor, which also controls a pneumatic shutter between the evaporation source and the substrate. The cryostat with the sample holder were completely surrounded by a cryogenic heat shield, held at liquid nitrogen temperature to reduce the thermal load on the substrate. In combination with a capsuled evaporation source the substrate temperature during the film deposition remains constant even at very low deposition temperatures of less than 30 K.
All presented experiments were performed at the beamline 8 at the DELTA storage ring. For the X-ray experiments a double-crystal monochromator with two flat Si(111) crystals and an energy resolution of about $\Delta E/E \approx 1.25 \times 10^{-4}$ was used. Incident and reflected intensities were measured by argon and nitrogen filled ionization chambers. The electrical resistivity measurements were performed using a conventional four point probe technique in parallel to the X-ray experiments. In order to minimize any effect of resistive heating, the measurement current was in all cases less than 2 μA.

As an example, in Fig. 1 the evolution of the electrical resistivity of a 5.9 nm ± 0.1 nm thick bismuth film deposited at T_S = 20 K (A) is depicted. As can be clearly seen, the isochronous annealing process to T_S = 80 K (B) induces an irreversible change of the electrical resistivity, after exceeding a critical temperature of about 43 K. This resistivity change is accompanied by an irreversible transformation of the film microstructure, from an highly disordered or even amorphous phase into polycrystalline film microstructure. Prior to the annealing process a linear and reversible resistivity behaviour was found for T_S < 40 K, showing a negative temperature coefficient of resistance (TCR) of $d\rho/dT_S \approx -1.5$ μΩcmK^{-1}, suggesting that weak localization and electron-electron scattering effects dominate the electronic transport in this temperature and film thickness region. A lower TCR value of about $d\rho/dT_S \approx -0.85$ μΩcmK^{-1} was observed after the annealing process to T_S = 80 K, suggesting that the film structure has been improved but nevertheless remains strongly disordered.
In Fig. 3, some typical specular X-ray reflectivity profiles which were in-situ recorded in the course of the deposition and annealing process are presented. Fitting of the experimental data gives the densities of the contributing materials, the surface and interface roughness between the different layers and the thickness of the deposited thin films. Within the error of the experimental uncertainty the film thickness derived from the X-ray reflectivity curves in the different stages of the annealing process (A-C) always yields the same value of about t = 5.9 ± 0.1 nm. Furthermore, the annealing process to T_S = 80 K exhibits no influence on the film density (mean value $\rho = 8.7 \pm 0.2$ gcm^{-3}) or the surface roughness ($\sigma = 0.8$ nm ± 0.1). Measurable changes can only be observed after the annealing process to T_S = 345 K (D)

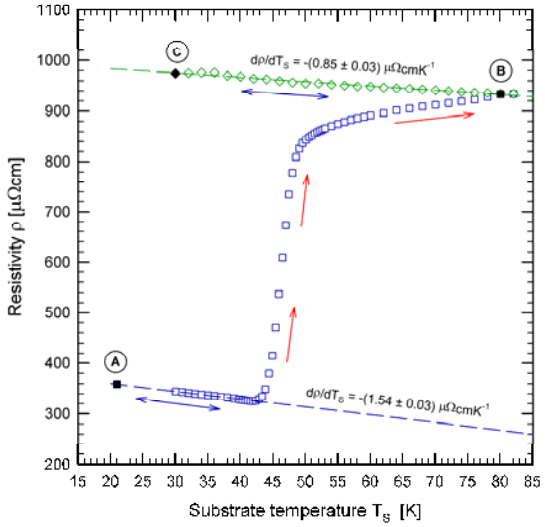

Fig. 1: *Annealing behaviour of the electrical resistivity ρ. After deposition onto a float-glass substrate held at T_S = 20 K (A) the thin Bi-film was annealed to 80 K (B) with a constant annealing rate of 2 Kmin^{-1} and recooled to 30 K (C).*

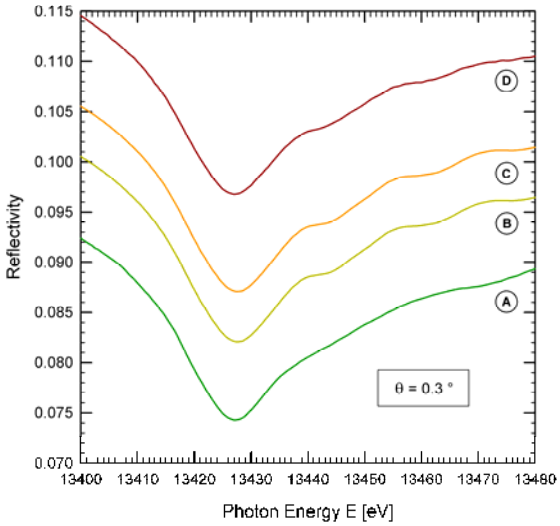

Fig. 2: *Reflectivity XAFS spectra taken at the Bi L_3-edge (13419 eV) at an incidence angle of Θ = 0.3 ° and different substrate temperatures. The curves are vertically shifted by 0.01with respect to each other for better comparison.*

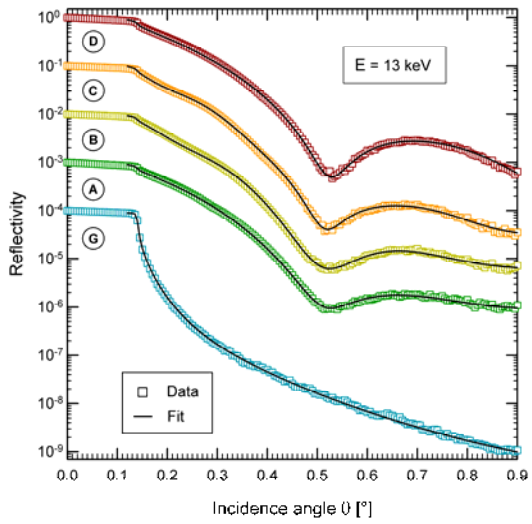

Fig. 3: *Specular reflectivity profiles for 13000 eV photons (λ = 0.9537 Å) as a function of the incidence angle Θ for the clean float-glass substrate, and the thin bismuth film at different substrate temperatures. The curves are vertically shifted by one order of magnitude with respect to each other. The full lines represent fits to the experimental data.*

A: T_S = 20 K (deposition temperature)
B: T_S = 80 K
C: T_S = 30 K
D: T_S = 345 K
G: T_S = 300 K (float-glass substrate)

where the best fit corresponds to a double layer system, consisting of a 1.4 ± 0.1 nm thick first layer with a density close to that of the bulk bismuth (ρ = 9.8 gcm^{-3}) and a 4.3 ± 0.1nm thick top layer with a density of ρ = 8.4 ± 0.2 gcm^{-3}. The surface roughness of both layers is less than σ = 0.3 nm. The specular X-ray reflectivity profiles therefore show no substantial changes with the annealing process to T_S = 80 K. Nevertheless, since there is a significant increase of the resistivity by a factor of more than 2.5 there must be some kind of structural change, which most likely corresponds to a change of the film structure in the atomic short range structure. As can be seen clearly in Fig. 2 we observe some irreversible changes of the XAFS profiles during annealing. Weak XAFS oscillations were observed directly after the deposition (A), which corresponds to a strongly disordered or even amorphous film structure. After annealing to T_S = 80 K, the amplitude of these oscillations increased substantially indicating that some crystallization occurred, leading to a more developed short range order around the absorbing Bi-atom. The higher oscillation frequencies after the annealing process can be understood as a increase of the inter-atomic distances, which is also in good agreement with a phase transformation from an disordered phase to a crystalline microstructure.

SAXS studies on Staphylococcal Nuclease

Martin Schroer[(a),*], Christina Krywka[(a),†], Saskia Schmacke[(a)], Michael Paulus[(a)], Christian Sternemann[(a)], Roland Winter[(b)], and Metin Tolan[(a)]

(*a*) Fakultät Physik/DELTA, Technische Universität Dortmund, Maria-Goeppert-Mayer-Str. 2, D-44221 Dortmund, Germany
(*b*) Physikalische Chemie I, Technische Universität Dortmund, Otto-Hahn-Str. 6, D-44227 Dortmund, Germany
† current address: Institut für Experimentelle und Angewandte Physik, Christian-Albrechts-Universität zu Kiel, Leibnizstr. 19, 24118 Kiel, Germany

* contact: martin.schroer@tu-dortmund.de

Investigating the structure of proteins and their stability is of fundamental interest as, e.g., destabilization may lead to protein unfolding, misfolding and aggregation. In this context, Staphylococcal Nuclease (SNase) has been proved as a model protein to study the influence of high pressure, temperature and various cosolvents [1,2]. However, little is known about the intermolecular interaction of the protein. Thus, the purpose of this small angle x-ray (SAXS) study was to analyze this interaction and how it is changed by the addition of different amounts of NaCl.

The measurements were carried out at the multi-purpose beamline BL9 of DELTA using the SAXS set-up [3]. A photon energy of 10 keV and a sample-to-detector distance of 1090 mm allowed to cover a q-range of up to 4 nm^{-1}. The SAXS spectra were obtained employing a two-dimensional *MAR345* detector. Measurements were done for different protein concentrations to determine the effective structure factor which is a function of the intermolecular protein-protein-interaction. The SAXS signal of the buffer was detected as a reference as well. Each sample was exposed to the x-ray beam for 1800 s.

Figure 1 shows the integrated raw data of the buffer and the solution as well as the form factor of SNase which is obtained by subtracting the pure buffer signal from the spectrum of the protein solution. The detailed analysis of the data showed [4] that the form of the protein used was different from that reported in other studies [1,5]. This indicates that the protein was partially unfolded. However, it is still possible to calculate the proteins' effective structure factor.

In contrast to previous measurements carried out on the proteins lysozyme and insulin [6,7], a less significant structure factor was detected for SNase [4]. This suggests

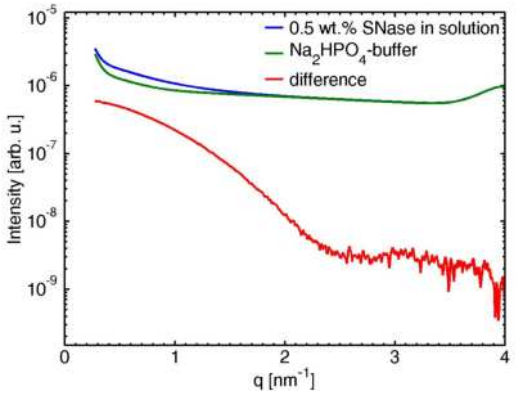

Figure 1: Raw data and form factor for a 0.5 wt.% SNase solution. 10 mM phosphate buffer were used at pH 5.4 at 25 °C.

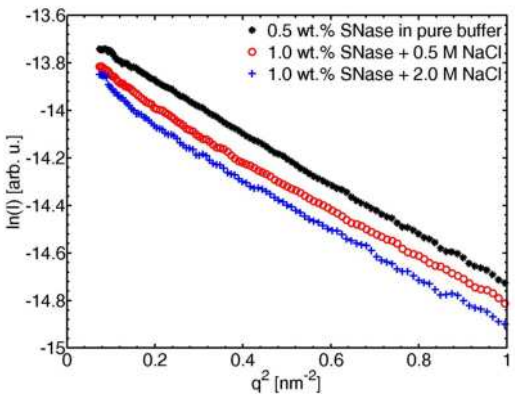

Figure 2: Guinier plot of the SNase form factor for different NaCl concentrations.

that the attractive part of the intermolecular interaction is more pronounced compared to the repulsive part than for the other proteins. The addition of NaCl induces the formation of aggregates which contribute to the scattering signal as is indicated by the nonlinear shape of the Guinier plot (see Fig. 2). Under these solution conditions the structure factor changes its shape reflecting the screening of the proteins' surface charge.

The observed shapes of the structure factors as well as the formation and precipitation of aggregates may be attributed to the non-native protein form which may lead to a different kind of interaction between the macromolecules. To verify this conclusion further measurements with a native SNase sample will be necessary.

References

[1] G. Panick, R. Malessa, R. Winter, G. Rapp, K.J. Frye, C.A. Royer, *Structural Characterization of the Pressure-denatured State and Unfolding/Refolding Kinetics of Staphylococcal Nuclease by Synchrotron Small-angle X-ray Scattering and Fourier-transform Infrared Spectroscopy*, J. Mol. Biol. **275**, 389 (1998)

[2] C. Krywka, C. Sternemann, M. Paulus, M. Tolan, C. Royer, R. Winter, *Effect of Osmolytes on Pressure-Induced Unfolding of Proteins - A High Pressure SAXS Study*, ChemPhysChem, doi: 10.1002/cphc.200800522 (2008)

[3] C. Krywka, C. Sternemann, M. Paulus, N. Javid, R. Winter, A. Al-Sawalmih, S. Yi, D. Raabe, M. Tolan, *The small-angle and wide-angle X-ray scattering beamline BL9 of DELTA*, J. Synchrotron Rad. **14**, 244 (2007)

[4] M. Schroer, *Röntgenkleinwinkelstreuung an dem Protein Staphylokokken Nuklease und dessen Mutanten*, Diploma-Thesis, TU Dortmund (2008)

[5] A. Paliwal, D. Asthagari, D.P. Bossev, M.E. Paulaitis, *Pressure Denaturation of Staphylococcal Nuclease Studied by Neutron Small-Angle Scattering and Molecular Simulation*, Biophys. J **87**, 3479 (2004)

[6] N. Javid, K. Vogtt, C. Krywka, M. Tolan, R. Winter, *Protein-Protein Interactions in Complex Cosolvent Solutions*, ChemPhysChem **8**, 679 (2007)

[7] N. Javid, K. Vogtt, C. Krywka, M. Tolan, R. Winter, *Capturing the Interaction Potential of Amyloidogenic Proteins*, PRL **99**, 028101 (2007)

In-situ reflection mode XAS measurements of non equilibrium dissolution processes in aqueous electrolytes at beamline 8

M. Valtiner[a,b], P. Keil[b], V. Möllmann[c], R. Wagner[d], D. Lützenkirchen-Hecht[d], R. Frahm[d], G. Grundmeier[a,c]

a) Christian Doppler Laboratory for Polymer/Metal interfaces, Max-Planck Institut für Eisenforschung GmbH, Max-Planck-Str. 1, 40237 Düsseldorf, Germany
b) Department of Interface Chemistry and Surface Engineering, Max-Planck Institut für Eisenforschung GmbH, Max-Planck-Str. 1, 40237 Düsseldorf, Germany
c) Department of Chemistry, University of Paderborn, Warburgerstr. 100, 33100 Paderborn, Germany
d) Fachbereich C – Physik, Bergische Universität Wuppertal, Gaußstr. 20, 42097 Wuppertal, Germany

The surface chemistry of oxide/liquid interfaces is a key issue in adhesion science and related areas such as corrosion science. The oxide dissolution promoting effects of H^+, OH^- and various anions, as e.g chlorides or sulphates, are an important aspect of metal corrosion, its inhibition and adhesion in corrosive environments. For example corrosion reactions, like a cathodic delamination of organic coatings or crevice corrosion, are accompanied by a change of the pH at the interface; chlorides can promote dissolution and corrosion of materials. Therefore, it is necessary to understand the stability, interface chemistry and dissolution behavior of materials as a function of the pH and anions activities. Due to this essential issue, the experimental setup for measuring in-situ grazing incidence XAS analysis of essentially non-equilibrium processes as the dissolution of oxides in electrolytes has been developed and tested on a ZnO system at beamline 8.

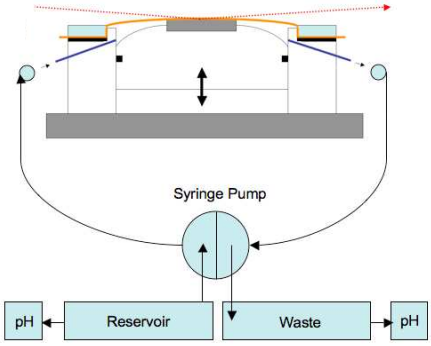

Fig. 1: Flowchart of the setup as installed at beamline 8. All parts of the cell that contact electrolyte are made of Peek. The cell is closed with an 8 µm Kapton foil. The foil is pressed on the surface, leading to a residual electrolyte film of some tenth of micrometer on top of the surface.

ZnO is in particular interesting, as zinc is a widely used metallic coating for steel. Hence the stability of passivating ZnO films is of high technical interest. In order to allow a defined study of oxides decoupled from any oxidative interfacial reaction a single crystalline ZnO(0001)-Zn surface was used. This polar ZnO surface can be prepared quite simple and efficient as a very well defined, single crystalline surface [1]. Between pH 11 and pH 5.5 the surface structure is inert against any dissolution. Below pH 5.5 the dissolution of the surface starts preferably from pre-existing edges of the surface [2]. Identification of inner and outer surface complexes by means of reflection mode XAS can give valuable information concerning the dissolution mechanism. In Fig. 1 the setup of the designed cell is depicted. The important aspect of this setup is the possibility to

exchange the electrolyte in situ as well as online while measuring spectra. This is achieved by using a syringe pump that allows a well defined and an almost pulsation free flow/ circulation of electrolyte through the cell. The XAS measurements described here were performed at the beamline 8 using a Si (111) double crystal monochromator, N_2- and Ar-filled ionization chambers as detectors for the incoming and reflected intensities, respectively. The grazing incidence XAS data were collected in the vicinity of the K-edge of Zn (9659 eV) under a grazing angle of 0.225°, witch is well below of the critical angle of total reflection.

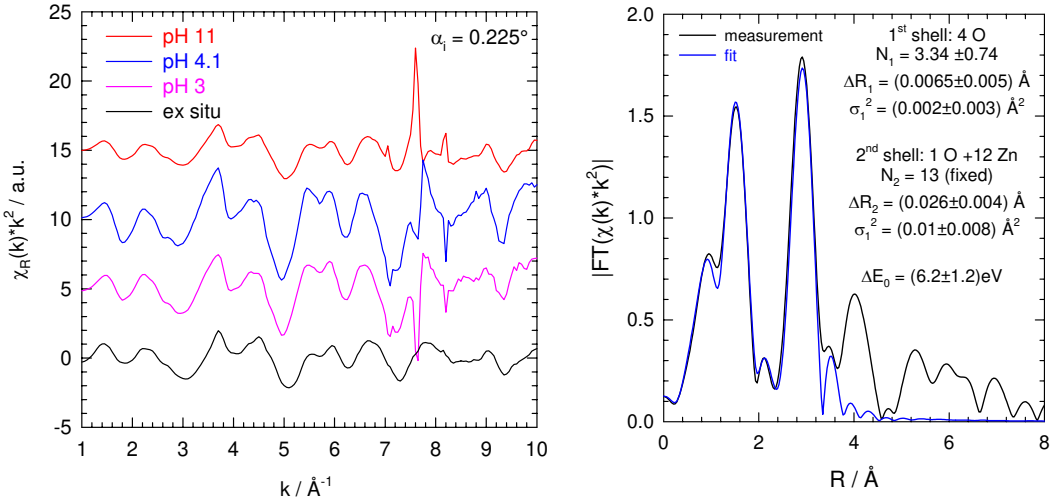

Fig. 2: Reflectivity fine structure from a single crystalline ZnO(0001)-Zn surface at the Zn K-edge for different pH levels in comparison to ex-situ experiments of the same sample, as indicated (left side). Fourier transformed true absorption fine structure (k^2-weighted) obtained form the ex situ measurements and respective fit (right side).

Comparison of the reflectivity fine structure data shown in Fig. 2 demonstrates that the data quality of the in-situ measurements is comparable to that of ex-situ measurments. Despite of some glitches between 7.5 and 8 Å^{-1} fine structure oscillations with very low noise are visible up to k > 10 Å^{-1}, allowing the transformation of the reflectivity structure into a true absorption fine structure by means of a Kramer-Kronig transformation analysis and a reliable fit of the received χ(k) on basis of ab-initio calculations. Exemplarily the Fourier transform of the ex situ measurement together with a preliminary fit of the first two neighbour shells assuming 4 O atoms in the first and 12 Zn + 1 O atoms in the second neighbour shell is shown in Fig. 2. The fit was performed using the FEFF6 [3] code. The presented data shows, that the cell setup works well for investigating non-equilibrium processes at the material/ electrolyte interface in-situ by means of reflection mode XAS allowing a detailed discussion regarding to the chemical dissolution of ZnO(0001) surfaces on the basis of FEFF calculations.

The financial support of voestalpine Stahl Linz AG, Henkel AG & Co. KGaA, Adhesives Technologies Division, as well as the Christian-Doppler Society in Vienna is gratefully acknowledged.

References:

1. Valtiner, M.; Borodin, S.; Grundmeier, G., PCCP 9 (2007) 2297.
2. Valtiner, M.; Borodin, S.; Grundmeier, G., Langmuir 24 (2008) 5350.
3. S.I. Zabinsky, J. J. Rehr, A. Ankudinov *et al.*, Phys. Rev. B 52 (1995) 2995.

Structural properties of $Ag@TiO_2$ nanocomposites measured by means of reflection mode XAS measurements at beamline 8

V. Möllmann[a], P. Keil[b], M. Valtiner[b], R. Wagner[c], D. Lützenkirchen-Hecht[c], R. Frahm[c], G. Grundmeier[a]

a) Department of Chemistry, University of Paderborn, Warburgerstr. 100, 33100 Paderborn, Germany
b) Department of Interface Chemistry and Surface Engineering, Max-Planck Institut für Eisenforschung GmbH, Max-Planck-Str. 1, 40237 Düsseldorf, Germany
c) Fachbereich C – Physik, Bergische Universität Wuppertal, Gaußstr. 20, 42097 Wuppertal, Germany

Silver nanoparticles embedded in TiO_2-films have received increasing attention during the last decade due to their various applications including solar energy conversion, photocatalysis, antibacterial coatings and unique optical components including photochromic devices. Most of the special optical properties arise from the localized surface plasmon resonance of the embedded nanoparticles and the dielectric properties of the surrounding matrix. For instance, the particle size, shape and the surrounding has a direct correspondence with their optical response, resulting in the so-called morphological dependent resonances. Thus, the performance of such devices is mainly determined by the structural properties of the embedded Ag and the surrounding TiO_2 as matrix material.

In the presented studies $Ag@TiO_2$-nanocomposite films were prepared by means of RF-magnetron sputtering from an Ag and a semiconducting TiO_2 target on top of a float glass substrate and using only Ar as process gas. The nanocomposite films were arranged in a layer-by-layer structure (TiO_2/Ag/TiO_2). By subsequent annealing at 500°C in inert atmosphere Ag nanoparticles of approx. 58 nm in diameter are formed within the TiO_2 matrix due to Ostwald-ripening. For the detailed determination of the structural properties of the embedding TiO_2 grazing incidence XAS investigations were performed at beamline 8 using a Si (111) double crystal monochromator and N_2-filled ionization chambers as detectors for the incoming and reflected intensities. The grazing incidence XAS data were collected in the vicinity of the K-edge of Ti (4966 eV) under grazing angles from 0.3° (below the critical angle of total reflection of TiO_2) to 0.45° (above the critical angle of total reflection of TiO_2), allowing a depth profiling through the thin nanocomposite film.

In Fig. 1 the XANES spectra of the $Ag@TiO_2$ nanocomposite film before and after annealing determined from the grazing incidence measurements at 0.3° are compared to those of reference compounds (transmission mode). In both cases, before and after annealing, the edge position of the nanocomposite films amounts approx. 4980 eV, demonstrating that the valance of the Ti is 4+, even though no additional oxygen was added during the sputter deposition process. Comparing the XANES it is obvious that after annealing the film is restructured from at least partly amorphous to the anatase phase, identifiable by e.g the typical pre-edge peak structure.

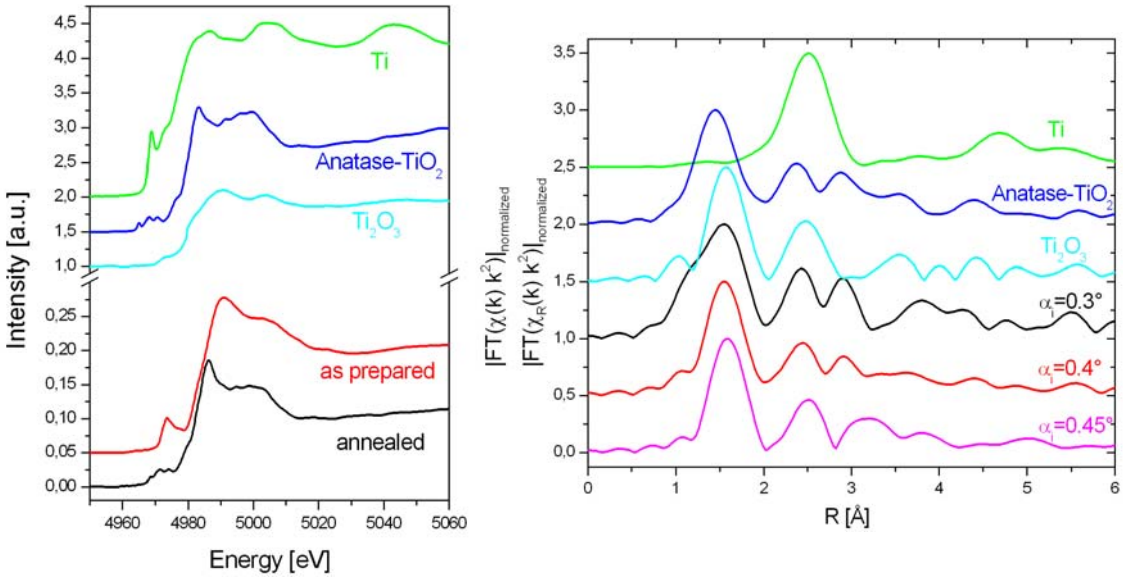

Fig. 1: *Right side*: XANES of the Ag@TiO_2 nanocomposite film before and after annealing in comparison to reference compounds (as indicated). The XANES of the Ag@TiO_2 film was determined from the grazing incidence measurements at 0.3° and the one of the reference compounds from transmission experiments. *Left side*: Normalized magnitude of the FT´s determined from grazing incidence XAS measurements from the annealed Ag@TiO_2 nanocomposite film in comparison to transmission mode XAS experiments of reference compounds (as indicated). The data are not phase-shift corrected.

The normalized magnitude of the FT´s determined from grazing incidence XAS measurements of the annealed film shown in Fig. 1 shown apparent differences between the measurements at small grazing angles (below (α_i = 0.3°) and in the vicinity (α_i = 0.4°) of the critical angle of total reflection) and the grazing angle above the critical angle of total reflection (α_i = 0.4°). While the normalized magnitude of the FT´s of the measurements at α_i = 0.3° and α_i = 0.4° are comparable to the one of anatase TiO_2, shifts in the position of the peaks corresponding to the second and third coordination shell at radial distances of approx. 2.45 Å and 2.95 Å are detectable for the measurement at α_i = 0.45°. This indicates that in the bulk the TiO_2 matrix is not completely restructured into anatase-TiO_2, even for the used curing conditions consisting of a relative high annealing temperature of 500°C and of an annealing time of 1 h. For further reading, the detailed discussion of the data regarding the structural properties of Ag@TiO_2 nanocomposites measured by means of reflection mode XAS at the Ti and Ag K-edges will be presented elsewhere.

Investigation of iron-based alloys by fluorescence EXAFS

D. Lützenkirchen-Hecht [a], S. Cammelli [a, b], R. Wagner [a],C. A. Degueldre [b], R. Frahm [a]

a) Fachbereich C – Physik, Bergische Universität Wuppertal, Gaußstr. 20, 42097 Wuppertal, Germany
b) Paul Scherrer Institut, CH-5232 Villigen PSI , Switzerland

In this report we want to describe our recent experiments on steel materials that are employed in nuclear reactor pressure vessels (RPV). Those materials are typically composed by an iron base alloy with traces of Ni and Cu and additional elements in the 0.1-1 wt.% range. The most important material degradation in RPV-steels during operation in a nuclear reactor is the embrittlement caused by the formation of small metal precipitates in the iron matrix. These precipitates, which are supposed to be mainly composed by small Cu and Ni atom clusters, are able to pin dislocations and hinder dislocation gliding, thus leading to a less ductile mechanical behaviour. On a macroscopic scale, these modifications of the elastic properties of the materials lead to a situation where the structural integrity of the reactor pressure vessel in a nuclear power plant can be critically affected. Therefore, significant work has been done in the past in studying RPV steel aging and coupling microstructural information with the mechanical behaviour of such steels (see e.g. Ref. [1]). In the present experiments, we want to investigate the distribution and the local environment of Cu and Ni in the RPV-steel and their changes induced by irradiation with high neutron fluxes and its relaxation by a subsequent annealing. The experiments were performed using the Si(111) monochromator optics of beamline 8 at the DELTA storage ring, a nitrogen-filled ionization chamber for the measurement of the incoming beam, and a Si pin-diode with a multichannel analyzer and digital pulse processor to measure the fluorescence signals excited in the sample. Typical raw fluorescence data obtained from an Fe base alloy with different other metal elements such as Ti, Cr and Mn in the 0.1-1 at% range are presented for several different excitation energies in the vicinity of the Mn K-edge (6.539 keV) are presented in Fig. 1.

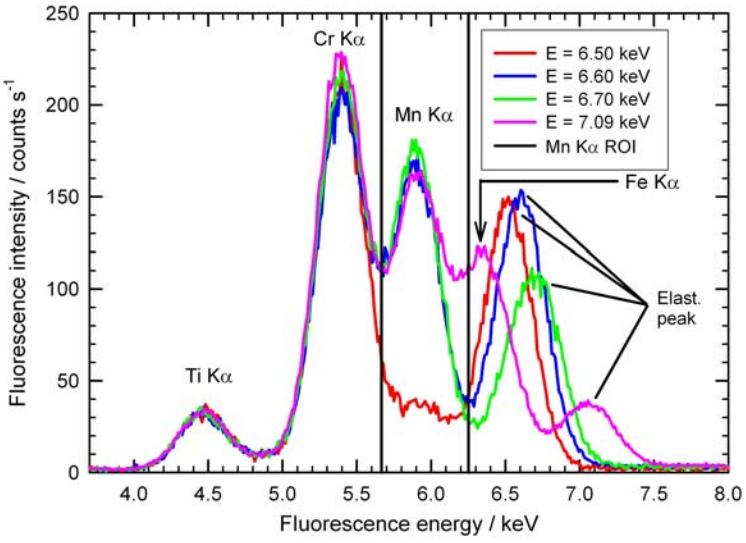

Fig. 1: Fluorescence spectra of an Fe alloy containing ca. 1 at% Mn for different excitation energies in the vicinity of the Mn K-edge (6.539 eV) as indicated.

As can be seen, clear signatures of Ti, Cr, Mn and Fe are detectable in addition to the different elastic contributions. In the case of the alloyed Mn, the respective signals were separated by means of a region of interest (ROI, see Fig. 1), and the counts in this region were integrated for each data point in an energy scan ranging from about 6.4 to 7.1 keV with ca. 500 data points. Although the concentration of Mn in the alloy is well below 1 at.%, the complete scan only took about 1 h, and the data quality is reasonable for a full EXAFS data analysis. The increase of the fluorescence yield for energies larger than ca. 6.8 keV is caused by the onset of the Fe K fluorescence, which cannot be completely discriminated in the present case due to a limited energy resolution of the used set-up of about 0.2 keV. As can be seen in Fig. 1, a significant contribution of the Fe Ka-radiation was found already for 7.09 keV, and due to the large Fe concentration in the sample compared to the small Mn-content, this signal has a strong influence already for lower excitation energies.

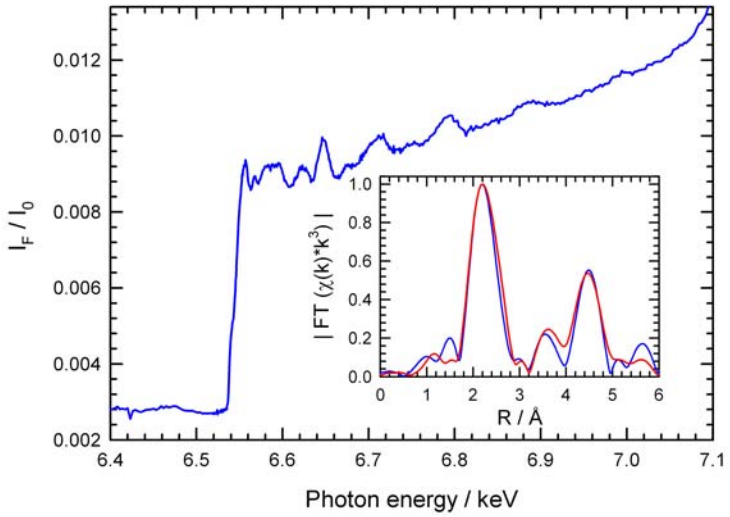

Fig. 2: Raw EXAFS at the Mn K-edge of the Fe base alloy within ca. 1 h of total integration time. The data are extracted from the data of Fig. 1. The inset shows the magnitude of the Fourier-transform of the k^3-weighted EXAFS fine structure (—) in comparison to that of a Fe metal foil at the Fe K-edge (—).

As can be seen from the evaluation of these data, Mn is obviously located in regular bcc Fe-sites: The Fourier-transformed data clearly resembles that of experiments at the Fe K-edge, with the same peak positions and intensities even for the second and third next neighbour atoms. However, a more detailed EXAFS analysis is required in order to obtain the atomic short range order information such as bond distances and the local disorder. Such an analysis as well as detailed structural investigations of irradiated samples will be described elsewhere [2].

References:

[1] W.J. Phythian et al., "The structure and hardening mechanism of Copper precipitation in thermally age or irradiated Fe-Cu and Fe-Cu-Ni model alloys", Effects of Radiation on Materials: 15th International Symposium, 1992, Philadelphia, ASTM.
[2] S. Camelli, PhD-thesis, University of Wuppertal, in preparation.

A XANES study of the aging of amorphous titania at room temperature

D. Lützenkirchen-Hecht [a], M. Wagemaker [b], W.J.H. Borghols [b], R. Wagner [a], R. Frahm [a]

a) Fachbereich C – Physik, Bergische Universität Wuppertal, Gaußstr. 20, 42097 Wuppertal, Germany
b) FAME, TU Delft, Mekelweg 15, 2629 JB Delft, The Netherlands

Nanomaterials are becoming important for use in Li-ion battery electrodes as these can deliver increased capacity and improved power performance. For example, due to the increased surface per weight or volume of the material, an enhanced charge transfer is resulting, and the reduced particle size is accompanied by a reduced diffusion/migration length, the latter is favourable for an enhanced power performance. Previous electrochemistry, neutron diffraction and EXAFS experiments have shown that nanosized anatase and rutile TiO_2 accept more Li in the surface shell than in the core, leading to a "novel" redox chemistry therefore [1-3]. Owing to the fact that nanosized materials also reveal a better acceptance of local strains which is comparable to that of zero-strain materials such as $Li_4Ti_5O_{12}$ [4], the possibility of interfacial Li storage has increasingly been investigated in the past few years (see e.g. [5, 6]). Furthermore, also amorphous materials are in the focus of interest thanks to their promising electrochemical properties [7]. However, there are problems with stability of the materials, more specifically with a degradation of those materials that leads to a reduced capacity and cyclability. This work is dedicated to the aging of amorphous TiO_2 phases which were prepared by hydrolysis of hydrolysis of titanium(IV)isopropoxide and the subsequent condensation and aggregation to titania agglomerates [8]. While crystallization and degradation effects are well known in the case of aging at elevated temperatures, only little is known of room temperature structural changes. The freshly precipitated TiO_2-samples as well as samples aged in a room temperature environment for about one year were investigated by transmission mode X-ray absorption experiments at beamline 8 at the DELTA-storage ring.

Raw X-ray absorption near edge spectra are shown in Fig. 1 for the freshly precipitated amorphous TiO_2 and the aged titania together with some selected Ti(IV)-oxide reference compounds, i.e. anatase and rutile. Clear differences are observed both in the pre-edge region, where the fresh precipitate has a strong pre-edge peak at about 4.972 keV. The intensity of this feature is significantly reduced for the aged precipitate, and slightly shifted to larger photon energies. Rutile and anatase reveal significantly smaller and more structured pre-edge region in comparison to the amorphous TiO_2 compounds. Further changes are also observed in the post edge region of the XANES spectra, where the freshly prepared precipitate shows only two broad maxima at about 4.990 keV and 5.005 keV. In contrast, the aged precipitate yields several smaller absorption features in this spectral range.

For a more detailed analysis of the spectra, we have performed a linear combination fit of the measured spectra, typical results are presented in Fig. 2. It has to be mentioned here that only negligible shifts of the energy scale of the used reference compounds are required for the fit, which stresses the meaning of such an analysis and proves the reliability of the results. For the spectrum presented in Fig. 2, we found a composition of

about 54.5 wt.% amorphous TiO_2, ca. 41.3 wt.% anatase, and only 4.2 wt.% rutile. These findings suggest that about half of the amorphous precipitate is transformed into a (nano-) crystalline anatase after storage in air at room temperature for one year. These findings are important for the use of amorphous or nano-sized titania as battery materials in reliable rechargeable devices, and it is planned to study these processes in more detail in the future.

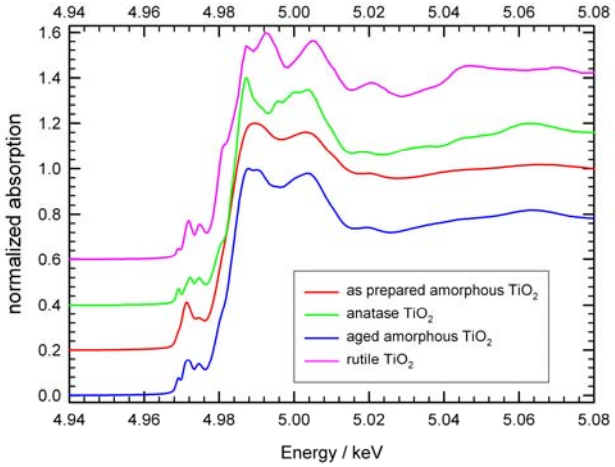

Fig. 1:

Comparison of the normalized Ti K-edge X-ray absorption near edge spectra of freshly precipitated amorphous TiO_2 samples to those of crystalline anatase and rutile reference compounds and the aged precipitate (storage in air at room temperature for about one year).

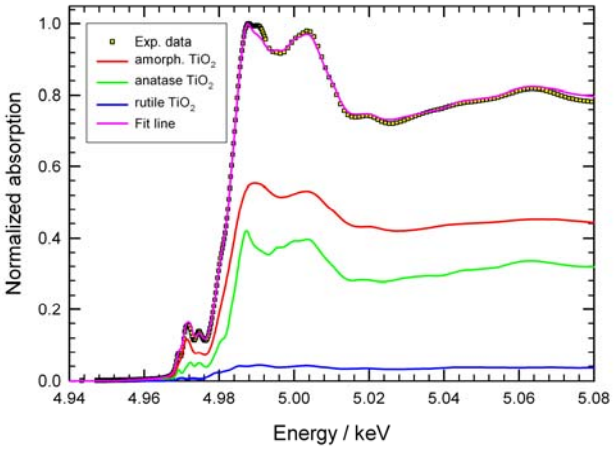

Fig. 2:

Modelling of the XANES spectrum of the aged precipitate by a linear combination of the Ti K-edge XANES spectra of anatase, rutile and the amorphous fresh precipitate. The contributions of the individual phases as well as the fit line are indicated.

References:

[1] M. Wagemaker, W.J.H. Borghols, F.M. Mulder, J. Am. Chem. Soc. 129 (2007) 4323
[2] M. Wagemaker,W.J.H. Borghols, E.R.H. van Eck, A.P.M. Kentgens, G.J. Kearley, F.M. Mulder, Chem. Eur. J. 13 (2007) 2023
[3] D. Lützenkirchen-Hecht, M. Wagemaker, P. Keil, A.A. van Well, R. Frahm, Surf. Sci. 538 (2003) 10
[4] M. Wagemaker, D.R. Simon, E.M. Kelder, J. Schoonman, C. Ringpfeil, U. Haake, D. Lützenkirchen-Hecht, R. Frahm, F.M. Mulder, Adv. Mat. 18 (2006) 3169
[5] J. Maier, Nature Materials 4 (2005) 805
[6] U. Lafont, C. Locati, E.M. Kelder, Solid State Ionics 177 (2006) 3023
[7] M. Hibino, K. Abe, M. Mochizuki, M. Miyayama, J. Power Sources 126 (2004) 139
[8] V. Luca, S. Djajanti, R.F. Howe, J. Phys. Chem. B 102 (1998) 10650

Report: EXAFS and XANES measurements of $Fe(phen)_2(NCS)_2$ spin crossover system

Bahia Arezki and Ullrich Pietsch (Universität Siegen)
Yves Bodenthin (PSI - Swiss Light Source)
Dirk Luetzenkirchen-Hecht, Ralph Wagner, Ronald Frahm (Bergische University of Wuppertal)

There is a continuous interest in spin transition (ST) systems where the spin state of metal ions can be switched by external stimulations [1]. Such tunable compounds are potential candidates for future molecular switching devices.
In the frame of our study of the structural changes associated with the ST of Metallo-supramolecular polyelectrolyte-amphiphile-complexes (PAC) induced by temperature [2] and light, Extended X-ray Absorption Fine Structure (EXAFS) and X-ray Near-Edge (XANES) measurements have been done on the well known ST compound $Fe(phen)_2(NCS)_2$ (phen=1,10-phenanthroline) [3]. This reference material has been used during our last beamtime in Delta/ beamline 8, in order to check if the setup is sensitive to the light (LIESST-Light-Induced-Excited-Spin-State-Trapping)-induced ST. Unfortunately, although the same conditions were applied in our experiment (HeNe laser irradiation at 10 K, λ= 633 nm, W~ 10 mW/cm^2), no changes have been observed in the XANES spectra. This is probably due to the fact that the thickness of the surface layer converted from the LS to the photo-induced HS state is much thinner than the volume probed by the X-rays. Nevertheless, we could identify the thermal ST for this complex. Although the structural modifications occurring during the thermal ST of $Fe(II)L_n(NCS)_2$ complexes are well known, it was interesting to use our experiment in order to extract some properties and compare them to those reported using XAFS or other techniques.

In Figure 1, we compare the XAFS spectra acquired at Fe K-edge of the sample at room temperature (HS) and after cooling (LS). The Fe-ligand distances obtained after EXAFS analysis are consistent with the significant shortening of the Fe-N(phen) and Fe-N(NCS) distances by about 0.2 Å and 0.1 Å respectively [4] within the octahedra after the thermally-induced spin transition.

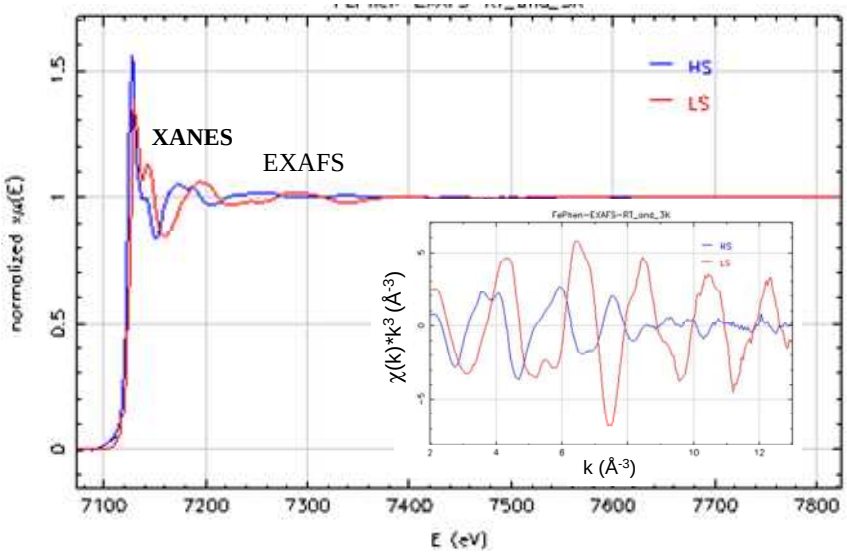

Figure 1: XAFS and k^3-weighted EXAFS spectra of $Fe(Phen)_2(NCS)_2$ before (HS) and after (LS) cooling, at the Fe K-edge

When cooling down the reference sample RT to less than 10 K, we could see clearly changes in the XANES profiles at low temperature, a signature of the thermally-induced ST. The pre-edge peaks labeled P_1, P_2 as well as the profiled near-edge structure A, B, C, D and E, change significantly after HS-LS transition, indicating a different arrangement of the Fe-N octahedra in both states. XANES spectra have been recorded at different temperatures between 10K and RT. This allows us to map out the evolution of the XANES profiles during the thermal ST as shown in Figure 2. The intensity and the position of the XANES features in Fig. 2 are in agreement with those reported earlier [5].

The two XANES scans of pure HS (RT) and pure LS (10K) have been used as standards to simulate the evolution of the percentage of the HS state as a function of the temperature. A weighted linear combination has been used to fit the spectra recorded at different temperatures. The result shown in Fig. 3 is consistent with the abrupt thermal transition reported by using magnetic measurements for the same complex [4]. Moreover, the temperature of ST is found at about 174 K which is in agreement with the reported value of T=176 K.

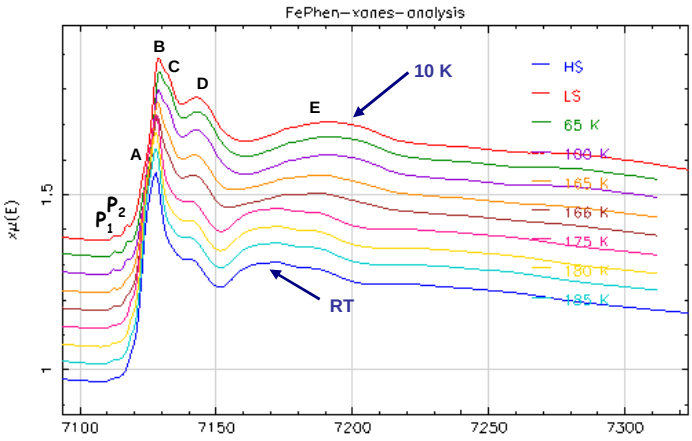

Figure 2: Evolution of the XANES spectra as a function of temperature

In summary, the evolution of XANES spectra with temperature can be used as alternative tool to mimic the behaviour of thermal ST and thus the magnetisation of SCO complexes. This will be helpful in the investigation of the structural changes around Fe during the transition for our own complexes in our next experiments.

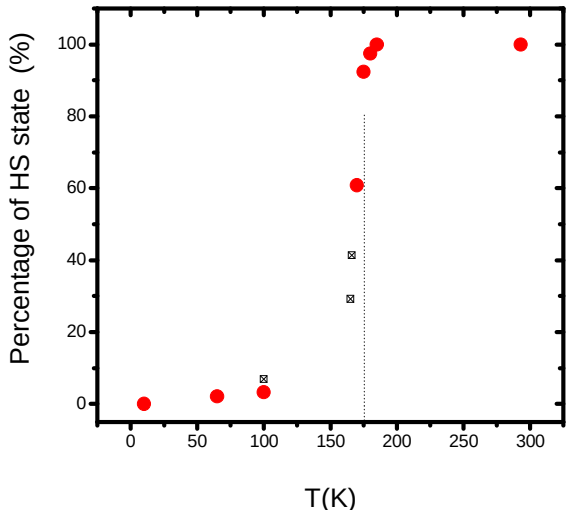

Figure 3: Percentage of HS state $Fe(Phen)_2(NCS)_2$ as a function of temperature after linear recombination analysis of the XANES spectra.

Aknowledgements

The authors thank the beamline staff and Christian Markert, for his kind help and assistance before and during this experiment. This work was funded by the DFG SPP1137 project.

References

[1] R. Chandrasekar, F. Schramm, O. Fuhr, M. Ruben, Eur. J. Inorg. Chem (2008) 2649.
[2] Y. Bodenthin , G. Schwarz, Z. Tomkowicz , A. Nefedov, M. Lommel, H. Möhwald, W. Haase, D. G. Kurth, U.Pietsch Phys.Rev. B76 (2007) 064422.
[3] M. Marchivie, P. Guinneau, J. A. K. Howard, G. Chastanet, J.F. Létard, A. E. Goeta, D. Chasseau, J. Am.Chem.Soc 124 (2002) 194.
[4] B. Gallois, J.A. Real, C. Hauw, J. Zaremblwich, Inorg. Chem. 29 (1990) 1152.
[5] V. Briois, Ch. Cartier dit Moulin, Ph. Sainctavit, Ch. Brouder, A. M. Flank, J. Am. Chem. Soc. 117 (1995) 1019.

Phase separation of bulk amorphous GeO

Ch.J. Sahle[(a),*], C. Sternemann[(a)], A. Hohl[(b)], R. Wagner[(c)], D. Lützenkirchen-Hecht[(c)], A. Herdt[(a,c)], O. Feroughi[(a)], H. Conrad[(a)], and M. Tolan[(a)]

(*a*) Fakultät Physik/DELTA, Technische Universität Dortmund, Maria-Goeppert-Mayer-Str. 2, D-44221 Dortmund, Germany
(*b*) Institute for Materials Science, Darmstadt University of Technology, D-64287 Darmstadt, Germany
(*c*) Fachbereich C - Abteilung Physik, Bergische Universität Wuppertal, Gaußstraße 20, D - 42097 Wuppertal, Germany

* contact: christoph.sahle@tu-dortmund.de

Bulk amorphous germanium monoxide (a-GeO_x, $x \approx 1$) was studied by means of fluorescence yield measurements at the Ge K-edge regarding its temperature-induced phase separation, i.e. the disproportionation of a-GeO into its constituents: $2GeO \rightarrow Ge + GeO_2$.

The study of amorphous germanium/oxygen systems, analogous to amorphous silicon/oxygen systems (a-SiO), has received great attention over the past years due to their notable optical [1] and electronic [2] properties relevant for opto- and microelectronic applications. Because of their high charge storage stability, structures containing germanium nanocrystals are candidates for ultra-fast non-volatile flash memories [3] and exhibit visible and near infrared photoluminescence [4]. Freestanding group IV metalloid nanocrystals have even been proposed as nontoxic diagnostic and therapeutic agents [2]. Furthermore, a-SiO and a-GeO represent the basic composites of $Si_xGe_yO_z$ alloys which are of relevance for light emitting and high speed electronic devices [5].

Measurements of the x-ray absorption near edge structure (XANES) are sensitive to the chemical state of the investigated element. Thus spectra of differently annealed a-GeO samples were taken employing fluorescence yield detection at the materials science beamline BL8 at DELTA. All samples were annealed under nitrogen flow in a quartz glass tube furnace for 30 minutes and characterized by x-ray diffraction measurements at the multi-purpose beamline BL9 at DELTA [6]. Figure 1 shows the normalized spectra at the Ge K-edge. For a quantitative analysis, the spectrum of the native sample was subtracted from the spectra (see figure 2) of the annealed samples. The phase separation parameter $A(T)$ was calculated by the integrated absolute value of these differences in the energy region where the sub-oxide contributions are expected (see shaded area in figures 1 and 2).

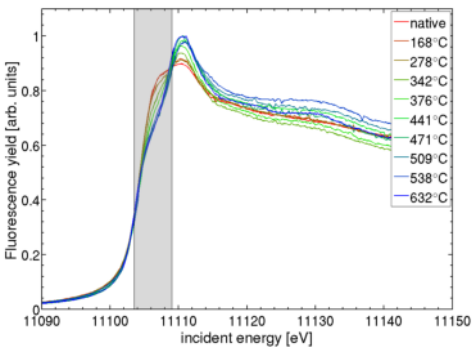

Figure 1: Spectra of differently annealed a-GeO samples. The shaded area represents the energy region of the onset of the sub-oxide contributions to the absorption edge.

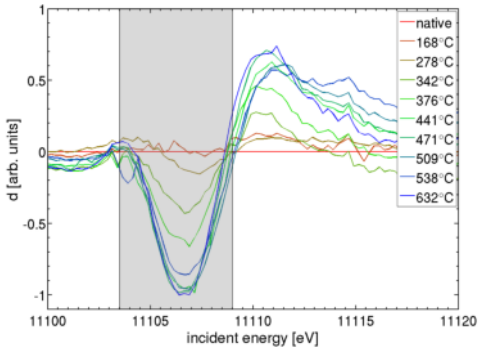

Figure 2: Differences d between the differently annealed a-GeO samples and the native sample.

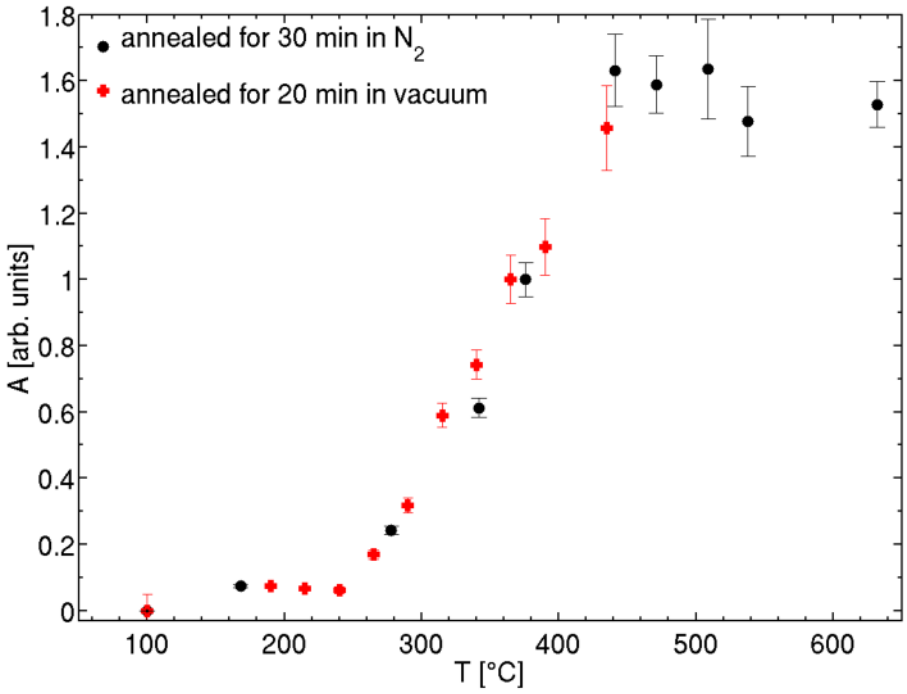

Figure 3: Phase separation parameter $A(T)$ as extracted from the current data and data which were taken earlier at BL9 employing partial fluorescence yield detection [8].

$A(T)$ is a measure of the relative decrease of the sub-oxide content in the samples. Figure 3 shows the phase separation parameter $A(T)$ as extracted from the data compared to results of an earlier experiment performed at beamline BL9 for samples annealed under vacuum conditions [7]. The temperature dependence of $A(T)$ indicates the growth of Ge and GeO_2 clusters at the cost of the sub-oxide contributions. The Temperatures T^{start} and T^{end} of the beginning and end of the phase separation process can be derived to be $T^{\text{start}} = 250 \pm 30$°C and $T^{\text{end}} = 440 \pm 30$ °C. Further measurements at BL8 and BL9 will include a detailed in-situ study of the disproportionation and nanocrystal formation process.

We would like to acknowledge the DELTA machine group for providing synchrotron radiation and technical support.

References

[1] L. Pavesi, L. Dal Negro, C. Mazzoleni, G. Franzo, F. Priolo, Nature **408**, 440 (2008).
[2] E.J. Henderson, C.M. Hessel, J. Am. Chem. Soc. **130**, 3624 (2008).
[3] T.Z. Lu, M. Alexe, R. Scholz, V. Talalaev, R.J. Zhang, M. Zacharias, Appl. Phys. **100**, 014310 (2006).
[4] S.S. Iyer, Y.H. Xie, Science, **260**, 40 (1993).
[5] S. Balakumar, S. Peng, K.M. Hoe, G.Q. Lo, R. Kumar, N. Balasubramanian, D.L. Kwong, Y.L. Foo, S. Tripathy, Appl. Phys. Lett. **90**, 192113 (2007).
[6] See report *Nanocrystal formation in Silicon- and Geermanium monoxide* by O. Feroughi Ch. Sahle, C. Sternemann, A. Hohl, M. Tolan, DELTA user report 2008.
[7] A. Schacht, C. Sternemann, A. Hohl, H. Sternemann, Ch. Sahle, M. Paulus, M. Tolan to be published.

X-ray Diffraction characterization of Metal-Organic Frameworks (MOFs) thin films grown on Functionalized Organic Surfaces

Osama Shekhah, Hui Wang and Christof Wöll[(1)]

[(1)]*Ruhr-Universität Bochum, Lehrstuhl für Physikalische Chemie 1, 44780 Bochum, Germany.*
woell@pc.rub.de

A novel approach for the synthesis and growth of Metal-Organic Open Frameworks (MOFs), based on organic ligands (OL) like benzenetricarboxylic acid (BTC) and inorganic connecters metal ions (ML_x) (like Zn(II) and Cu(II)), on an appropriately functionalized organic surface prepared by self assembly of organothiols on Au has been developed in our group [1]. The approach is based on the sequential immersion of the SAM (self assembled monolayer) covered substrate separately in both of the ML_x and OL solutions.

The synthesis and growth of the HUKST-1 [$Cu_3BTC_2(H_2O)_n$] MOF using this approach on two different types of SAMs a COOH terminated SAM, namely the 16 mercaptohexadecanoic acid ($HS(CH_2)_{15}$-COOH) (**MHDA**) and an OH terminated SAM, namely the 11-Mercapto-1-undecanol ($HS(CH_2)_{11}OH$) (**MUD**), was characterized using different techniques like XPS, IRRAS, NEXAFS, SEM, AFM and XRD (using both a laboratory (Cu Kα) as well as a synchrotron radiation source (DELTA, Dortmund). [1].

a. COOH functionalized SAMs:

HUKST-1 [$Cu_3BTC_2(H_2O)_n$] was synthesised and grown using this approach on (**MHDA**). IRRAS data show a linear increase in the thickness of the deposited MOF with the number of immersion cycles. AFM and SEM data demonstrated the homogenous and selective growth of the MOFs on COOH-terminated surfaces. In the case of Cu(II)-BTC the out-of-plane XRD-data (Fig. 1.c), reveal the presence of a highly ordered and preferentially oriented crystalline material, which exhibits the same structure for the bulk compound of HUKST-1 [1] .

b- (OH) functionalized SAMs

HUKST-1 was also synthesised and grown using this approach on an OH terminated SAM (**MUD**). IRRAS data show a linear increase in the thickness of the deposited MOF with the number of immersion cycles. In the case of Cu(II)-BTC the out-of-plane XRD-data (Fig. 1e), reveal the presence of a highly ordered and crystalline material which has a preferentially different orientation from the COOH terminated SAMs [1].

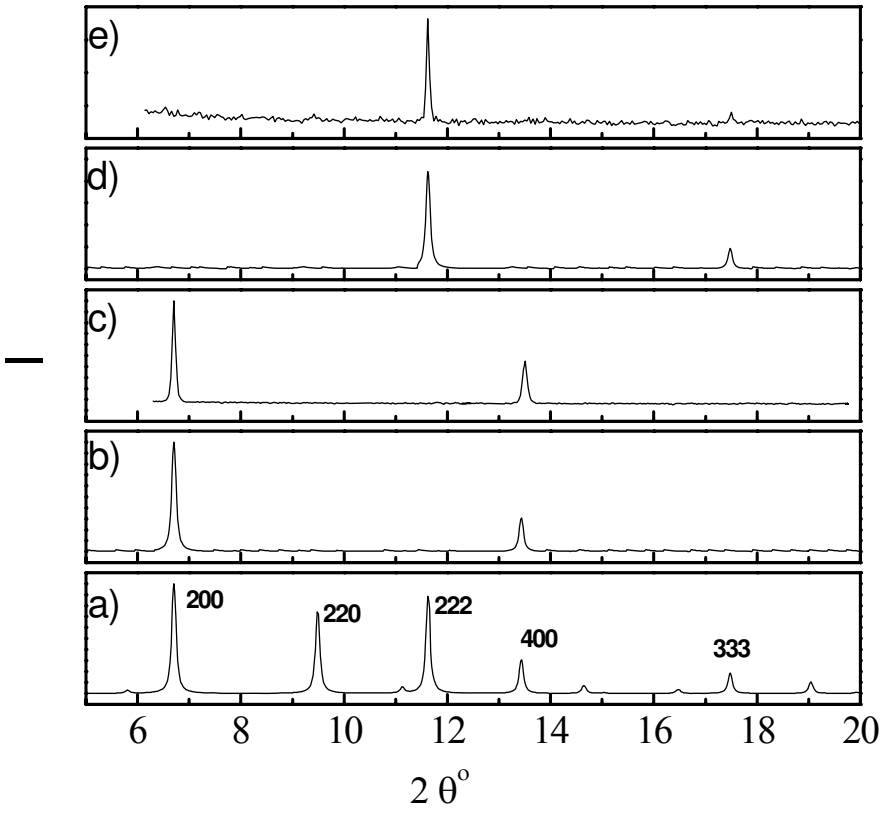

Figure 1. Out-of-plane XRD data for a $Cu_3BTC_2.xH_2O$ MOF a) Bulk, b) growth on a MHDA SAM (Simulation), c) experimental growth on MHDA SAM (experimental), d) growth on MUD SAM (Simulation), e) grown on MUD SAM (experimental).

This new approach will also allow – at least in some cases – to provide insights in the growth mechanism of MOFs. To some extend this new approach is complementary to the growth of MOFs on organic substrates as reported recently for SAMs on Au [2, 3] and on Si [4].

Acknoledgment:

We thank Dr. M. Paulus, Dr. C. Sternemann, F. Eves, F. Wielnad and Prof. M. Tolan for their assistance and support with the XRD measurements at Delta Beamline-09.

References:

1. Shekhah, O., et al., Journal of the American Chemical Society, **2007**. 129(49): 15118.
2. Hermes, S., et al., J. Am. Chem. Soc., **2005**. *127*(40): 13744-13745.
3. Biemmi, E., et al., JACS, **2007**. *129*(26): 8054.
4. Zacher, D., et al., J. Mater. Chem., **2007**. *17*: 2785.

Nanocrystal formation in silicon and germanium monoxide

Omid Feroughi[(a),*], Christoph Sahle[(a)], Christian Sternemann[(a)], Achim Hohl[(b)], and Metin Tolan[(a)]

(a) Fakultät Physik I/DELTA, Technische Universität Dortmund, Maria-Goeppert-Mayer-Str. 2, D-44221 Dortmund, Germany

(b) Institute for Materials Science, Darmstadt University of Technology, D-64287 Darmstadt, Germany

* contact: omid.feroughi@tu-dortmund.de

The study of bulk amorphous silicon monoxide and germanium monoxide (a-SiO_x and a-GeO_x with $x \approx 1$) attracted significant interest over the past years due to their relevance for opto- and micro-electronic applications. Germanium nanocrystals are candidates for non-volatile flash memories [1,2,3] and exhibit visible and near-infrared photoluminescence [4,5,6]. Structures containing Si nanocrystals in an oxide matrix are valuable alternatives to fragile, porous Si on the way towards high-efficient photoluminescence from Si-based materials [7,8]. This is why the synthesis of germanium and silicon nanocrystals has been studied intensively. One of the ways to produce nanocrystals in oxide matrices is to anneal native amorphous monoxides. During temperature treatment native a-SiO (a-GeO) shows a phase separation (disproportionation) in which regions of Si (Ge) and SiO_2 (GeO_2) grow at the cost of the sub–oxides contained in the bulk material resulting in a formation of Si (Ge) nanocrystals [9,10]. Therefore, these systems have attracted great interest as a starting material for the production of photoluminescent structures.

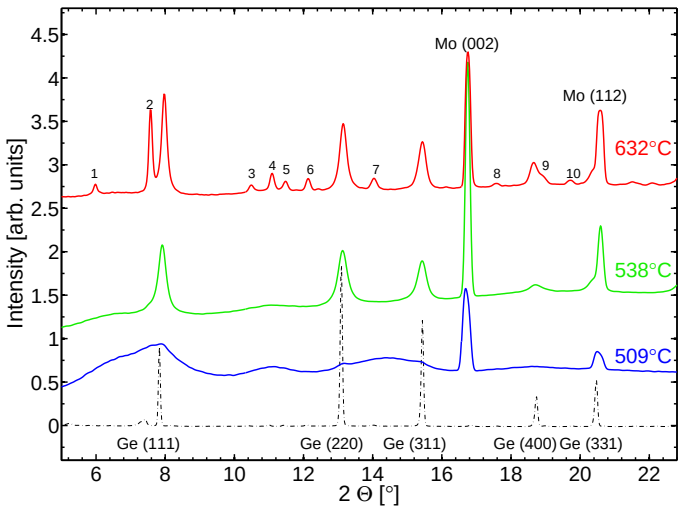

Figure 1: X-ray diffraction pattern of differently annealed GeO samples together with a reference spectrum of crystalline Ge. For the highest annealing temperature also crystalline GeO_2 diffraction peaks can be observed.

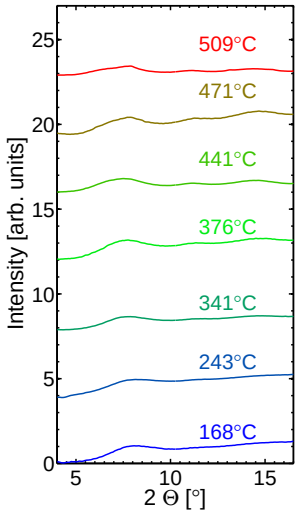

Figure 2: X-ray diffraction pattern for annealed GeO samples are found to be amorphous up to temperatures of 500°C.

In order to characterize the formation process of Ge (Si) nanocrystals in GeO (SiO) x-ray diffraction data of differently annealed native a-GeO (a-SiO) samples were measured at beamline BL 9 of DELTA using the MAR345 image plate detector with an

incident energy of 27 keV. SiO powder samples were measured in transmission and GeO films prepared on molybdenum foils were studied in reflection geometry.

The native a-GeO and a-SiO starting materials were produced at temperatures of about 100 °C and 600 °C, respectively. All samples were heated under N_2 atmosphere for 30 minutes at temperatures between 168 °C (800 °C) and 632 °C (1150 °C) for GeO (SiO). The obtained radially integrated diffraction patterns are presented in Figs. 1,2 (GeO) and Fig. 3 (SiO). From the data the onset temperature for nanocrystal formation (T_c) was estimated and the average size of the observed nanocrystals (d_n) was determined using the Scherrer equation. The corresponding results are summarized in Tab. 1. The samples studied in this experiment will be charactarized further using different x-ray techniques such as x-ray absorption and x-ray Raman scattering to obtain a detailed understanding of the disproportionation and nanocrystal formation process in these materials.

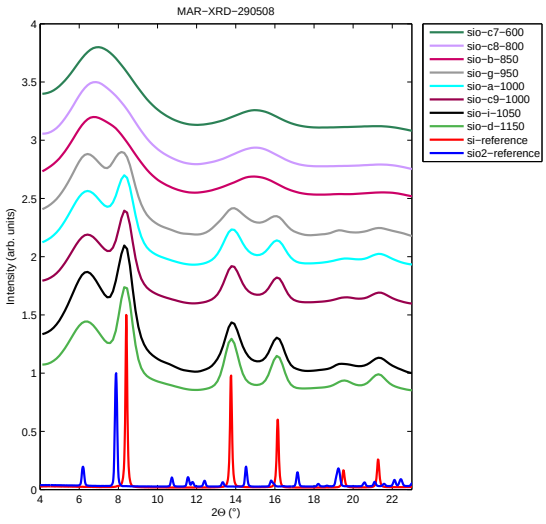

Figure 3: X-ray diffraction data of annealed SiO samples together with a Si and SiO_2 reference spectrum. Crystallization of Si occurs around 950 °C.

monoxide	T_c [°C]	d_n [nm]
SiO	900 ± 50	3.3 ± 0.5 (annealed at 950°C)
GeO	510 ± 40	13.5 ± 2.5 (annealed at 538°C)

Table 1: Crystallization temperatures and average size of the Si (Ge) nanocrystals in annealed SiO (GeO).

We would like to acknowledge the DELTA machine group for providing synchrotron radiation.

References

[1] Y. Batra, D. Kabiraj, S. Kumar, and Kanjilal, J. Phys. D: Appl. Phys. **40**, 4568 (2007).
[2] V. Beyer, J von Borany, M. Klimenkov, J. Appl. Phys. **101**, 094507 (2007).
[3] M. Y. Chan, P. S. Le, V. Ho, H. Ö. Seng, J. Appl. Phys. **102**, 094307 (2007).
[4] Y. Maeda, N. Tsukamoto, Yazawa, Y. Kanemitsu, and Y. Masumoto, Appl. Phys. Lett. **59**, 3168 (1991).
[5] M. Zacharias and P.M. Fauchet, Appl. Phys. Lett. **71**, 380 (1997).
[6] W. Wang, K. Wang, D. Han, B. Poudel, X. Wang, D.Z. Wang, B. Zeng, Z. F. Ren, Nanotechnology **130**, 075707 (2007).
[7] L. Pavesi, L. Dal Negro, C. Mazzoleni, G. Franzo, and F. Priolo, Nature **408**, 40 (2000).
[8] A. Zimina. S. Eisebitt, W. Eberhardt, J. Heitmann, and M. Zacharias, Appl. Phys. Lett. **88**, 163103 (2000).
[9] See report *Phase separation of bulk amorphous GeO* by Ch. J. Sahle, C. Sternemann, A. Hohl, R. Wagner, D. Lützenkirchen-Hecht, A. Herdt, O. Feroughi, H. Conrad, and M. Tolan, DELTA user report 2008.
[10] H. Sternemann, C. Sternemann, A. Hohl, G. T. Seidler, T. T. Fister, and M. Tolan, submitted.

Residual Stresses Analysis in Cobalt-Diamond Composites

H.-A. Crostack, U. Selvadurai-Laßl

[1]Lehrstuhl für Qualitätswesen; Universität Dortmund, Joseph-von-Fraunhofer Str. 20, 44227 Dortmund, Germany

Cobalt-diamond composites are suitable as cutting tools due to their mechanical and physical properties. During the sintering of diamond particle reinforced cobalt composites thermally induced residual stresses can be initiated due to the mismatch of thermal expansion coefficients. Unfavourable residual stresses reduce the lifetime of cutting tools made of such composites. In this work, the distribution of residual stress in the cobalt matrix of vacuum sintered composite was studied near single diamonds and in a matrix region without any influence of a diamond. This study (contained investigations on samples after sintering and after additional thermal treatment in order to improve) improves the knowledge about the correlation between manufacturing parameters and residual stresses [1,2].

The residual stresses in the cobalt matrix of composites were analysed by means of X-ray diffraction and the $d/\sin^2\psi$-method [3] using synchrotron radiation at beamline B9 of DELTA at TU Dortmund, Germany. The high brilliance and intensity of synchrotron radiation allow to reduce the size of measuring field for local residual stress values to areas of 2 and 1 mm^2. An energy of 7500 eV (Ni-K_α radiation,λ= 0.16532 nm) was chosen. By means of this radiation the cubic (222) and (113) reflections were analysed. In some samples the (113) reflection is overlapped partially by a smaller hexagonal (112) reflection of cobalt and was analyzed also. According to the $d/\sin^2\psi$ method these reflections were analysed under 2θ-θ conditions and at different ψ –angles. (This ψ-angle is an angle between the normal of the sample surface and the normal of the lattice plane.) It can be chosen by changing the angles χ or an ω offset. The stress induced deformation of the lattice result in an reflection shift. In a linear case a plot of the measured d-values or the lattice distortions against $\sin^2\psi$ result in a line. The slope of a regression function of this line correlates with the residual stress. The correlation factors are the X-ray elastic constants. Because the X-ray elastic constants of sintered cobalt are unknown the approximated values were calculated by the Young´s modulus of 208 GPa and Poisson constant of 0.32 according to the Voigt method [4]. The error of the stress values is calculated by the standard deviation from the slope of the straight line.

It was known from previous studies that compressive residual stresses exist in sintered pure cobalt. These stresses are due to inhomogeneous sintering and can be reduced by the incorporating of diamond particles [2]. To understand this effect, local residual stresses were analysed on composites samples, which were manufactured by vacuum sintering at 1100 °C or 1200 °C [2]. The samples have a disc form with a diameter of 12-15 mm. The particle size of cobalt powder was between 1 and 40 µm whereas the size of diamond particles ranged from 300 - 450 µm. Only a few number of diamond particles were incorporated in this composite in order to find isolated diamonds for the local measurements. Various masks made of Pb with different apertures (quadratic and circular with areas of 2 mm^2 and 1 mm^2 and diameters of 2 mm and 1 mm, respectively) were used to define areas of different sizes and positions for local measurements. These masks were fixed onto the surface of the sample at isolated diamonds and far away from a diamond. By this way the irradiated matrix area chances and the measurements provides information on the residual stress at the distances 0.5, 1 and 5 mm to the diamond. Here the stresses were analysed during rotating the sample in ψ- mode [5].

In Fig. 1, the local stresses measured with round masks is shown as function of the distance to diamond for a sintered composite (sample 51) and three samples (32, 58, 26) thermally treated at 450 °C.

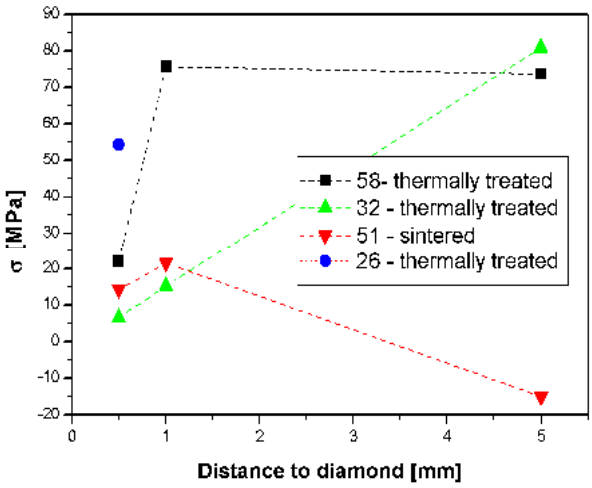

Fig. 1: Local residual stress of cobalt matrix near a diamond

Sample 51 sintered without any thermal treatment shows the typical stress state of pure cobalt matrix at a distance of 5 mm: compressive stresses due to inhomogeneous density. Tensile stresses were found in the direct neighbourhood of a diamond (0.5 – 1 mm). That means, in this area the effect of mismatch of TEC on residual stress is strong enough to exceed compressive stresses in pure cobalt.
In contrast to the sample 51 the thermal treatments of the samples 26, 32 and 58 lead to a change from compressive to tensile stress far from the diamond.
But local stresses near the diamond is unchanged.

An analysis by X-ray tomography revealed that the diamond in sample 58 was 1 mm below the sample surface. Therefore the real distance to the diamond is higher than 1 mm and the stress value is similar to the one at 5 mm distance.

As found before the stress state of composite samples depends on sintering temperatures, also [5]. The stress near the diamond in sample 26 sintered at 1200 °C is higher than in the samples 32, 51 and 58 sintered at 1100 °C. This difference is not influenced by the thermal treatment.

Additionally the stresses were measured by shifts of the cubic (311) and hexagonal (112) reflection in radial and tangential directions in ψ- and ω-mode. This reflections were chosen because their theoretical intensity is much higher than the very small cubic (222) and hexagonal (004) reflections. But the (311)+(112) reflections overlap partially. We analysed this reflection group after sintering and after additional thermal treatment at 450 °C. Due to the high overlapping state and the strong texture of hexagonal phase the position of both reflections could not separated yet. But first reflection profile analysis give hints for higher stresses in the hexagonal than in the cubic phase of cobalt. After this thermal treatment the hexagonal reflection intensity decrease strongly and point at a phase transformation. For that reason the cubic phase of cobalt should to be analysed in future, exclusively.

This work was supported by the German Research Foundation (DFG) in the scope of the research project Cr 4/110 which is gratefully acknowledged.

References

[1] H.-A. Crostack, U. Selvadurai-Laßl: Residual Stresses in Cobalt-Diamond Composites. HASYLAB-Jahresbericht 2005

[2] H.-A. Crostack, U. Selvadurai-Laßl, W. Tillmann, M. Gathen, C. Krohnholz, T. Wroblewski, A. Rothkirch: Residual stresses in sintered diamond-cobalt composites". ECRS7, Berlin, 13.-15. September 2006, Material Science Forum Vols. 524-525 (2006) pp. 787-792

[3] V. Hauk and E. Macherauch (Hrsg.): Eigenspannungen und Lastspannungen (HTM Beiheft), Carl Hanser Verlag München, Wien (1982)
[4] W. Voigt: Lehrbuch der Kristallphysik, Leipzig, B.G. Teuber Verlag (1928)
[5] H.-A. Crostack, U. Selvadurai-Laßl, G. Fischer, A. Rothkirch: Local residual stresses in sintered diamond–cobalt composites. MECASENS IV, Vienna, 24.-26. September 2007, submitted

X-ray investigation of CdSe/CdS and CdSe/CdS-ZnS core-shell nanorods

Özgül Kurtulus[1,2] and Ullrich Pietsch[1]
[1]Fachbereich Physik, Festkörperphysik, Universität Siegen
[2]Dogus University, Istanbul, Turkey

Improving the performance of nanodevices can be done by effective surface passivation. The best passivation to date is the creation of core-shell heterostructures. In order to protect the electronic performance, both core and shell materials have to have the lowest lattice mismatch as much as possible. For II-VI semiconductor nanomaterial systems, CdSe/CdS, CdSe/ZnS, and CdSe/ZnSe core-shell structures are under investigation up to now [1]. CdSe/CdS and CdSe-CdS/ZnS core-shell nanorods (NR) have been prepared by solution-liquid-solid (SLS) approach [2]. X-ray investigations were performed in ROBL beam line at ESRF and BL9 at DELTA. Filled into a capillary, the NRs are randomly oriented and each of them exhibit the admixture of wurtzite and zinc blende structure separated by stacking faults which is common in CdSe nanomaterials. The aim of this work consists of the determination of aspect ratios and the strain acting parallel and perpendicular with respect to NR axis by using x-ray diffraction.

CdSe nanowires have been prepared by solution-liquid-solid (SLS) approach in which three types of Bi nanocatalysts stabilized with oleylamine, l-hexadecylamine and trioctylphosphine are used. Briefly, a mixture of CdO, TOPO and octanoic acid (oleic acid) was loaded into a flask. The mixture was dried and degassed under vacuum. Then the flask was filled with Ar and the temperature was increased to 330°C. Afterwards a mixture of Bi nanoparticles and TOPSe was injected. When the temperature was decreased to 80°C, toluene was added to the solution. Then butanol was added to precipitate the nanowires. The dark-brown precipitate was washed with toluene/butanol [2]. When both CdS and ZnS are added for shell growth, CdS is preferentially grown first to reduce the interfacial energy since its lattice mismatch with CdSe is less than that of ZnS.

Due to the random orientation of NRs, we performed X-ray powder diffraction. The X-ray diffraction measurements have been done in ROBL beam line at ESRF and BL9 at DELTA. The energy of the beam used is 8.3keV and 11-15keV, respectively. During the experiments either an image plate or a point detector was used. Using the image plate a ring like scattering pattern was found which was radial averaged using Fit2D software. The angular values and the background of raw data have been calibrated with respect to the distance and beam centre position in x and y coordinates, using silicon powder as a reference material.
Fig.1 shows the scattering pattern taken from pure CdSe (b) and from CdSe/CdS-ZnS core-shell NW fractions (c). By comparision we can make the following conclusions:

- The X-ray diffraction pattern of CdSe/CdS-ZnS shows broad peaks which are in accordance with wurtzite crystal structure of CdSe suggesting that the diffraction is predominantly due to the CdSe core [3].
- The (002) peak is much stronger and narrower than the other peaks for both nanowires, indicating that both were elongated along the c-axis and the shape was well preserved in the conversion reaction.
- The reflection peaks of the core-shell NRs are shifted only little with respect to the peak positions found for pure CdSe.
- The FWHM of the peaks get narrower for the core-shell NRs. Using these values, according to Scherrer formula, the lengths along the growth direction are changing

between 160A° and 240A° for both of the NRs while the diameters are determined between 50A° and 80A° for pure CdSe NRs and 60A° and 150A° for core-shell NWs.

The data will be evaluated in terms of stacking faults density and strain applied along and perpendicular the c-axis of NWs using the procedure presented in [4].

We would like to thank all the BL9 beamline staff at DELTA for their help during the measurements.

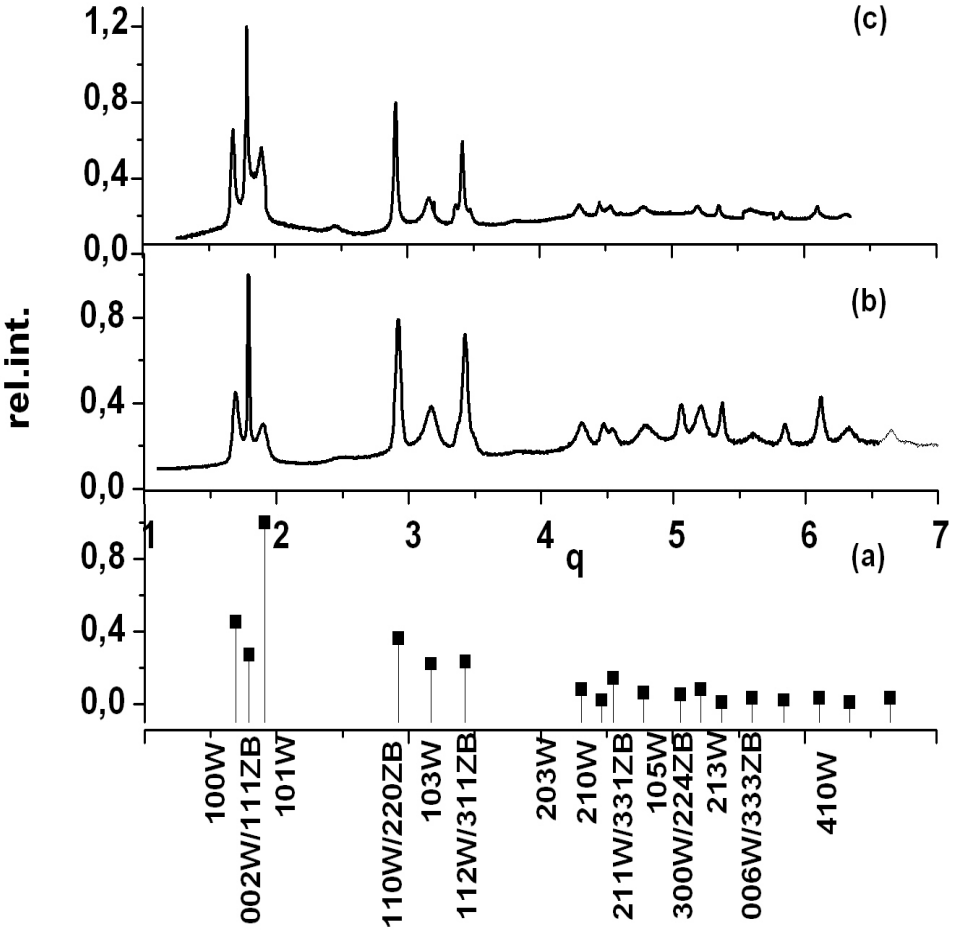

Fig. 1. The diffraction diagram of (b)CdSe, (c)CdSe/CdS-ZnS core-shell NW fractions while (a) is showing the relative intensities of a pure wurtzite CdSe NW. Each peak is indexed by Miller indices of either wurtzite and/or zinc-blende structure.

References:

1. S.Kar et al., Journal of Physical Chemistry C ***112***, 4036 (2008)
2. Z.Li et al., submitted
3. L.Manna et al., J.Am.Chem.Soc. ***122***, 12700 (2000)
4. O.Kurtulus et al. phys.stat.sol.(c) 2008, submitted

Characterizing the Structure and Kinetics of Protein Adsorbates by X-Ray Reflectivity at DELTA beamline BL 9

Florian Evers,* Kaveh Shokuie, Michael Paulus, Christian Sternemann, and Metin Tolan
Fakultät Physik / DELTA, TU Dortmund, Maria-Goeppert-Mayer-Str. 2, 44221 Dortmund

Claus Czeslik
Fakultät Chemie, TU Dortmund, Otto-Hahn-Str. 6, 44221 Dortmund

We demonstrate that the X-ray reflectivity set-up of DELTA beamline BL9 using 27 keV X-rays is well-suited for the study of organic thin films at buried solid-liquid interfaces. Thus, the structure and the time-evolution of biological systems can be investigated with highest accuracy in a previously inaccessible manner. The power of this technique will be discussed in the context of recent experiments: the adsorption of lysozyme at the hydrophilic silica-water interface and the adsorption of BSA at the hydrophobic polystyrene-water interface.

1. INTRODUCTION

Protein adsorption onto solid surfaces often plays the central role in a wide variety of processes occurring in medicine, biochemistry, biotechnology and daily life [1]. That is why protein adsorption has been widely studied by various techniques, such as ellipsometry or optical reflectometry. However, in order to understand the mechanisms of protein adsorption in detail, it is decisive to probe the interfacial structure of adsorbed protein layers in situ with angstrom resolution. We have recently shown that the X-ray reflectivity (XRR) technique is capable of exploring the interfacial structure of protein adsorbates on atomic length scales and the kinetics of protein adsorption with a time resolution on the order of minutes [2–4]. The potential of XRR will be illustrated by recent studies on the adsorption of lysozyme at the hydrophilic silica-water interface and on the adsorption of BSA at the hydrophobic polystyrene-water interface.

2. HOW TO ACCESS SOLID-LIQUID INTERFACES BY X-RAY REFLECTIVITY

A detailed overview of the XRR technique is presented in [5]. XRR provides information about the laterally averaged electron density profile perpendicular to the sample surface from which layer thicknesses and roughnesses can be obtained. Reflectivity measurements are predominantly sensitive to electron density differences, and, consequently, the investigation of solid-liquid interfaces of low contrast, e.g., as present in biological systems under natural conditions, exhibits a great challenge.

The high energy reflectivity set-up of DELTA beamline BL9 [4] is well-suited for the characterization of buried interfaces. For this purpose, a photon energy of

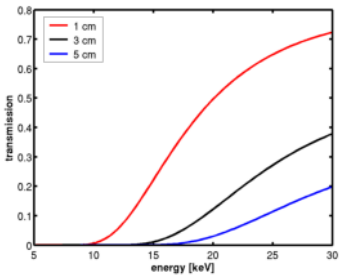

FIG. 1: Transmission through liquid H_2O as a function of photon energy [8]. In our study, the x-ray beam has to penetrate about 3 cm of water through the sample chamber.

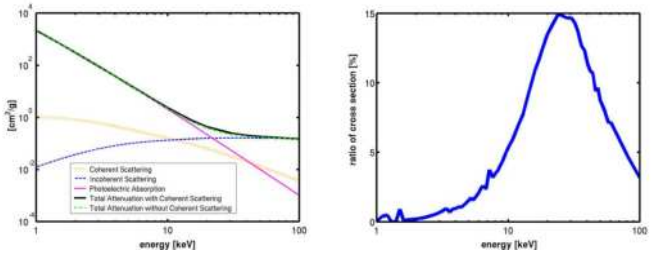

FIG. 2: (Left) X-Ray interaction cross section of carbon as a function of energy [7]. (Right) Assuming that scattering from biological thin films at solid-liquid interfaces is dominated by C and H_2O, the according ratio of coherent and incoherent cross sections is shown as a function of energy [7].

$E = 27$ keV is used. This photon energy has been chosen because of several reasons [6]: First of all, the transmission through the water filled sample cell should be high, cf. Fig. 1. Second, incoherent scattering processes cause beam damage. This is a serious issue in the context of biomolecules, and, hence, beam damage should be minimal. Third, the diffraction signal from the interface which is given by the coherent cross section should be high. It can be deduced from Fig. 2 that the investigation of organic materials is favoured by X-ray energies in the regime between 20 keV and 30 keV.

*Electronic address: florian.evers@tu-dortmund.de

The proteins were dissolved in 10 mM buffer solutions with a protein concentration of 0.1 mg/mL. Silicon wafers were cut into small pieces and cleaned with piranha solution. For details of the preparation, we refer to [2, 3].

3. THE ADSORPTION OF LYSOZYME AT THE HYDROPHILIC SILICA-WATER INTERFACE

XRR data on the effect of pH on the adsorption of lysozyme have been presented at the 3rd DELTA user meeting [9]. By analyzing these data, we have proposed a model for the influence of the pH value on the adsorption behavior of lysozyme onto hydrophilic silica as schematically shown in Fig. 3 [2]. According to this structural model, the lysozyme layers for pH 4 and pH 7 both consist of lysozyme molecules with their long axis parallel to the surface (side-on), but they differ in their packing density. The protein layer adsorbed at pH 11 comprises lysozyme molecules oriented with their long axis parallel (side-on) and normal (end-on) to the surface.

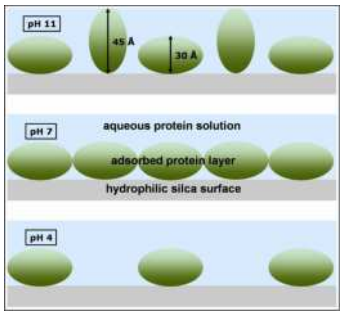

FIG. 3: Simple model for the adsorption of lysozyme at the silica-water interface [2].

XRR is able to measure the kinetics of protein adsorption on timescales of minutes, while other methods are not able to access these timescales for nm-thick films. For the time-dependent XRR scans [9], it is suggested that the time-evolution of the adsorbed layer might be interpreted as a structural reorganization which affects the protein layer by increasing its roughness [2].

4. THE ADSORPTION OF BSA AT THE HYDROPHOBIC POLYSTYRENE-WATER INTERFACE

XRR data on the adsorption of BSA at the hydrophobic polystyrene-water interface and corresponding electron density profiles are shown in Fig. 4 [3]. In the presence of 1 M NaCl, the Kiessig fringes become more pronounced. Although this might partially be due to a slightly different density of the PS layer, the drastic effect of salt on the protein layer is shown in the inset in Fig. 4. Accordingly, the adsorbed amount is drastically enhanced. An enhanced adsorption at a hydrophobic surface in the presence of salts underpins that the hydrophobic effect acts as the dominating driving force for protein adsorption in this case.

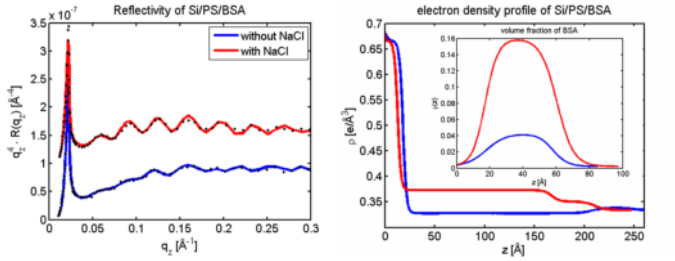

FIG. 4: (Left) XRR data (dotted) and refinements (solid lines) for the adsorption of BSA at the hydrophobic polystyrene-water interface in the presence and absence of NaCl (1 mM) [3]. (Right) Corresponding electron density profiles [3]. To visualize details of the adsorbed layers, the volume fraction profiles are displayed in the inset.

5. CONCLUSION

Our recent studies on the adsorption of lysozyme at the hydrophilic silica-water interface and the adsorption of BSA at the hydrophobic polystyrene-water interface show that detailed density profiles of protein adsorbates at solid-liquid interfaces can be obtained by XRR. Thus, valuable insights on protein-surface interactions are gained. By means of time-resolved XRR, the kinetics of the adsorption process and the structure of the adsorbed layer can be studied simultaneously. High energy XRR is able to investigate buried solid-liquid interfaces with an accuracy in the angstrom regime, which is of particular interest probing interfacial aspects of manifold biophysical systems, e.g. model membrane systems.

We woud like to thank the DELTA machine group for providing synchrotron radiation and technical support.

[1] C. Czeslik, Z. Phys. Chem. **218** (2004) 771.
[2] F. Evers et al., Langmuir **24** (2008) 10216.
[3] F. Evers et al., Eur. Phys. J. S.T., submitted.
[4] M. Paulus et al., J. Syn. Rad. **15** (2008), DOI:10.1107/S0909049508026745.
[5] M. Tolan, *X-Ray Scattering from Soft Matter Thin Films*, (Springer, Berlin 1999).
[6] C. Reich et al., Rev. Sci. Instr. **76** (2005) 095103.
[7] M. J. Berger et al., Photon Cross Sections Database XCOM , NIST.
[8] B. L. Henke et al., At. D. Nucl. Data Tab. **54** (1993) 181.
[9] F. Evers et al., 3rd DELTA user meeting (2007).

Phase Behavior Characterization of Monomer-Clay Dispersions by X-ray Scattering Method.

Nadeem Javid [1], Neil Bradley[2], Jan Sefcik [1], John Liggat [2], Richard Perthrick [2]
[1] Department of Chemical and Process engineering
[2] Department of Pure and Applied Chemistry, University of Strathclyde, Glasgow,United Kingdom.

Polymer nanocomposites is a multicomponent system in which the major constituent is a polymer or blend and the minor constituent has at least one dimension below 100 nm[1]. Polymer-clay nanocomposites (PNCs) are formed through the union of two very different materials with organic (monomer or its polymer) and mineral (clay particle) pedigree [2]. The organic material like monomer of the polymer is intercalated in the interlayer space of the clay and *in situ* polymerized or the polymer itself is intercalated within interlayer spaces of the clay directly through heating the mixture. Exfoliated PNCs are synthesized by homogenously dispersing the clay platelets in the polymerizable monomeric solvent following the *in-situ* polymerization which yields huge interfacial area between polymer and clay [3] giving enhanced properties materials.

Polymer-clay nano-composites, synthesized chemically by dispersing functionalized and naturally occurring inorganic clays in organic polymers have the potential to rival the highly advanced natural materials and have prospect of the morphologically controlled high-performance new materials with value added functionalities. Polymer-clay nano-composites exhibit enhanced properties, such as gas impermeability, flame retardance and exceptional mechanical properties [4] (i.e. tensile strength and Young's modulus giving high stiffness ultrastrong materials), relative to unmodified polymers due to nanoscopic spatial and orientational distribution of the suitably modified clay particles. Consequently, these materials have found application in food and drink packaging, construction, automotives and aerospace and hence could potentially have much wider application considering the range of plastics in use today (e.g. plastic films, membranes and components). The knowledge of phase behaviour (isotropic, nematic or columnar) is essential to control and achieve these enhances properties.

Different types of laponite and cloisite (montmorillonite) clays (Laponite RDS, Laponite RD, Laponite RD with CTAB modification, Laponite RD modified with hydrogenated tallow, Cloisite 6A, Cloisite 15A, Cloisite 20A, Cloisite 10A and Cloisite 30B were used to prepare exfoliated suspensions by using ultrasonication-Stirring procedure. Styrene is used as solvent with and without help of cationic surfactants and stabilizers. Cetyltrimethyl ammonium bromide (CTAB) with concentration used are 0.2 and 0.4 wt % was used as surfactant and Isobutylene based stabilizers SAP was used with added concentration 0.5 wt %.

The small angle scattering data was collected at the beamline Bl9 at DELTA.

[1] K. I. Winey and R. A. Vaia, *MRS BULLETIN* (2007) **32**, 314-322
[2] T. J. Pinnavaia and G.W. Beall, *Polymer-clay nanocomposites* (2000), John Wiley & Sons Ltd.
[3] X. Fu and S. Qutubuddin, *Polymer* (2001), **42**, 807-813.
[4] Paul Podsiadlo and *et al*, *Science* (2007), **318**, 80-83.

Representative Results

Laponite (organically modified) with CTAB and SAP

For a thin disc, the form factor is described as[5],

$$I(Q) = (\Delta\rho)^2 v_p^2 \int_0^{\pi/2} \left\{ \frac{\sin[QH\cos(\beta)]}{QH\cos(\beta)} \right\}^2 \left\{ \frac{2J1[Qr\sin(\beta)]}{QR\sin(\beta)} \right\}^2 \sin(\beta)\, d\beta \qquad (1)$$

The form factor was calculated for different values of R and H (Fig. 1) and the best fit yielded the R about 9 nm and H about 0.9 nm corresponding to diameter of 18 nm and thickness about 1.8 nm. The clay laponite is modified with quaternary ammonium cation having one long chain tallow group which increases the thickness of the clay disc from 1 nm (single disc thickness) to approximately 1.8 nm . The degree of exfoliation was checked by calculation of the slope of the scattering intensity which shows that scattering intensity follows power law Q^{-2} behavior. As discussed above the single clay disc shows this power law Q^{-2} behavior and the absence of any pseudo-bragg's peak in higher Q-region indicates that the clay platelets are fully oxfoliated or delaminated. The size parameters evaluated estimated the diameter of about 18 nm and thickness of 1.9 nm. All of these results indicate that the laponite 1 wt % suspension is isotropic in nature and have maximum exfoliation.

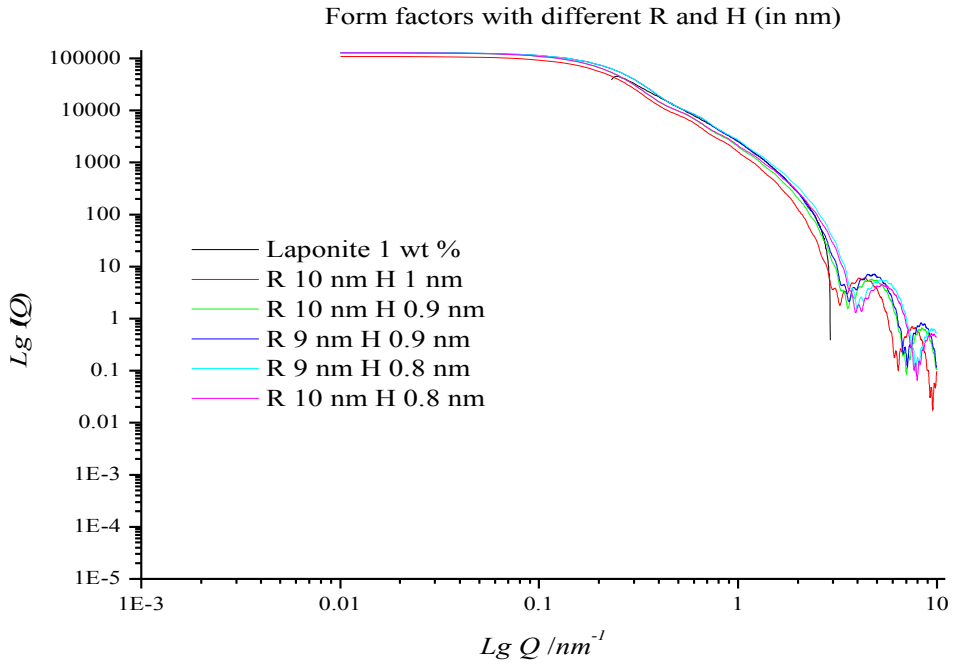

Figure 1: Calculation of form factor of a single thin disc for different values of R and H with experimental data of Laponite 1 wt % in the presence of CTAB and SAP.

[5] O. Glatter, Small angle X-ray Scattering, *Academic*, Newyork, (1982)

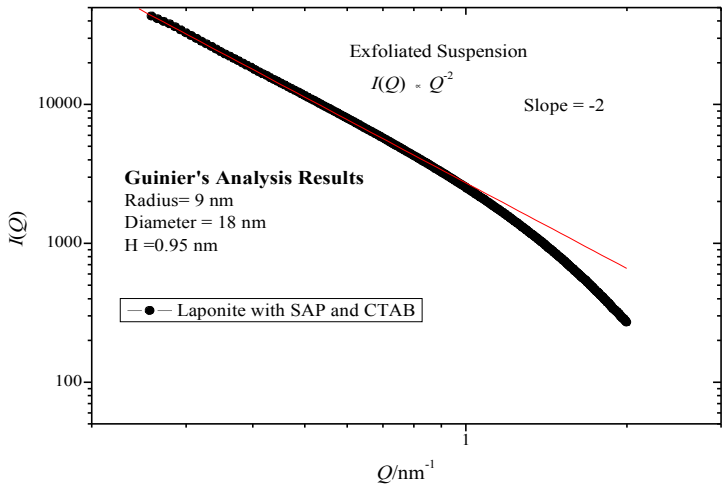

Figure 2: Slope calculation for 1 wt % Laponite solution in the presence of CTAB and SAP.

The plot of $I(Q)$ vs Q from SAXS data has a Q^{-2} power law dependency at very small Q values only, which indicates that clay is isotropically distributed and has some extent of exfoliation, as with the 1% (wt) dispersion. However in this sample there is a peak due to stacking, which can be attributed to the possibility of CTAB causing the formation of adducts with laponite. The basal spacing ('*d*'-spacing) for these stacks or adduct is of about 26 Å.

Laponite RD (non-modified) in styrene with CTAB

The data from SAXS for 1% and 2% both show stacking, possibly as a result of a CTAB-laponite adduct. In both plots there is a small height peak at Q 1.2 nm^{-1} and large peak at Q 2.4 nm^{-1}.The basal spacing ('*d*'-spacing) for these stacks or adduct is of about 26 Å. The very small peak at Q-value approximately at 1.2 nm^{-1} also shows basal spacing of about 26 Å. The relative peak positions are at ratio of 1:2 of Q-values which is indication of stacking in the form of a lamellar structure. These results favour the presence of aggregation and clusters within the dispersion.

Laponite (organically modified) in styrene

The scattering pattern from Laponite I wt % in styrene follows the power law behavior of Q^{-2} which is indication of exfoliation of the sample. The guinier's analysis gives the diameter of about 18 nm and thickness was calculated about 2.2 nm. Laponite suspension in styrene was not stable and separates into layers with time. The same concentration laponite suspension in the presence of CTAB and SAP is stable and does not separate into two layers with time, hence the isobutylene based stabilizer SAP in presence of surfactant CTAB helps to exfoliate the sample and increases the stability of system to stay suspended. In case of laponite 2 wt %, the intensity follows the Q^{-2} power law behavior in very small range of Q but shows a hump in Q value of 1.2 nm corresponding to stacking with basal spacing of 26-28 Å. These results are indication of isotropic phase

with maximum exfoliation in case of 1 wt % and some stacked structures for 2 wt % concentration but still in isotropic phase.

Cloisite 6a in styrene

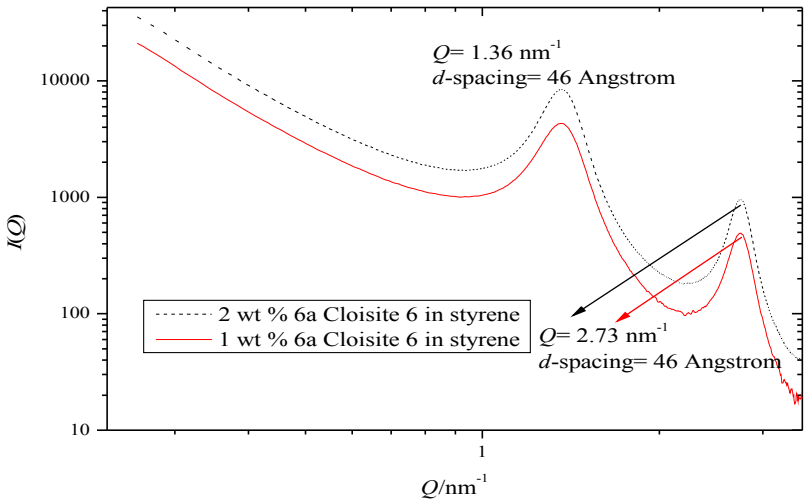

Figure 3: Comparison of background subtracted scattering intensity of Cloisite 6a suspension in styrene.

Cloisite 6a dispersed in styrene for concentrations of 1 and 2 wt % show two pseudo-Bragg's peaks and the relative peak positions are in 1:2 ratio which is indication of lamellar stacked structure with *d*-spacing of about 46 Å. These lamellar structures are formed by tactoids (repeating units in stack) having layers of individual clay discs. The X-ray diffraction *d*-spacing (001) is around 35.7 Å. It means that the clay stacks are now swollen structures and solvated by styrene molecule due to the presence of organic modification on the clay discs. All other measurements are shown in Fig 4 and 5 showing isotropic or stacking behaviour. None of these suspensions showed nematic phase possibly due to lower concentrations.

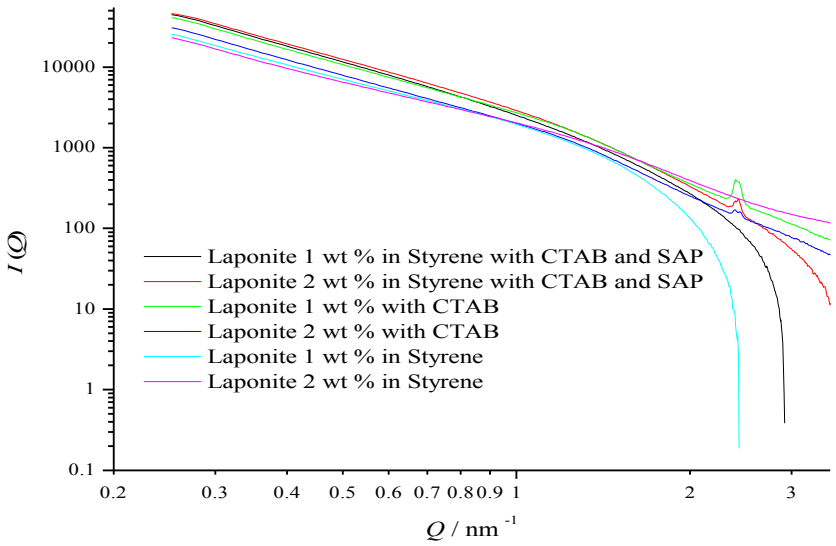

Figure 4: Background subtracted scattering intensity curves of Laponite samples with and without CTAB and SAP.

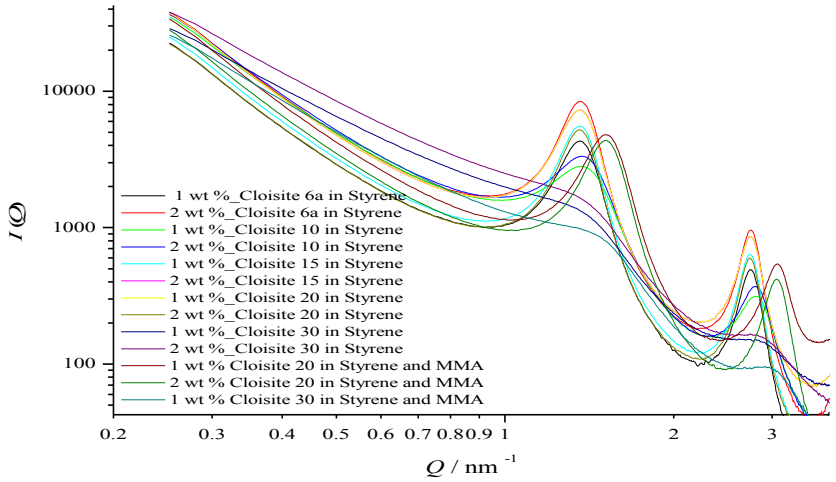

Figure 5: Background subtracted scattering intensity curves of differently modified Cloisite in styrene and MMA

Further studies are required to achieve the phase diagram of nano-clay suspensions, especially in lower Q-range from approximately 0.01 nm^{-1} to 4 nm^{-1} and with higher concentrations and at high temperatures.

Structural properties of CoFeB/MgO multilayers

M. Vadalà, K. Zhernenkov, B.P. Toperverg, H. Zabel
Department of Physics and Astronomy, Ruhr-Universität Bochum
44780 Bochum, Germany

H. Kubota, S. Yuasa
National Institute of Advanced Industrial Science and Technology (AIST)

In recent years there has been a great deal of interest in using magnetic tunnel junctions (MTJs), which can achieve high tunnel magnetoresistance (TMR) ratios [1,2] for use in devices and sensors such as in non-volatile magnetic random access memories and magnetic read heads of hard disk drives. The selection of materials used in a MTJ stack needs to be targeted at technological applications, usually requiring low switching fields, low saturation fields, and low device resistances.
Originally, most studies were devoted to MTJs with amorphous aluminium oxide barriers, yielding TMR ratios of 50-70%. Currently, the international focus of the scientific community in MTJ research is on CoFeB/MgO junctions, which in their amorphous state have the advantage to be homogenous at small scales, as required for high density recording media. As the CoFeB layers are amorphous during sputtering deposition and the MgO are supposed to be in a fine grain polycrystalline state after growth, annealing up to 360°C has been proven to be a necessary prerequisite for reaching the high TMR values reported in the literature. During annealing it is assumed that MgO acts as a seed for the recrystallization of the amorphous CoFeB layers, while the B concentration of up to 20% somehow redistributes or escapes the sample.

The AIST laboratory (S. Yuasa, Japan) has prepared a number of CoFeB/MgO multilayers for our investigations, following exactly the same procedure used to fabricate their standard MTJs, which presently hold the world record for the highest TMR.
We performed specular and off-specular X-ray reflectivity scans in order to achieve information about the multilayer periods, thickness fluctuations and interface roughness. The measurements were performed at the BL9 at a fixed X-ray energy of 11 keV [3].
The samples investigated have the following design: Si/SiO2/ [CoFeB(3 nm) / MgO (2 nm)]n / Ru 8 nm, (n=5 and 10). We proposed to have a maximum of 10 bilayers to prevent the roughening of the interfaces along the multilayer stacks.

In **Fig.1** we plot X-ray reflectivity curves for the multilayers $[CoFeB/MgO]_n$ annealed at T = 360°C, T = 300°C and T = 240°C, respectively. We observe Bragg peaks up to high order revealing very flat interfaces and low roughness. The hump between the first and the second order Bragg peak is due to the presence of the Ru cap layer; furthermore, Kiessig fringes which exactly correspond to the number of bilayer repetitions, can be resolved up to the sixth order Bragg peak.

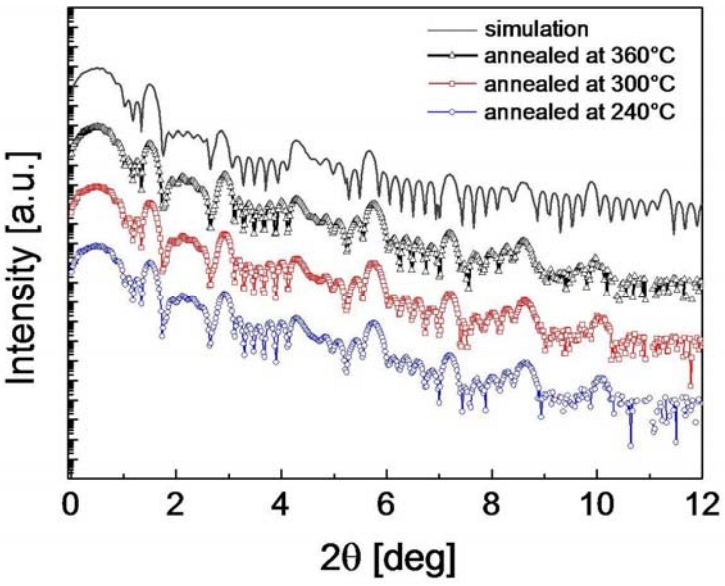

Fig. 1 Experimental X-ray reflectivity curves and simulation for the multilayers $[CoFeB/MgO]_5$ annealed at T = 360°C (black curve), T = 300°C (red curve) and T = 240°C (blue curve), respectively.

Surprisingly, the reflectivity curves for the samples annealed at different temperatures, do not present any variation. Annealing the samples at high T should cause some structural changes, as observed in [4] from a different set of CoFeB/MgO samples grown by different methods, where the high order Bragg peak vanished for an annealing temperature of T = 360°C. From the simulation of the reflectivity curve we derive the experimental thickness values for the ferromagnet and insulator, respectively, yielding d_{CoFeB} = 3.2 nm and d_{MgO} = 2.1 nm. The corresponding interface roughness obtained is σ_{CoFeB} = 0.2 nm and σ_{MgO} = 0.1 nm. The roughness values which we obtained for this set of samples are much lower than those obtained for similar systems investigated at DELTA in our previous work [4]; the bilayer periodicity is quite well respected.

The authors gratefully acknowledge Christian Sternemann and Micheal Paulus for their kind assistance during the experiments at the Beamline 9. The financial support provided through the European Union's Marie Curie actions (Research Training Networks) ULTRASMOOTH under contract MRTN-CT-2003-504462 is also kindly acknowledged.

[1] T. Miyazaki and N. Tezuka: J.Magn. Magn. Mater. **139** (1995) L231.
[2] J. S. Moodera, L. R. Kinder, T. M. Wong, and R. Meservey: Phys. Rev. Lett. 74 (1995) 3273.
[3] C. Krywka, M. Paulus, C. Sternemann, M. Volmer, A. Remhof, G. Nowak, A. Nefedov, B. Pöter, M. Spiegel, and M. Tolan, *J. Synchrotron. Rad.*, **13**, 8 (2006).
[4] M. Vadalá, K. Zhernenkov, M. Wolff , B. P. Toperverg, K. Westerholt, H. Zabel et al. *in preparation for JAP*

XSW measurements of sulphur distribution in polymer layers

M. Brücher[1], A. von Bohlen[1,2], R. Wagner[3], D. Lützenkirchen-Hecht[3], R. Hergenröder[1], R. Frahm[3]

[1] ISAS Dortmund, Bunsen-Kirchhoff-Str. 11, 44139 Dortmund
[2] DELTA, University of Dortmund, Maria-Goeppert-Mayer-Str. 2, 44221 Dortmund
[3] Fachbereich C Physik, Bergische Universität Wuppertal, Gauß-Str. 20, 42097 Wuppertal

In the field of semiconductors, organic LEDs are of increasing importance. The samples analysed in the presented experiments are polymer layers used for the development of a new OLED fabrication method. Figure 1 shows the cross-section of a sample: a Si wafer substrate is coated with a layer of PEDOT/PSS (thickness ca. 20 nm), covered by a crosslinkable polymer. The crosslinking provides semiconducting properties of the polymer and is induced by thiol groups of the PEDOT/PSS (Polyethylenedioxythiophene/Polystyrenesulfonate) layer. The crosslinking process releases thiol groups, which accumulate in an S containing front between the two phases. The S front was to be detected separately from the PEDOT/PSS layer, whereas the distance to the Si-Polymer interface was theoretically known from the fabrication process.

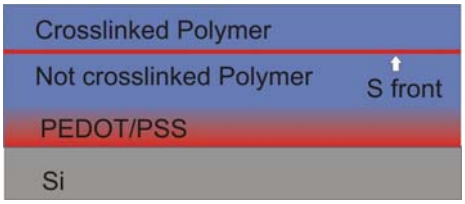

Fig. 1: Sample composition. A crosslinkable polymer covers a PEDOT/PSS layer. The extension of the crosslinked region is marked by a front of sulphur containing thiol groups.

Measurements were performed at BL 8 with 10 keV photon energy over an angular range from 0.02° to 0.3° in steps of 0.001°. X-ray Standing Waves (XSW) were generated on the Si substrate and passed the sulphur distribution of the sample exciting fluorescence photons, which were collected by an energy dispersive detector. The reflectivity of the samples was measured simultaneously. Oscillations of the sulphur K-fluorescence intensity verify the existence of the sulphur front and allow quantitative analysis. The oscillation period indicates the vertical position above the Si/polymer interface; the relative amplitude gives information about the sulphur atomic density. Maximal thickness of the front could be measured to 1 nm, the extension of the lower PEDOT/PSS layer varied from sample to sample between 7 and 15 nm.

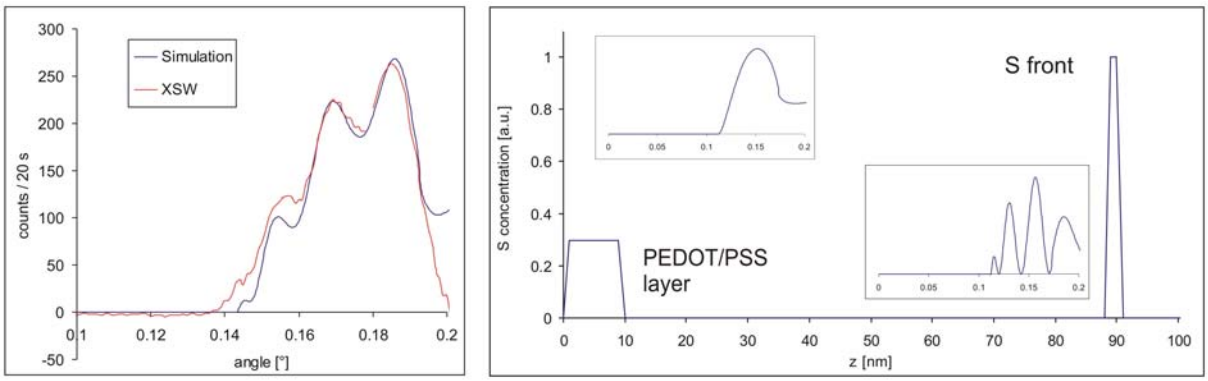

Fig.2: Left: XSW scan of polymer sample with sulphur front 90 nm over substrate. Oscillations of sulphur fluorescence are generated by alternating XSW maximum/minimum passage through the sulphur front.
Right: Sulphur distribution model used for the XSW simulation with the single intensity contribution of each sulphur layer.

Five samples were analysed, with a sulphur front at 70, 85, 90 and 130 nm above the Si surface. The values were theoretically known from the production process as mentioned previously. The sulphur fronts were located with a high precision (± 2 nm) at the expected positions.
Fig. 2 (left) shows the XSW signal of the sulphur front 90 nm above the interface, the simulation is calculated applying the sulphur distribution model shown right. The PEDOT/PSS layer generates an unmodulated XSW signal beginning at the critical angle of the air/polymer interface and fading to normal excitation at the critical angle of polymer/Si transition. The XSW induced fluorescence from the S front visualizes the passage of alternating maxima and minima of the electric field, which can be more clearly be seen in Fig. 3, where the complete fluorescence spectra are presented as a function of the incidence angle.

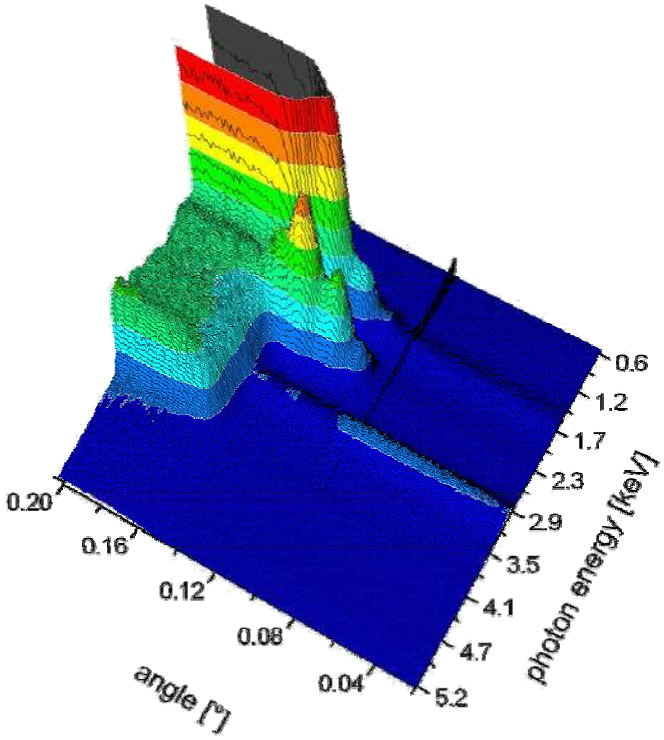

Fig.3: XSW measurement of S front 70 nm over Si substrate. Occurrence and oscillations of S fluorescence (E = 2.31 keV) are clearly visible between 0.1° and 0.16°. At the critical angle of polymer/substrate interface Si fluorescence intensity rises as the beam penetrates into the substrate. For smaller angles, the spectral background is very low. The fluorescence signal at 3.1 keV results from Ar escaping from the ionization chambers.

For the future, further experiments are planned in order to analyse such multilayered structures for OLED-fabrication processes in more detail.

2D-GISAXS investigation of crystal structure in thin polymer films

Yun Gu, Anton Davydoc, U.P. ,Uni Siegen

In this study, a Grazing Incidence Small Angle X-ray Scattering was used to determine the structure of crystalline thin polymer film made from PDI8CN2 on silicon substrates. The crystallographic analysis of the diffraction spots enables to determine the space group and the lattice parameters of the unit cell. In addition the two-dimensional GISAXS pattern provides the possibility to find the major orientation of crystallites with respect to the substrate surface. We have analysed polymer film (PDI8CN2) spin coated on silicon which differ in thickness, the pre-treatment of the substrates before spin-coating and the kind of subsequent chemical treatment.

The GISAXS measurements were carried out at DELTA with an X-ray radiation source of 15.5 keV and an incident angle close to the critical angle at 0.1˚. The image plate detector was used and two-dimensional pictures were recorded; where one of them is shown in Figure 1. The measured pattern shows a number of distinct Bragg reflections and each spot refers to a certain lattice plane of nano-crystals. From the structure analysis, the unit cell is determined as a triclinic cell with lattice parameters a_1=20.48Å a_2=8.77Å, a_3=5.00Å and α=88.1˚, β=88.2˚, γ=101.4˚. A model of crystal orientation is found by fitting the simulation of Bragg reflection peaks to the measured pattern. The pattern can be interpreted by the assumption that the nano-crystals having an average in-plane size of about 30nm are randomly oriented around the 100 axis which coincides with the surface normal. From reflectivity pattern we found that the crystal size in normal direction corresponds with the whole film thickness. The resulting Miller indices of the Bragg reflections are given in Figure 1. Comparing the different pattern taken from various samples, we found that the crystalline structure does not depend on the thickness, but strongly from preparation condition.

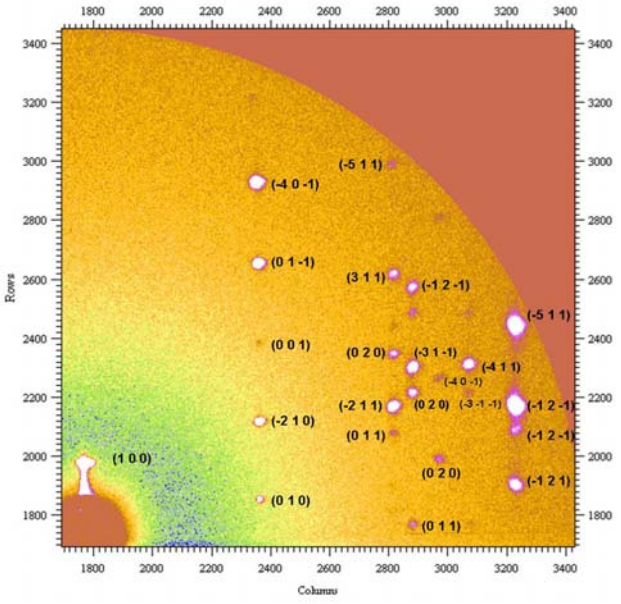

Figure 1
Two-dimensional GISAXS pattern for 100nm PDI8CN2 on Si substrate, measured by grazing incidence angle using image plate detector.

The CO_2 and THF hydrate formation process

Felix Lehmkühler, Heiko Conrad, Christian Sternemann, Michael Paulus, Lars Böwer, and Metin Tolan

Fakultät Physik/DELTA, Technische Universität Dortmund, Maria-Goeppert-Mayer-Str. 2, D-44221 Dortmund

Introduction

Clathrate hydrates are ice-like inclusion compounds where a guest molecule is enclosed into a water cage network [1]. These structures are common in nature, e.g. methane hydrates in ocean floor or permafrost regions. They are usually formed at low temperatures and high pressures. Furthermore, hydrates are promising candidates for future technological applications. CO_2 hydrate in particular can potentially be used for CO_2 recovery from flue gas emitted from power plants in terms of deep ocean storage of CO_2 [2, 3]. Tetrahydrofuran (THF, C_4H_8O) - hydrates were shown to be a candidate for hydrogen storage [4, 5]. CO_2 forms the cubic structure I (sI) hydrate with a lattice constant of $a_{CO_2} \approx 12$ Å and a stoichiometry of $(H_2O)_{46}(CO_2)_8$. THF in contrast forms cubic structure II (sII) hydrate with a lattice constant of $a_{THF} \approx 17.3$ Å and a stoichiometry of $(H_2O)_{136}(C_4H_8O)_8$. At $T = 0°C$ the minimum pressure for stable CO_2 hydrate is $p = 12.5$ bar, THF hydrate is stable at atmospheric pressure and temperatures below $T = 4.4°C$.

Although hydrates have been in the focus of numerous studies during the last 50 years the microscopic formation process of hydrates is still not understood. Three different theories for this process are proposed in literature: the *cluster nucleation theory* [6], the *local structuring hypothesis* [7], and a *surface driven model* [8]. In the framework of the *cluster nucleation theory* small water-guest clusters form immediately after dissolution of gas molecules, agglomerate and finally the nucleation sets in. The *local structuring hypothesis* predicts the formation of hydrates after stochastic arrangements of the dissolved guest molecules in the water similar to the hydrate structure are achieved. In contrast, the *surface driven model* bases on the high gas concentration at the water surface. Due to the high offer of gas molecules hydrate cluster form, grow and agglomerate in a similar way as in the framework of the *cluster nucleation theory* [6].

In order to favor one of these models, the hydrate formation process at the water - liquid CO_2 interface was examined by means of x-ray diffraction measurements. Furthermore, first experiments of THF hydrate growth applying a new in-situ stirring sample cell which allows detailed studies of the formation applying different x-ray scattering methods are presented in this report.

Experimental methods

CO_2 hydrate

Due to its importance for future application CO_2 was chosen as sample system. Furthermore, the low induction time for hydrate formation of $t_i \approx 2$ h, the high dissolubility of CO_2 in water, and thus the possibility for hydrate formation at the water surface or in the bulk, the system CO_2-water is an ideal sample to study the hydrate formation in-situ. Investigations of hydrate formation at the water-gas interface did not show any hydrate formation [9, 10]. The formation of CO_2 hydrate at the water-liquid CO_2 interface was observed by x-ray diffraction utilizing an improved sample cell with a decreased sample thickness of $d_{2008} = 6$ mm compared to $d_{2007} = 80$ mm [9]. This allows a higher resolution in space for the diffraction experiments. The experiments had to be performed at a CO_2 pressure above the condensation pressure of $p_{CO_2} = 35$ bar at $T = 0°C$ which makes the use of a high pressure sample cell and thus high energy x-rays to penetrate this cell necessary.

High energy x-ray diffraction measurements ($E_\gamma = 27$ keV) were performed at BL9 at DELTA [11] to examine the hydrate formation. The MAR345 image plate detector was used in order to measure the whole spectrum at once and investigate the occurrence and disappearance of different Bragg reflections simultaneously which gains access to fluctuations of hydrate crystallites.

THF hydrate

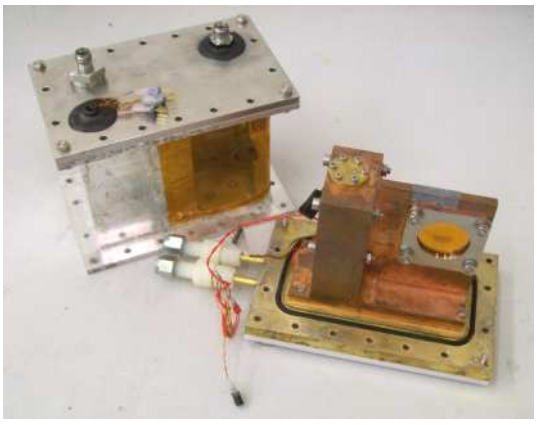

Figure 1: Sample cell with embedded magnetic stirrer.

Owing to the perfect miscibility of water and THF, this system is well suited to study hydrate formation.

The freezing process of THF hydrate at a supercooled temperature of $T \approx 0.5°C$ was examined utilizing a new in-situ-stirring sample cell, see Fig. 1. Therefore, medium energy x-ray diffraction measurements ($E_\gamma = 15.5$ keV) were performed at BL9 at DELTA [11].

Data analysis and discussion

CO_2 hydrate

After condensation of a few mm thick CO_2 layer on the water surface the formation of small hydrate crystallites starts immediately. Extracts of MAR345 images taken from the water-liquid CO_2 interface are shown in Fig. 2. Due to the narrow aluminum windows a large area of the image plate is shadowed by the sample cell. Bragg peaks according to a CO_2 hydrate diffraction pattern are clearly visible as white dots. The strong diffraction rings stem from the aluminum windows. The images were taken every 90 seconds. Thus, the effect of time on the formation is clearly visible due to the change of the positions of Bragg reflections and suggests the stochastic formation of small hydrate crystallites which can be explained by the *local structuring hypothesis*.

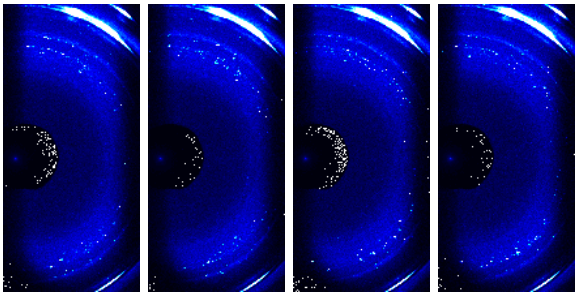

Figure 2: Four diffraction patterns taken at the water-liquid CO_2 interface after liquid CO_2 condensed at the water surface. The time interval between two measurements is 90 seconds (left to right).

THF hydrate

A diffraction pattern of the liquid water-THF mixture before stirring is shown in Fig. 3 (left). The structure peak of the solution is clearly visible. After stirring the liquid utilizing a magnetic stirrer which is embedded inside the cell in order to offer nucleation seeds the nucleation and growth of THF hydrate sets in. A diffraction pattern taken after the growth had been finished is shown in Fig. 3 (right). Since THF hydrate growth as a single crystal only few very sharp Bragg peaks are visible. Thus, more measurements with this cell to study the hydrate formation applying different scattering techniques will be performed.

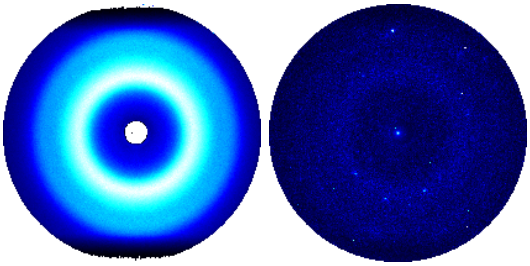

Figure 3: Diffraction patterns of the water-THF solution before stirring (left) and THF hydrate after stirring and crystallization (right).

Acknowledgments

We thank the DELTA machine group for providing synchrotron radiation and technical support. The BMBF (project nos. 05KSPE1 and 05KSPEA) and DFG (project no. TO 169/12-1) are gratefully acknowledged for financial support.

References

[1] E.D. Sloan Jr., *Nature* **426**, 353 (2006).

[2] S.P. Kang and H. Lee, *Environ. Sci. Technol.* **34**, 4397 (2000).

[3] R.P. Warzinski et al., *Annals of the New York Academy of Science* **912**, 226 (2000).

[4] L.J. Florusse et al., *Science* **306**, 469 (2004).

[5] H. Lee et al., *Nature* **434**, 743 (2005).

[6] E.D. Sloan Jr. and C.A. Koh, *Clathrate Hydrates of Natural Gases*, Boca Ranton, 2007.

[7] R. Radhakrishnan and B.L. Trout, *J. Chem. Phys.* **117**, 1786 (2002).

[8] B. Kvamme, *Annals of the New York Academy of Science* **912**, 496 (2000).

[9] F. Lehmkühler et al., *Hydrate formation in the system CO2-water: High energy x-ray scattering.* DELTA User report 2007.

[10] F. Lehmkühler et al., submitted to *J. Am. Chem. Soc.* (2008).

[11] C. Krywka et al., *J. Synch. Rad.* **13**, 8 (2006).

Investigating the molecular structure of polyethylene gas pipes

Saskia Schmacke[(a),*], Thomas Theisen[(b)], Dirk Grahl[(b)], Michael Paulus[(a)], Christian Sternemann[(a)], and Metin Tolan[(a)]

(a) Fakultät Physik/Delta, Technische Universität Dortmund, Maria-Goeppert-Mayer-Str. 2, D-44221 Dortmund, Germany
(b) RWE Energy AG, Rheinlanddamm 24, D-44139 Dortmund, Germany

* contact: saskia.schmacke@tu-dortmund.de

Polyethylene (PE) is a thermoplastic material which exhibits on nanometer length scales PE regions of randomly arranged (amorphous phase) and of highly ordered PE chains (crystalline phase). The balance between the amorphous and crystalline phase within the pipe material is one key parameter which defines macroscopic properties such as elasticity, brittleness and density [1]. PE pipes have become highly complex materials containing a significant amount of buffered flexibilizers. These additives which disappear with time assure the conservation of original material properties. Using additives has lead to estimated lifetimes above hundred years for the latest PE based products. However, first generation PE63 pipes are still in use. Thus, the study of stability of these gas pipes is of high economic interest.

The ageing of polyethylene PE63 gas pipes was investigated by wide angle x-ray scattering at BL 9 [2] of the synchrotron radiation source DELTA [3]. Several gas pipes were artificially aged applying temperature, pressure and humidity treatments. Samples were prepared from the different parts of the tube ranging from the inner to the outer surface ot the pipe wall. Diffraction patterns of the samples were recorded using an image plate set-up in order to identify indicators of abrasion by x-ray diffraction.

Diffraction images, one taken from the inner part (volume) and one from the outer surface of an artificially aged gas pipe are presented in Figs. 1 and 2, respectively. Both images show typical Debye-Scherrer rings originating from the crystalline parts of the PE63 material. The results show a clear texture of the material which can be observed most significant close to the surface of the outer part of the pipe wall and less intense in the volume of the pipe. The arrows indicate the [200], [400] and [020] reflections which show the strongest texture. The observed texture indicates that the chains of the polymer are alinged parallel to the pipe wall. New pipes show a similar texture so

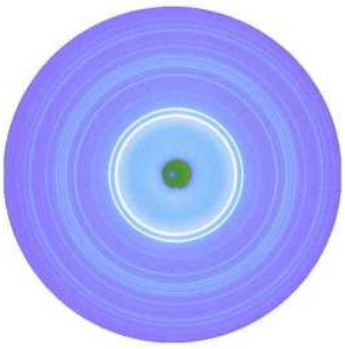

Figure 1: Diffraction image measured in the volume of an artificially aged gas pipe showing only small texture.

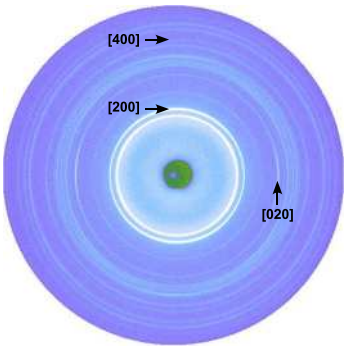

Figure 2: Diffraction image from the outer surface of the same pipe. The [200], [400], and [020] reflections are indicated.

that it can be inferred that the texture is due to the production process. Nevertheless, to study changes in texture due to ageing a more detailed data analysis is in required.

Changes in the ratio between crystalline and amorphous regions due to ageing of PE pipes can be extracted by azimuthal integrations of e.g. the first two Debye-Scherrer rings taken from the outer side of a native and an aged gas pipe. In Fig. 3 normalized data of the [110] and [200] diffraction peaks are shown.

After normalization the amorphous contribution was subtracted and the analysis of the diffraction peaks indicates a reduction of the integrated intensity by approximately 5% for the aged sample. This gives a hint that the crystallinity of aged gas pipes increases on cost of the amorphous regions. This observation might be one of the indicators which may serve as a precursor of ageing and possible failure of gas pipes. The widths of the diffraction peaks point to an averaged size of the crystallites of about 30 nm.

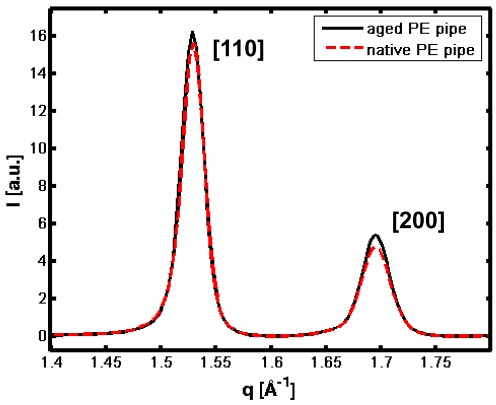

Figure 3: Diffraction peaks of the [110] and [200] reflections of a native and an aged gas pipe after normalization and subtraction of the amorphous contribution.

A whole series of samples taken from differently aged pipes was measured and data analysis is under progress, to obtain a more detailed understanding of the effects of ageing on the diffraction results. These results will give a deeper insight into the changes of crystallinity and its effect on stability by various treatments of PE pipes.

References

[1] H. Gräfen, *Lexikon der Werkstofftechnik*, VDI-Verlag Düsseldorf, 779 (1993).

[2] C. Krywka, M. Paulus, C. Sternemann, M. Volmer, A. Remhof, G. Nowak, A. Nefedov, B. Pöter, M. Spiegel, M. Tolan, *The new diffractometer for surface diffraction at BL9 of DELTA*, Journal of Synchrotron Radiation **13**, 8 (2006).

[3] C. Krywka, C. Sternemann, M. Paulus, N. Javid, R. Winter, A. Al-Sawalmih, S. Yi, D. Raabe and M. Tolan, *The small-angle and wide-angle X-ray scattering set-up at beamline BL9 of DELTA*, Journal of Synchrotron Radiation **14**, 244 (2007).

[4] M. Tolan, T. Weis, C. Westphal, K. Wille, *DELTA: Synchrotron Light in Nordrhein-Westfalen*, Synchrotron Radiation News **16**, 9 (2003).

X-ray diffraction studies of thick Vs thin films of low and high molecular weight poly(3-hexylthiophene) P3HT fraction

Siddharth Joshi[1], Souren Grigorian[1], Ullrich Pietsch[1], Patrick Pingel[2],Dieter Neher[2],Michael Forster[3], Ulrich Scherf[3]
1 Festkörperphysik, Universität Siegen, Walter Flex strasse 3, D-57068, Siegen, Germany
2 Institut für Physik, Universität Potsdam, Am Neuen Palais 10, D-14469, Potsdam, Germany
4 Macromolecular Chemistry, Universität Wuppertal, Wuppertal, Germany

Conjugated polymers are the one of the most promising candidates for the active layer of low-cost Organic-field-effect transistors (OFETs). The charge carrier mobility of these conjugated polymers is the key material property, limiting the performance of the devices. Poly(3-hexylthiophene) (P3HT) specially high molecular fraction is one of the promising material for such opto-electronic devices. By its structural modification one can further improve its electrical properties to make it more useful for fast speedy devices. The aim of the experiment was to understand and improve the structural properties of HMW fraction for a bulk as well as for thin films via surface engineering [1, 2].

All the X-ray measurements were performed at BL 9 beamline of Delta Synchrotron source at Dortmund technical University, Dortmund, Germany. The energy used was 15.2 keV, utilising an Image plate having 3450x3450 pixels of 100 µm size set at 48 cm apart from the sample. The beam size was 0.1x0.3 mm². In all measurements, the incident angle and the angle of exit within the incident plane are α_i and α_f, resp., and the in-plane scattering angle is 2θ. For better comparison all angular coordinates are transformed into q-space [1]. HMW (M_n = 30,000 g/mol) as well as LMW (M_n = 2500 g/mol) thin films of having different concentration exposed to X-ray on top of various substrates (Si/SiO_2, Si/SiO_2/HMDS, Si/SiO_2/OTS). All the results are summarized below -

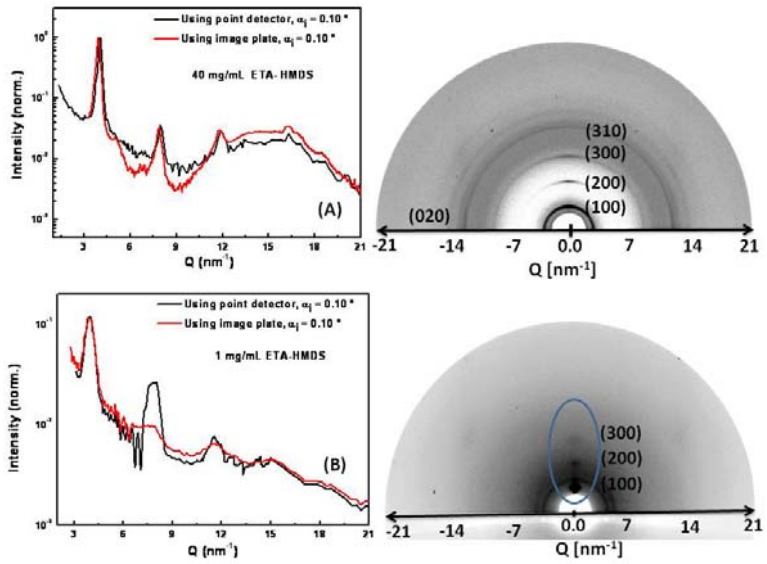

Fig. 1. 2D images taken in grazing-incidence geometry of sample 1(thick) (A) and sample 2 (thin) (B) at 15.2 keV (right). Extracted line scans are compared with point detector measurements taken at equal

Fig. 1 shows the image plate measurements of LMW P3HT of thick and thin films. Here $\alpha_i < \alpha_{cs}$ was fixed, and the 2D scattering of the film was recorded for 30 min. For sample 1(thick) we find closed rings with **Q** radii corresponding to (100) and its higher multiples with a small preference along the surface normal. In addition, one finds a ring related to (020) as well as (310) peaks. The peaks appear onto a non-uniform background caused by diffuse scattering from disordered P3HT, the SiO_2, and the background scattering of the experiment.

A line scan extracted from image plate data shows the (*h*00) and (020) peaks which coincide well with a scan taken with a point detector under same geometric conditions. In contrast to this, sample 2 (thin) displays distinct scattering spots in out-of plane direction without a remarkable ring structure. Also, there is no indication for the (020) peak. The different structural behaviour found in both images can be interpreted by the transition from a random to a preferential orientation of the crystallites as a function of film thickness.

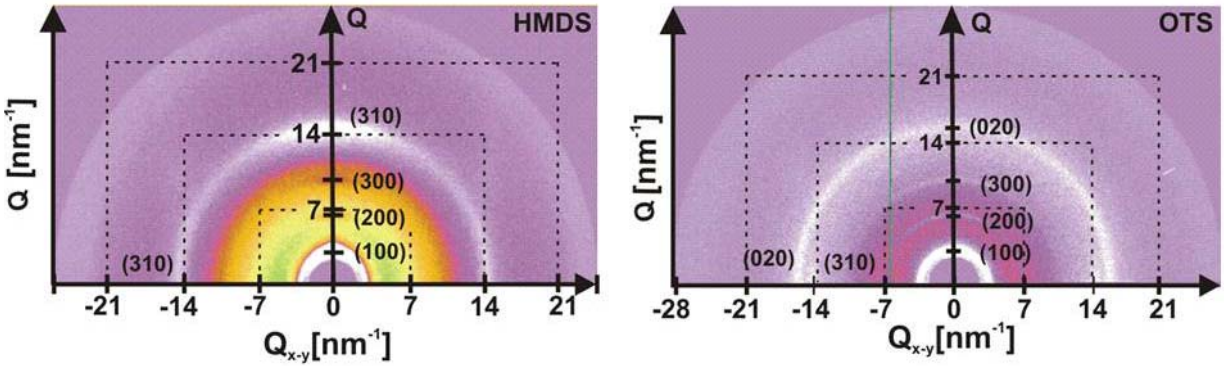

Fig. 2 A. Image plate measurements of virgin sample of type B treated with HMDS (a) or OTS (b) for α_i = 0.10 °.

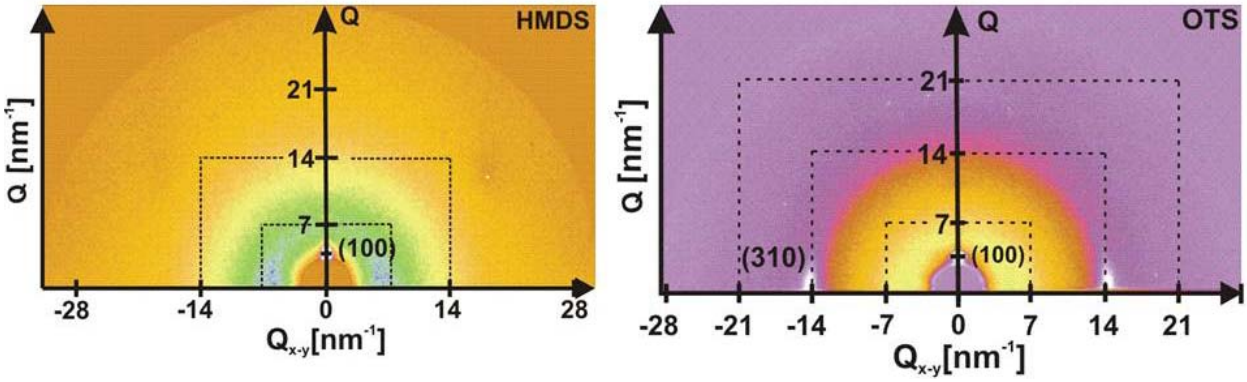

Fig. 2 B. Image plate measurements of as prepared sample of type A treated with HMDS (a) or OTS (b) for α_i = 0.10 °.

The typical structures of as-grown samples of HMW fraction are shown in Fig. 2(A, B) recorded by image plate exposure at room temperature (RT). Thick samples (Fig. 2A) on both HMDS and OTS coated substrates show a typical ring structure of wide angle reflections with a preferred orientation of (100) planes along normal direction, where (*h00)* peaks appear with certain angular distribution increasing with increasing *h*. For HMDS coated sample, there is a presence of a ring corresponding to the texture of (310) plane with stronger intensity along the normal direction.

For OTS coated substrate there is a clear presence of (020) ring as well as a lower intense (310) peak along the in plane direction. Comparing the OTS and HMDS substrates for thick films, there is a complete absent of (020) peak for HMDS substrate, while the appearance of (020) ring indicates the random orientation of (020) plane for OTS substrate. At the same time the (310) peak appears for both substrates either textured or sharp along in-plane direction. This could be the indication that the main chains for HMW films are not exclusively parallel to each other or there is a twisting of chains along in-plane direction. In general, both samples indicate the presence of mixed orientation (edge on as well as flat on) where still edge on is dominating along the whole thickness of film.

In contrast, for thin films (Fig. 2B) samples on both HMDS and OTS coated substrates

have shown much narrower angular distribution of (*h00)* reflections, one can see the presence of spots rather than rings, which directly indicate the preferential orientation of crystals in such thin films along normal direction. For OTS coated sample one can also see the presence of (310) peak, which could indicate the rather poor alignment of in plane stacking or non parallelism of main chain. At the same time as there is a clear absence of (020) peak from thin films of HMW fraction on both HMDS and OTS coated substrates, therefore it is just hard to distinguish from image plate about which one is providing better dielectric –polymer layer interaction.

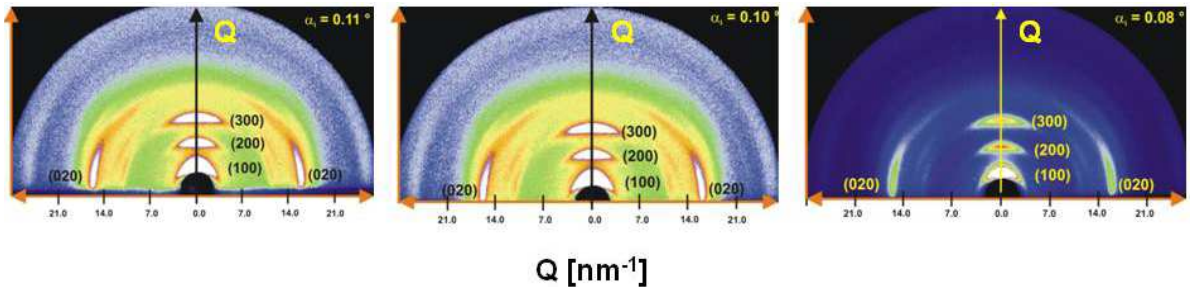

Fig. 3. Image plate measurements for HMW P3HT thick film prepared by drop Casting technique at different angle of incidence α_i^s.

Comparing Fig. 3 with Fig. 1 and 2, one can clearly see the difference between drop cast (thick film) and spin coating samples (thick films). Fig 3 clearly shows the well pronounced of 2d lamella orientation where alkyl chains are oriented normal to substrate while there is a strong thiophene-thiophene interaction along lateral direction due the appearance of (020) peak. The appearance of well pronounced (100), (200), (300) peaks indicates the edge-on orientation along the whole thickness of film, this is also clear from three different images for three different angle of incidence. Comparing all three α_i^s, its looks that the top morphology of drop cast film is more pronounced compared to any range of thickness accessed by varying the α_i^s for the drop cast film. Comparing the size of crystallites with other spin coating samples of low as well as high molecular weight fraction, the size of crystallites calculated for drop casting is 14 ±1 nm, where as for LMW fraction it is 25 ±1 nm and for HMW fraction it is 9 ±1 nm at RT. Whereas the inter-planar distance for drop casting is 1.63±0.02 nm, for HMW it is 1.64±0.02, where as for LMW fraction it is 1.57±0.02, clearly give hints that 'd' spacing could be the function of molecular weight.

In general, comparing the spin coated samples of LMW and HMW fraction, we can say that that the crystalline order of films made of LMW and HMW P3HT changes as a function of film thickness. For film thicknesses above 20 nm the film structure consists of randomly oriented nanocrystallites of 25–40 nm size diluted in an amorphous matrix. Whereas thin films are preferentially orientated and shows diffraction spot not the powder rings.

Whereas comparing the thick films prepared by spin coating and drop casting, drop casting films look more promising in terms of structural ordering. One can clearly see the 2d crystallites orientation, where the size of crystallites is higher than HMW but still lower then LMW spin coated films. Parallel to it drop cast films are not flat, instead it shows curved surfaces. At the same time it is not easy to control the thickness of such self-organised drop cast films up to few nm.

[1] Joshi, S.; Grigorian, S.; Pietsch, U.; Physica status solidi (a) **2008**, 205, 488-496

[2] Joshi, S.; Grigorian, S.; Pietsch,U.; Pingel, P.; Zen, A.; Neher, D. and Scherf, U.; Macromolecules **2008**, 41 (18), 6800–6808

XRD Studies of different Metal-Organic-Frameworks

D.C. Florian Wieland[(a),*], Osama Shekhah[b], Michael Paulus[(a)], Christian Sternemann[(a)], Christof Wöll[b], and Metin Tolan[(a)]

(a) Fakultät Physik/DELTA, Technische Universität Dortmund, Maria-Goeppert-Mayer-Str. 2, D-44221 Dortmund, Germany
† Physikalische Chemie I, Ruhr-Universität Bochum, Universitätsstraße 150 D-44780 Bochum, Germany

* contact:florian.wieland@tu-dortmund.de

Metal organic frameworks (MOFs) are a new class of porous materials, which have been recently used for storage, sensing and separation of gas. In contrast to the usual synthesis protocol a new route for the synthesis was developed, which could help to understand the dynamics and the process of MOF formation. Two different MOF were prepared by Christof Wöll et al. following their step-by-step synthesis approach [1]. Both samples had a support consisting of a wafer covered by a self assembled monolayer (16-mercaptohexadecanoic acid ($HS(CH_2)_{15}COOH$)). Sample (1) consisting of HKUST-1 [$Cu_3BTC_2(H_2O)_n$] (BTC=benzentricyrboxylacid) and sample (2) consisting of ZnBDC (BDC=benzendicarboxylic acid) were grown on top of the support. When grown on top of the functionalized organic surface sample (1) exhibits the same

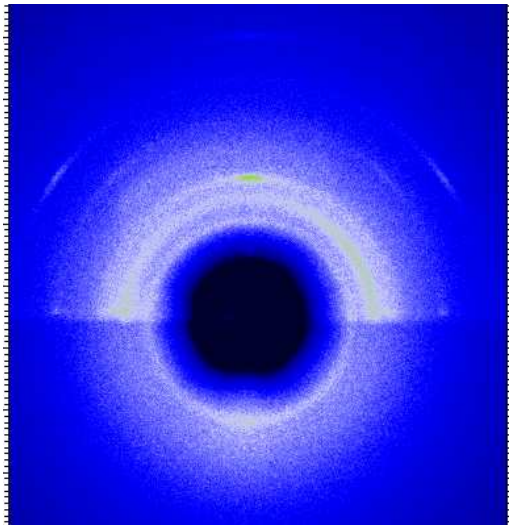

Figure 1: Two dimensional scattering pattern of HKUST-1 as-sythesized

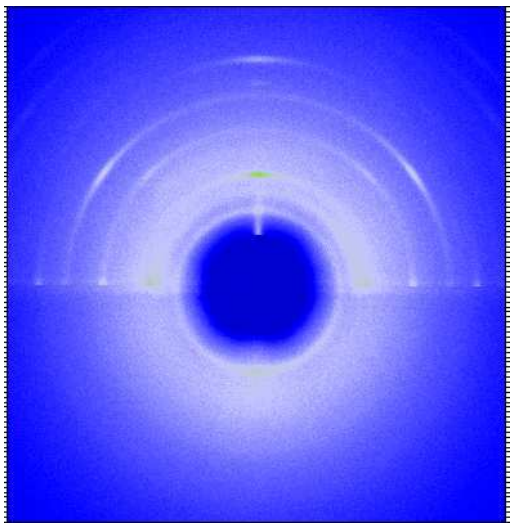

Figure 2: Two dimensional scattering pattern of HKUST-1 annealed up to 250°

structure as in the bulk-phase,where as sample (2), which was previously charactirised at a laboratory diffractometer, revealed a completely new structure yet unknown in the bulk-phase. The samples were investigated regarding their structure and temperature stability. Measurements were carried out at the multi-purpose beamline BL9 using two experimental setups. For the structure analysis the XRD setup employing a two-dimensional MAR345 detector was used. In the case of the sample (1) also the x-ray reflectivity setup was utilized.

It is known from foregoing measurements that samples of HKUST-1 show a change in orientation after a period of weeks. In order to understand the process that leads

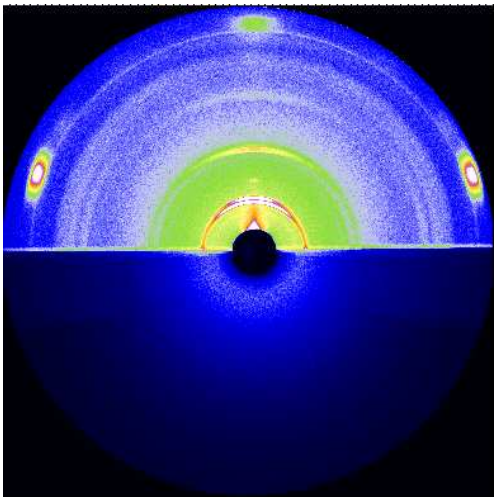

Figure 3: Two dimensional scattering pattern of ZnBDC

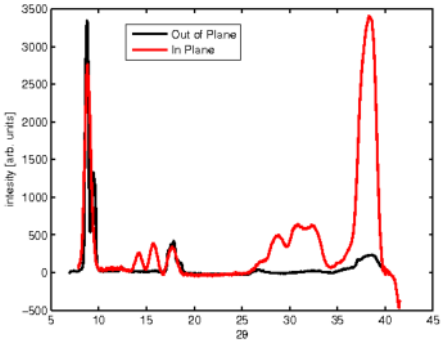

Figure 4: Intergrated intensity of ZnBDC, perpendicular to surface (out-plane-signal) and parralell to the surface (in-plane-signal)

to this reorientation sample of HKUST-1 (sample(1)) was annealed at temperatures up to 250°C. A scattering pattern was recorded at temperature intervals of 20°C. Also XRR spectra for the as-synthesized sample and the sample annealed at 250°C were measured. A scattering pattern of the as-synthesized sample and the sample annealed up to 250°C is shown in figure 1 and figure 2. The sample shows a continuous change of structure from a well ordered state where all MOF crystals are orientated along the (001)-direction to a polycrystalline state where no preferred orientation exists, indicated by the change from spot-like to ring-like reflexes. The XRR data shows that the SAM is destroyed during the annealing process. The data analysis is still in progress.
In figure 3 the obtained two-dimensional scattering pattern and in figure 4 the integrated intensities for the in-plane and out-of-plane structures of ZnBDC (sample(2)) are shown. The structure on top of the surface is highly oriented, as indicated by the single scattering spots in figure 3. Six different scattering reflexes which are originating from the MOF structure could be identified. A theoretical scattering pattern from a model proposed by Christof Wöll et al. possibly matches the measured scattering pattern, but due to the fact that some theoretical reflexes of this modeled structure are masked by the beamstop, the structure is still ambiguous. Further measurements are needed.

References

[1] O. Shekhah, H. Wang, S. Kowarik, F. Schreiber, M. Paulus, M. Tolan, C.n Sternemann, F. Evers, D. Zacher, R. A. Fischer, and C. Wöll, *Step-by-Step Route for the Synthesis of Metal-Organic Frameworks* , J. Am. Chem. Soc. **129** 15518 (2007)
[2] O. Shekhah, H. Wang, T. Strunskus, P. Cyganik, D. Zacher, R. A. Fischer, and C. Wöll, *Layer-by-layer Growth of Oriented Metal Organic Polymers on a Functionalized Organic Surface* , Langmuir **23** 7440-7442 (2007)
[3] See report *X-ray Diffraction characterization of Metal-Organic Frameworks (MOFs) thin films grown on Functionalized Organic Surfaces* by O.Shekhah, H. Wang, and C. Wöll,DELTA user report 2008.

Current status and activities at the XAS/XRD Beamline 10

Together with University of Wuppertal (R. Wagner, D. Lützenkirchen-Hecht and R. Frahm) and Technical University of Dortmund (Chr. Sternemann) the solid state physics group of Siegen University (K. Istomin, S. Gorfman and U. Pietsch) is building up a new beamline for charge density analysis at DELTA Synchrotron. Present scientist in charge is Dr. Konstantin Istomin. The installation is based on the fact that the German charge density community is searching for new experimental station. Due to the future projects at DESY the D3 beamline at HASYLAB, used by many groups of the SPP, will come to an end soon. The main European synchrotron source ESRF still does not offer a dedicated beamline for charge density analysis up to now. Therefore new options at German synchrotron radiation sources are strongly demanded. TU Dortmund is running a 1.6 GeV synchrotron source providing soft and hard x-ray radiation with sufficient flux for charge density measurements. In 2006 University of Siegen (U.Pietsch) , University of Wuppertal (R.Frahm) and TU Dortmund (M.Tolan) have signed a contract to install BL10 for charge density (Siegen) and Quick EXAFS (Wuppertal) experiments. The beamline is realized without external money using resources from collaborating university groups only. As example the main goniometer (60 k€) was purchased by welcome money of Prof. Pietsch at Uni Siegen, similar resources of university of Wuppertal made it possible to buy the components for the monochromator. One important component (y-z-table (20T€) was bought by DFG via this project.

Due to lack of money and compared to large facilities the progress of BL installation is slow. Main components, as tilt absorber or crystals for the monochromator were constructed and manufactured in the workshops of Siegen and Wuppertal universities. However the first beam is expected for spring 2009. Therefore first charge density experiments can be realized in autumn 2009. The experiment is offered to all members of SPP. One of them (Ch. Lehmann, Max-Planck-Institute für Kohlenforschung, Mülheim/Ruhr) has expressed his strong interest already and offered to deliver a cryo-unit for low temperature measurements.

At present the status of the BL10 is as follow:

A special tilt absorber working as a white beam slit system has been designed using a dynamical simulation approach at the University of Siegen (Figure on the left). Most of its parts have been already manufactured. The last two missing parts are delivered by the mechanical workshop in Dortmund in November 2008. The entire slit system will be assembled and tested for leakage in November/December 2008. A new stepping motor and its power unit stage have to be bought from Pyhton (Berlin)

The vacuum chamber and most of the inner parts for the optics of the channel-cut Si(111)-monochromator suited for diffraction and absorption measurements are machined or delivered and ready for assembly. Assembly and testing of the components as well as the later implementation and first measurements is part of a diploma work (University of Wuppertal) started in September 2008 and expected to be complete in early 2009.

The four circle Huber-diffractometer and its adjustment table have been already delivered (Figure on the left) and the implementation into the experimental hutch is in progress and will be finished in December 2008. Power supply units have to be bought for the motors of the adjustment table as well. Installation of a setup for absorption spectroscopy measurements is performed by the University of Wuppertal.

The personal safety interlock system has been rewired completely. The signal flow has been tested and is ready for operation. As a next step the vacuum control system will be installed. The assembly of the front-end section of the BL10 had been postponed due to a service event which caused the exchange of the photon absorber. In this regard a completely new vacuum section has been installed during the last summer shut-down which is already in operation. Other few minor installations and the vacuum testing of the remaining front-end section are scheduled for the next weeks of shut-down in the second half of 2008 and depending on this, first conditioning with synchrotron radiation is planned.

A new point detector has to be bought. The spectrum of detectors on the market is rather broad with the prices ranging between ca. 10.000 - 40.000 Euros and depending on the performance characteristics.

There is already interest from the MPI Mülheim concerning possible experiments with X-Ray diffraction at lower temperatures. In this regard the Oxford Cryosystems cooling stage will be implemented in the experimental set-up.

Expected parameters of the beamline:
Energy range: *4,5 – 15 keV*
Energy resolution: $dE/E \sim 10^{-4}$
Beam size: *1.5 x 4* mm^2 to *0.5 x 0.1* mm^2 (depending on aperture)
Photon Flux: 5×10^9 *Photons / s* mm^2
Ambient environment, as well as opportunity for sample cooling in prospect.
Runs in standard SPEC shell.

The time schedule is presented in the following table:

November – December 2008	Assembling and Installation of the absorber / slit system
November – December 2008	Alignment of the diffractometer system
December 2008 – Febraury 2009	Assembling and testing of the monochromator
December 2008 – February 2009	Installation and testing of the vacuum system
February 2008 -	Installation and testing of detectors and motors
April –May 2009	Beginning of comissioning

Bonding configuration of cyclopentene and benzene on GaAs(001) surfaces

R. Paßmann[1,2], T. Bruhn[1,2], C. Friedrich[2], D. Weier[3], F.Schönbohm [3], C. Westphal[3], N. Esser[1,2], P. Vogt[2]

[1]ISAS – Institute for Analytical Sciences – Department Berlin, Albert-Einstein- Str. 9, 12489 Berlin, Germany
[2]Institute for Solide State Physics, TU Berlin, Hardenbergstr. 36, 10623 Berlin, Germany
[3]Experimentelle Physik , TU Dortmund, Otto-Hahn-Strasse 4, 44221 Dortmund

During our beamtime we investigated the different bonding configuration of benzene (C_6H_6) and cyclopentene (C_5H_8) adsorbed on the three 'main' GaAs(001) surface reconstructions, the c(4x4), (2x4) and (4x2). Our aim was to obtain information about the electronic interface properties required to elucidate the role of intra-molecular bonds within the adsorption process. In this particular case, the influence of a different amount of intra-molecular C=C double bonds onto the resulting adsorption structure was investigated. Therefore cyclopentene and benzene were chosen in order to identify differences in the adsorption configuration of a hydrocarbon ring molecule consisting of one and three double bonds, respectively. These results are also important for a systematic understanding of the interface formation between organic molecules and semiconductor surfaces in general.
Up to now, no comprehensive study of this parameter on the important organic/inorganic interfaces can be found in literature. In this report we focus on the results concerning the adsorption of benzene (cyclopentene) on the GaAs(001)c(4x4) reconstruction as an example.
In order to clarify the chemical composition and surface bonding sites for the different molecules on the surfaces SXPS measurements were carried out at BL11 at DELTA.

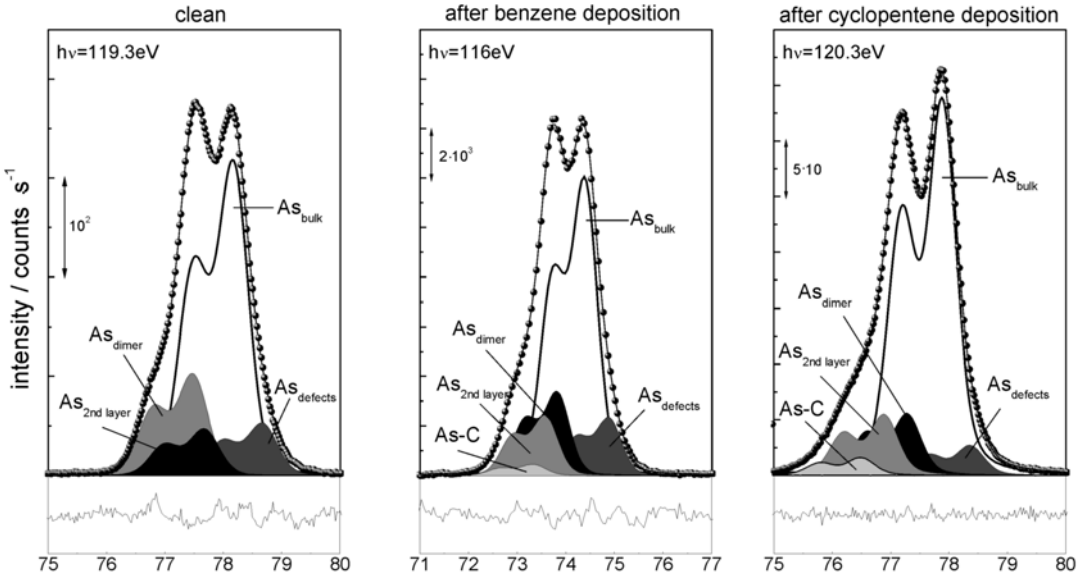

Fig.1:
As3d core level emission lines for the clean, benzene saturated and cyclopentene saturated surfaces, respectively.

In Fig. 1 the As3d core level spectra of the clean surface (left), and the surfaces after saturation with benzene (middle) and cyclopentene (right) are depicted. The components found in the core level emission line shape analysis for the clean

reconstructed surface are comparable to previous work. The core level spectra taken after the saturation with benzene (cyclopentene) reveal a new component (As-C) after the molecule adsorption. This component can be assigned to a covalent bond formation of the benzene (cyclopentene) to the topmost arsenic atoms of the surface.

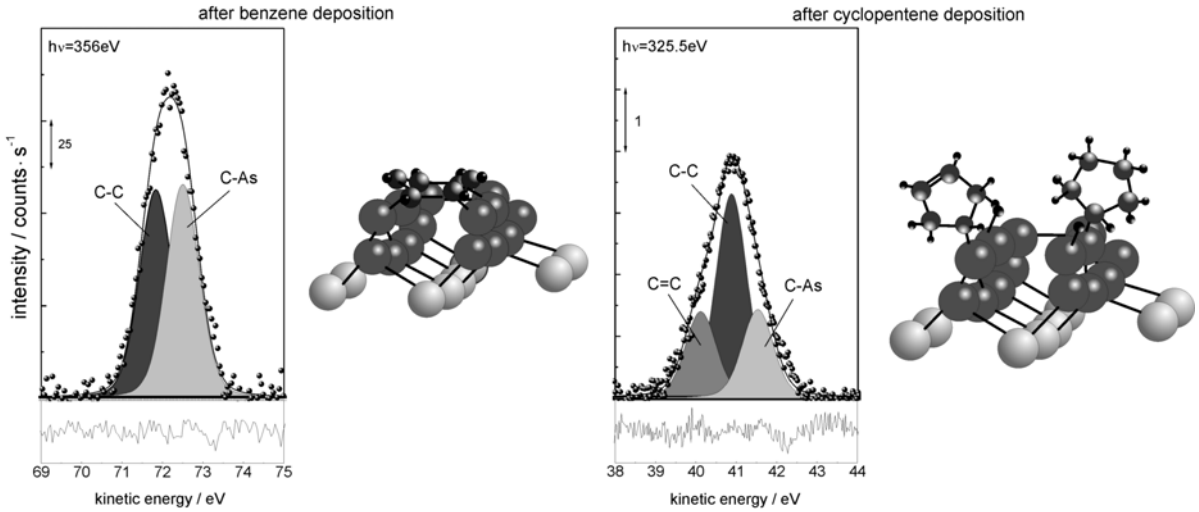

Fig.2:
C1s core level emission lines for the benzene (left) and cyclopentene (right) saturated GaAs(001)c(4x4) surface resonstruction, respectively

Within the Ga3d core level emission line no additional components were found in the line shape analysis.
A more detail information on the bonding configuration is obtained from the C1s core level emission lines. After the saturation of the GaAs(001)c(4x4) surface with benzene (cyclopentene) two (three) components were found in the line shape analysis. In the case of the saturation with benzene these components can be assigned to C-C and C-As bonds whereas for cyclopentene deposition additionally to these components (C-C, C-As) also a clear third component shows up, which is assigned to C=C bonds whithin the cyclopentene molecules. A comparison of the different intensities of the
C-As components after the saturation with benzene and cyclopentene leads to the conclusion that in the case of the adsorption of benzene more bonds to arsenic atoms of the surface are formed than in case of cyclopentene. Hence different adsorption structures for benzene and cyclopentene on the GaAs(001)c(4x4) occur. The measurements so far indicate that the adsorption of benzene results in a bridge-bond-like configuration while cyclopentene molecules only form a single bond to the topmost As atoms of the surface resulting in an upright configuration. Further data analysis, in particular of photoelectron diffraction experiments of benzene on GaAs(001)c(4x4), is currently underway.
In summary the SXPS measurements could help to clarify the different adsorption configurations of benzene and cyclopentene on the GaAs(001)c(4x4). These results show the important role of the number of double bonds on the chemical, electronic, and geometric aspects of the bond formation between GaAs(001) surfaces and small ring molecules. This results will serve as a basis for a better understanding of the organic/inorganic interface formation in general.

Photoelectron spectroscopy (XPS) and photoelectron diffraction (XPD) studies on the local adsorption of benzene on Si(100)

D. Weier[1,2,*], A. Beimborn[1], T.Lühr[1], F. Schönbohm[1,2], S. Döring[1,2], U. Berges[1,2], C. Westphal[1,2]

[1] Institute of Physics - University Dortmund, Otto-Hahn-Str.4, D 44221 Dortmund, Germany
[2] DELTA - University Dortmund, Maria-Goeppert-Mayer-Str. 2, D 44227 Dortmund, Germany
[*] corresponding author: daniel.weier@uni-dortmund.de

There has been considerable interest in the behaviour of the bonding process of unsaturated hydrocarbons with semiconductor surfaces. These systems offer a potential route to optoelectronic and bioanalytical devices if functional groups are added to the base molecules. One example of these systems is the interaction between benzene and silicon. Within the silicon surfaces the Si(100) surface oriantation is very important because it's relevance in industrial applications. For the benzene-Si(100) interaction many different structures have been proposed including Standard Butterfly (SB), Pedestal, Tight Bridge (TB), Tilted, Twisted Bridge and Diagonal-Bridge Butterfly. The most stable structures identified by density functional theory (DFT) are the TB und SB structures [1]. In our measurement at the beamline 11 at DELTA this structure is studied using x-ray photoelectron spectroscopy (XPS) and x-ray photoelectron diffraction (XPD) and the experimental data are compared to simulation calculations in order to identify the interaction parameters.

The experiments were carried out in a UHV-chamber with a base pressure of $5{\cdot}10^{-11}$mbar. Sample preparation was started with the clean (2x1)-reconstructed Si(100) surface. The reconstruction was obtained by using a standard annealing procedure via flashing the sample at approximately 1100°C and slowly cooling down the sample in a time interval of 15 minutes. A quality check of the surface was performed by LEED and XPS. As the next step a benzene partial pressure of approx. $1{\cdot}10^{-5}$ mbar was applied for 5 minutes. The growth of the C 1s peak was measured afterwards. This step was repeated until the saturation coverage of a monolayer was achieved [2]. All measurements were carried out at the beamline 11 which provide high flux and sufficient energy resolution in the soft x-ray range for the planned XPS and XPD studies. Photoelectron diffraction patterns were recorded for an azimuthal and polar range of 0–358° and 0–80°, respectively. The step width of 2° was kept constant for both angular settings. In total, around 7000 XPS spectra of the C 1s signal region were taken.

Figure 1(a) shows overview spectra, high resolution XPS spectra of the C 1s (Fig. 1b), silicon 2p (Fig. 1c) signals before and after the preparation cycles and the experimental and simulated XPD pattern of the C 1s signal (Fig. 1d). In Figure 1(a) no carbon contamination is detectable before exposure to benzene, and a strong signal afterwards. An asymmetric peak shape for the C 1s signal in the high resolution spectrum (Fig. 1b) is observable. This can be explained due to the different bonding types of the carbon atoms. One carbon species is bond to silicon whereas others are bond to carbon. Further the silicon 2p signal shows a strong change in its line shape (see Fig 1c). At higher kinetic energies the observed asymmetry for clean surfaces is not visible after benzene adsorption, but there is an additional component at lower kinectic energies. The asymmetry at higher kinetic energies is typical for silicon (2x1)-reconstructed surfaces, because Si dimers at the surface experience a different chemical

environment compared to the normal silicon-silicon bond. This is displayed as a chemical shift in the high resolution XPS spectra. Appearently, exposure of the surfrace to benzene removes the dimers and therefore the chemical shifted component is not visible anymore. The additional component at lower kinetic energies appears due to the new silicon-carbon bonds.

Figure 1(d) compares the experimental XPD pattern of the C 1s signal with a first simulation. As discussed above, the C 1s peak consists of 2 different chemical components, and the XPS pattern shown in Figure 1(d) corresponds to the carbon-silicon bonded carbon atoms. The first simulation performed for the standard butterfly structure shows an acceptable agreement between experiment and simulation. However, a more detailed calculation including the Tight Brigde model is needed. Presently, the experimental XPD patterns of the silicon 2p signal is being analyzed. Here, the component reflecting the silicon-carbon bond is of high interest.

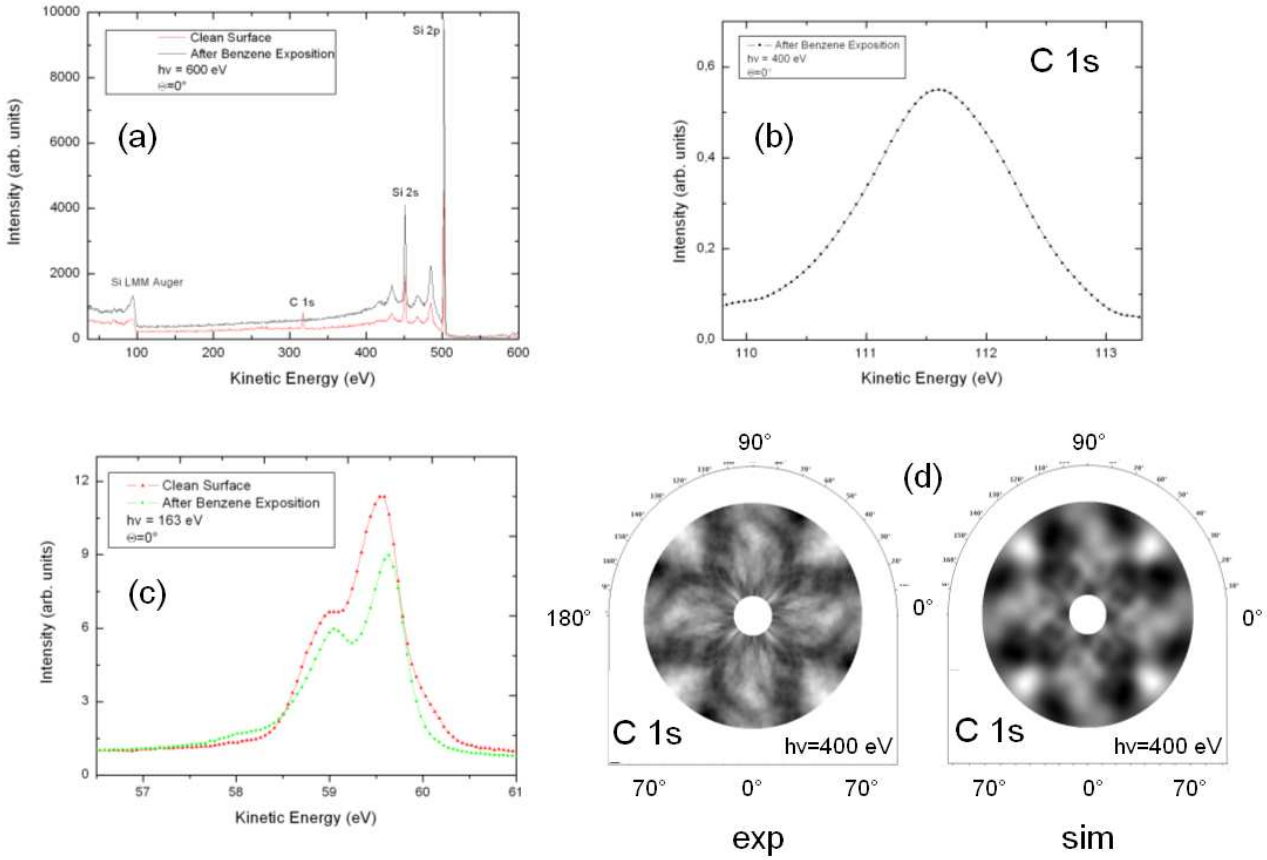

Figure 1: Overwiew spectra (hv = 600 eV) (a), high resolution XPS spectra of the C 1s (hv = 400 eV) (b), high resolution XPS spectra of Si 2p peak before and after benzene exposure (hv = 163 eV) (c), and experimental XPD pattern of the C 1s peak (left) compared with the simulated pattern (right) (d)

[1] Lee J Y and Cho J H, Phys. Rev B **72**, 235317 (2005)

[2] Gokhale S et al., J. Chem. Phys. **108**, 5554-64 (1998)

Photoelectron spectroscopy (XPS) studies on the system zirconium oxide on Si(100)

F. Schönbohm[1,2,*], D. Weier[1,2], U. Berges[1,2], C. Westphal[1,2]

[1] Experimentelle Physik 1 - TU Dortmund, Otto-Hahn-Str. 4, D 44221 Dortmund, Germany
[2] DELTA - TU Dortmund, Maria-Goeppert-Mayer-Str. 2, D 44227 Dortmund, Germany
[*] corresponding author: frank.schoenbohm@uni-dortmund.de

(October 2008)

Following Moores Law the consistent decrease of the aspect ratios of semiconductor devices leads to a problem when the SiO_2 gate dielectric is reduced below 2 nm. A further miniaturization of this insulating layer leads to an increase of tunneling currents and an increased power consumption of the device. This behaviour finally causes a loss of efficency. However, a thin gate dielectric is desired in order to obtain high gate capacities and a fast switchable MOSFET. In order to overcome this obstacle research activities were performed in order to examine possible replacement materials for the classically used SiO_2 gate dielectric. Among the so-called high-k materials there are some promising candidates such as hafnium oxide and zirconium oxide which could substitute the SiO_2 gate dielectric. These group of materials has a higher dielectric constant (k) than SiO_2. Due to the importance for technical applications ultrathin ZrO_2 films on a Si(100) surface were studied.

The measurements were carried out at beamline 11 of DELTA. The undulator beamline provides a high photon flux and a high energy resolution at the applied energy of 320 eV. The sample cleaning and preparation was performed in-situ in the measurement chamber. The base pressure within the chamber is about $5 \cdot 10^{-11}$ mbar. After cleaning the sample by annealing at 1050°C a Si(100)(2×1) surface reconstruction was prepared. On top of the silicon surface 11 Å of ZrO_2 were evaporated by means of an electron beam evaporator. Figure a) shows an survey scan of the sample surface before and after evaporation of ZrO_2. The small yttrium and hafnium signals arise due to a contamination of ZrO_2. It is difficult so separate these materials, therefore small residue amounts can not be omitted. After the evapoaration process the samples were stepwise annealed at increasing temperatures ranging from 550°C to 750°C in order to study variations of the surface with respect to the annealing temperature. Figure b) shows the thermal behaviour of the Si 2p and Zr 3d peak area as a function of the annealing temperature. For temperatures above 600°C the intensity of the overlaying ZrO_2 intensity starts to decrease, whereas the burried silicon intensity starts to increase. Further heating to temperatures from 650°C to 725°C results in a strong intensity change of the Si 2p and the Zr 3d intensity. For temperatures above 725°C the intensities of the Zr 3d and the Si 2p remain constant. Furthermore, the intensity of the Si 2p peak resembles the intensity of a clean silicon surface. The ZrO_2 is completely transformed into $ZrSi_2$ which is confirmed by a chemical shift of 3.7 eV of the Zr 3d signal. This observation as a function of temperature is a strong indication for the formation of $ZrSi_2$ islands on the sample surface. Between the islands the previously burried silicon substrate becomes free and terminates the surface.

In order to examin the formation of $ZrSi_2$ on the Si(100) surface XPD pattern were recorded. Figure c) shows the XPD pattern of the clean silicon surface. The kinetic energy of the emitted electrons was E_{kin}=219 eV. Figure d) shows the sample after ZrO_2 evaporation and annealing

at 760°C at an electron energy of $_{kin}$=138 eV. The differences in the pattern show that the intensity variation in the Zr 3d pattern (Figure d)) is caused by the $ZrSi_2$.

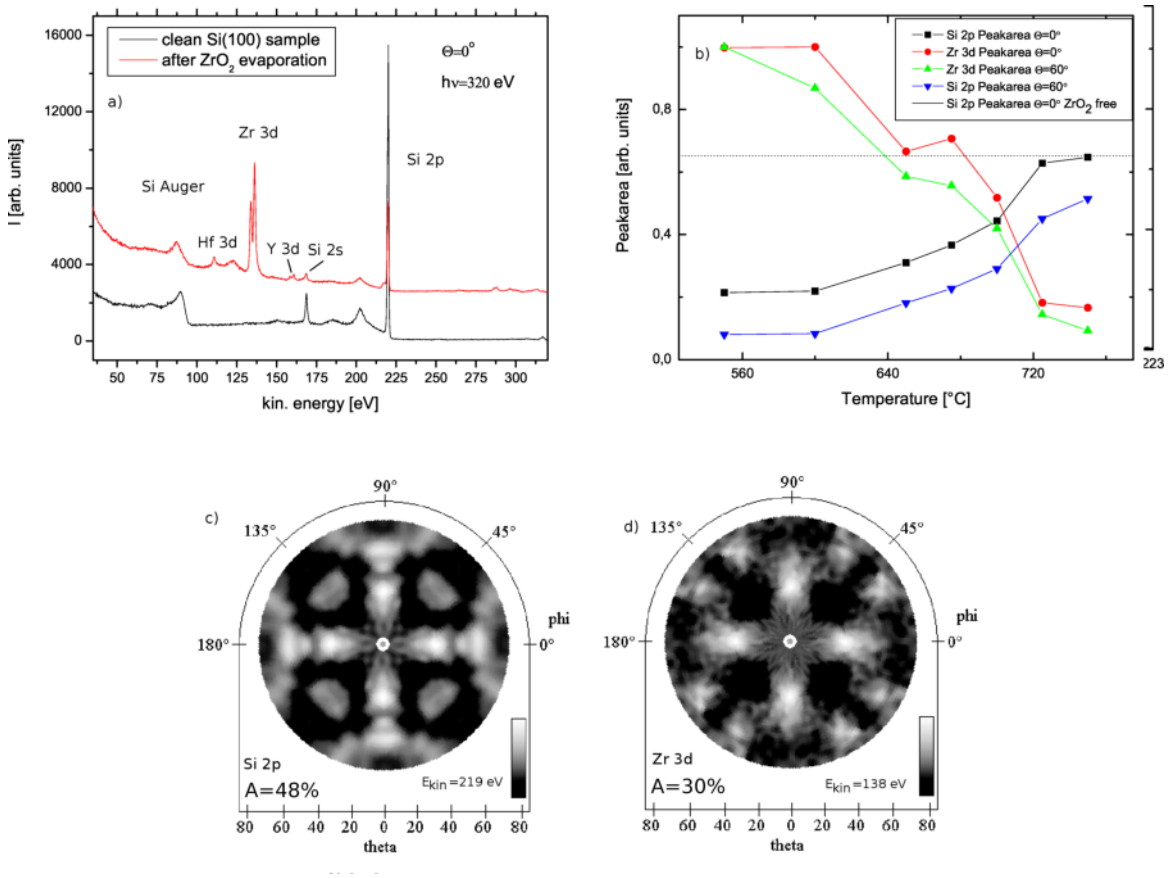

Figure 1: Survey scan of the clean sample and after ZrO_2 evaporation. The contaminations are caused by the evaporation material and are typical for these elements (a). Peak area of the Si 2p and Zr 3d signals as a function of the annealing temperature. For higher surface sensitivity the intensities were measured for an emission angle θ =60° (b). XPD pattern of the Si 2p intensity of a clean surface (c). XPD pattern of the Zr 3d signal after Zr 3d evaporation and annealing at 760°C (d).

Acknowledgments:
This work was financially supported by the DFG (We 1649/7-1, Germany) and the Land Nordrhein-Westfalen. Thanks go to the staff of DELTA for continuous support during the beamtimes.

XPD-Measurement of the Si/SiO_2-interface on Si(110)

T. Lühr[1,2], D. Weier[1,2], F. Schönbohm[1,2], S. Döring[1,2], U. Berges[1,2], C. Westphal[1,2]

[1] Institute of Physics - University Dortmund, Otto-Hahn-Str.4, D 44221 Dortmund, Germany
[2] DELTA - University Dortmund, Maria-Goeppert-Mayer-Str. 2, D 44227 Dortmund, Germany

The Si/SiO_2-interface of the Si(100) surface orientation is of great relevance in the semiconductor technology. The investigation of the silicon (100) surface was in the center of many research activities in the past. However, the structure of the interface for the Si(110)-surface is relatively unknown.

In order to determine the structure of the oxidized Si(110)-surface XPS and XPD experiments were conducted. The preparation and the measurements were performed in a UHV-chamber with a base pressure of $5 \cdot 10^{-11}$mbar at the beamline 11 of DELTA. This beamline provides high flux and sufficient energy resolution in the soft x-ray range. After thermal desorption of the native silicon oxide the Si(110)-wafer was heated at 700°C with a partial oxygen pressure of $1 \cdot 10^{-5}$mbar for 15 minutes. At these preperation parameters a coverage of approximately 5 Å is expected at the surface [1]. Figure 1 (a) shows a high resolution XPS-spectrum of the Si 2p-signal recorded at normal emission. The spectrum contains seven components which correspond to photoemission from emitters located in the interface region and the bulk. Three signals can be assigned to the bulk atoms and non-oxidized silicon atoms located near the interface. The remaining four of signals correspond to the different oxidation states of silicon. All photoelectron signals except the Si^{α} signal are shifted to lower kinetic energies relative to the bulk signal. We observe a shift of -0.9eV per oxygen neighbor atom, as reported in literature for other surface orientations previously [1, 2].

The photoelectron diffraction patterns were recorded for an azimutal range of 0° - 358° and a polar range of 0° - 70°. Both angles were variied with a step width of 2°. In that way over 6000 XPS-spectra of the Si 2p-signal were recorded at a photon energy of $h\nu = 180$eV. Figure 2 shows two examples of the obtained diffraction patterns resulting from clearly defined structures inside. The diffraction patterns clearly indicate a crystalline interface structure below the amorphous SiO_2-layer. The patterns also differ from each other as a consequence of the different chemical environment.

Since the photon energy was not changed during the measurments the inelastic mean free path of the emitted electrons is constant for all spectra and therefore a plot of the intensity versus polar angle provides information about the relative positions of the components. The intensity slope is correlated with the distance of the atoms to the surface. Figure 1 (b) shows an only shallow increase of the intensities of the Si^{1+}- and the Si^{2+}-components as a function of emission angle. This indicates that the Si^{1+}- and the Si^{2+}-atoms are located close to the bulk and within the same layer. Above these components there is a layer of Si^{3+}. Because differnet variation of the intensity slope of the Si^{3+}-signal, this layer is separated from the $Si^{1+/2+}$-layer. The highest increase in intensity as a function of emission angle is shown by the Si^{4+}-component which is part of the SiO_2-film at the surface.

In order to determine the accurate structure from the recorded data it is necessary to simulate the XPD-pattern. For that reason a genetical algorithm was developed that creates and combines different interface structures. Each structure is defined by a number of static parameters and a reasonable size of variable parameters. The static parameter are equal for every generated structure. After generating a random set of structures the algorithm calculates the multiple scattering pattern for each structure and evaluates the pattern with an R-factor [3]. If no R-factor has reached a specified value, the algorithm creates a new generation of parameter sets by combining the variable parameters of two structures in each instance. Parameter sets with a low R-factor are preferred to be chosen for this procedure. If the stoichiometry of the layers or films is known, the algorithm already works very well. For the Si/SiO_2-interface the algorithm needs some expansions, that are tested at the moment. The obtained information about the order of the components provides a foundation for the simulations.

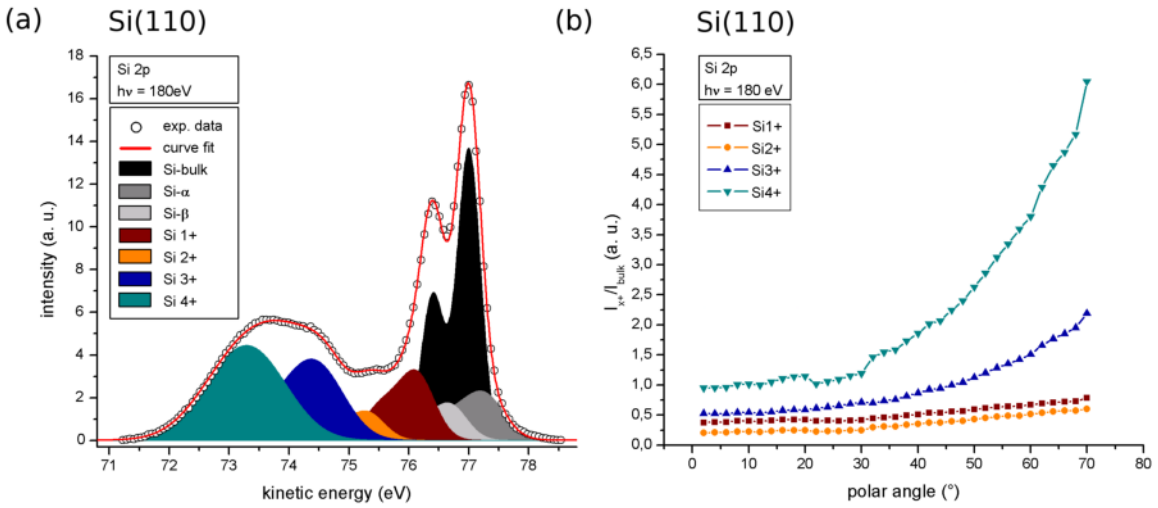

Figure 1: High resolution XPS-spectrum of the Si 2p-signal of an oxidized Si(110)-surface at normal emission. Additionally the decomposed signals of the different silicon components are presented (a); Intensity versus polar angle plot of the different oxidized silicon species (b).

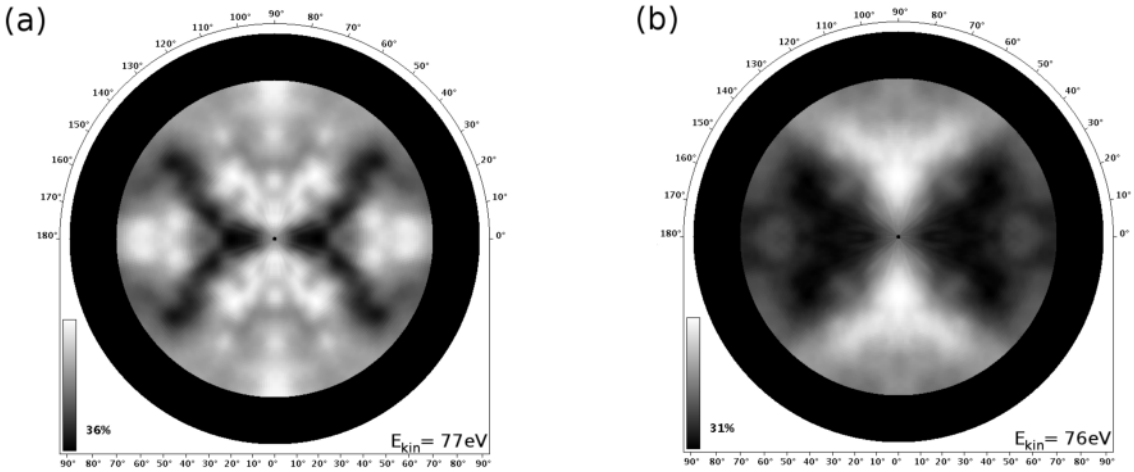

Figure 2: Experimental XPD-pattern of an oxidized Si(110)-surface: Si 2p-signal of the bulk-component (a); Si 2p-signal of the Si^{1+}-component (b).

Acknowledgement

We would like to thank the DELTA-staff for their support.

References

[1] F. J. HIMPSEL et al., Phys. Rev. B 38 (1988) 9.
[2] D.-A. LUH, T. MILLER, T.-C. CHIANG, Phys. Rev. Lett. 79 (1997) 16.
[3] C.R. FLÜCHTER et al., Surf. Sci. (2008), doi:10.1016/j.susc.2008.09.033

Characterization of the TGM Beamline (BI12) at DELTA

Martin Schmidt, Ulf Berges, and Carsten Westphal

DELTA, TU Dortmund, Maria Goeppert Mayer Str.2, Dortmund, Germany
Experimentelle Physik 1, TU Dortmund, Otto HahnStr.4, Dortmund, Germany

In the last year the commissioning of the TGM-Beamline proceeded. During the last year, all three gratings of the monochromator were energy-calibrated. Further, the energy-resolution of the two gratings in the high energy-range were measured, the energy resolution at the low-energy side at hν = 5-30 eV is still in progress. As experimental test experiments, the group of Prof. Neumann (Universität Osnabrück) recorded first photoemission spectra with their experimental end-station at BL12.7

All energy-calibration measurements for grating 1 and grating 2 were performed with the beam-line integrated gas-cell. Grating 1 with 18000 lines/mm and grating 2 with 600 lines/mm cover an energy range of hν =90-200 eV and hν =30-90 eV, respectively. The photoionization-spectra of He, Ne, Ar, and Kr consist of narrow lines at well-known energies. For grating 1 the 3d lines of Krypton and for grating 2 the He 2s and Xe 4d lines were used.
Since the photoionization lines are Voigt-shaped it is possible to determine the energy resolution from these spectra. This was carried out by the standard procedure*[1]* of a deconvolution of the experimental Voigt-shaped spectra into a Lorentz-function and a Gaussian-contribution, representing the resolution of the beamline.

In a second step, the energy-calibration and resolution of both gratings were calibrated with the Al 2p absorption edge at 72.7 eV. The step decrease in the transmitted intensity through a thin Al foil due to the increase of the Al absorption coefficient is well suited for energy calibration measurements. This transmitted intensity was measured with a thin aluminium foil and a photo-diode behind.

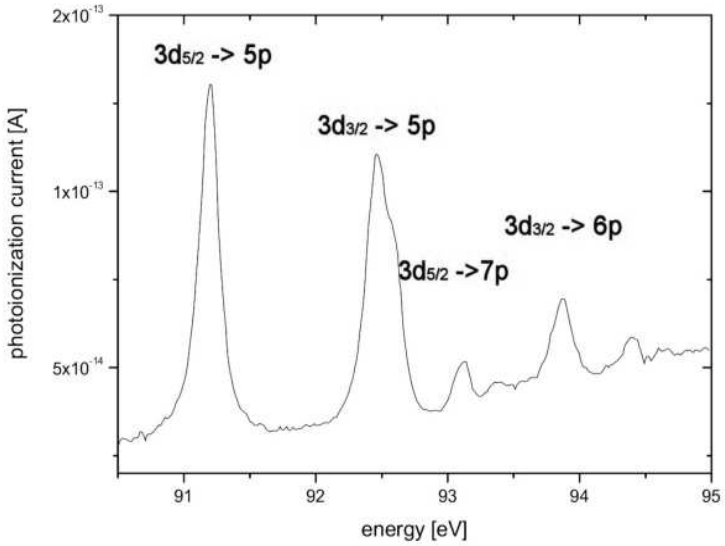

Figure 2: Photoionization spectrum of the Kr 3d lines, used for the energy-calibration of grating 1

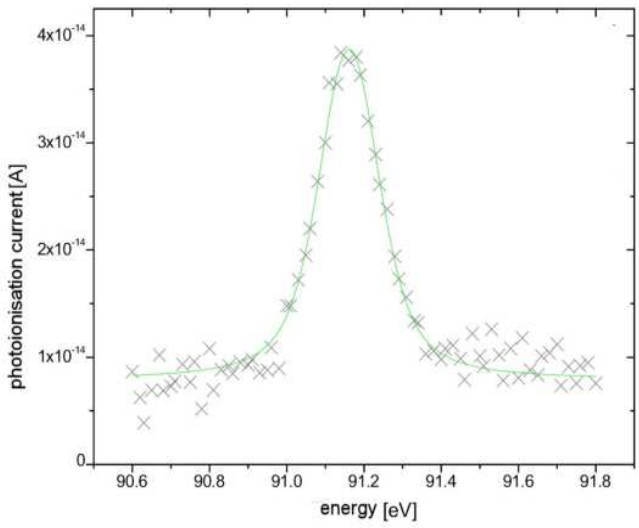

Figure 1: Photoionization spectrum of the Kr 3d(5/2) → 5p transition with a fitted Voigt function (green). The Lorentz width is set to the natural line width of 0.1eV, the Gaussian width was calculated as 0.13 eV

Grating 3 with 200 lines/mm for the energy range of hν =5-30 eV was energy-calibrated by measuring the Fermi-edge of the Au(111) surface. These measurements were carried out in the experimental end-station. Measuring the Fermi-edge as a function of the grating settings provides a way to calibrate mirror 1 over the complete range. However, in this approach, the quality of the calibration depends on the accurateness of the used photoelectron spectrometer, and this data analysis is currently still in progress.

A calibrated GaAs-diode was positioned behind mirror 2 (in down-stream direction) in order to measure the photon flux. Figures 3 and 4 present the photon flux of all three gratings before mirror-chamber 1 was replaced in summer 2008. The displayed photon-flux is normalized to an electron-beam current of 100mA. While the dependence of the photon flux as a function of energy is as expected, the flux itself was much lower than calculated. It was suspected that the low flux is a result of mechanical instabilities. After replacing mirror-chamber 1 the first measurements of the flux showed a strong increase of at least two orders of magnitude. We expect to have BL 12 fully operational after the commissioning of the new mirror chamber in mid 2009.

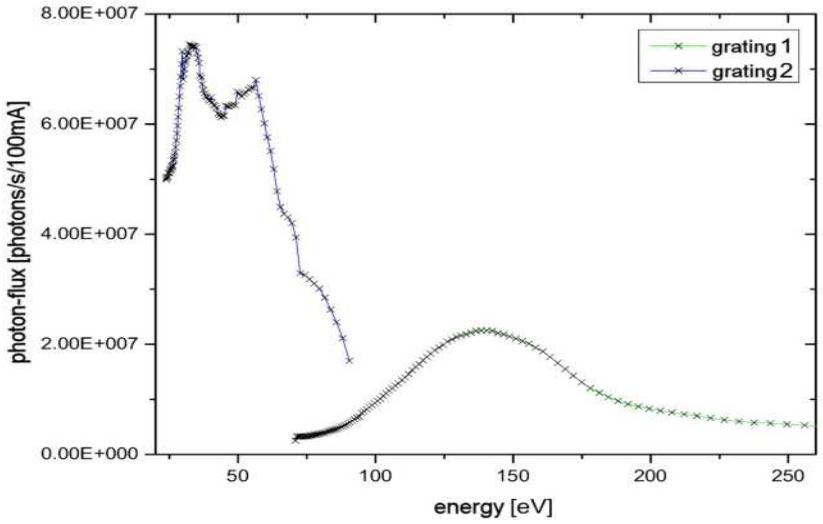

Figure 3: Measured photon flux of gratings 1 and 2, the entrance and exit slit size were set to of 2mm x 1mm

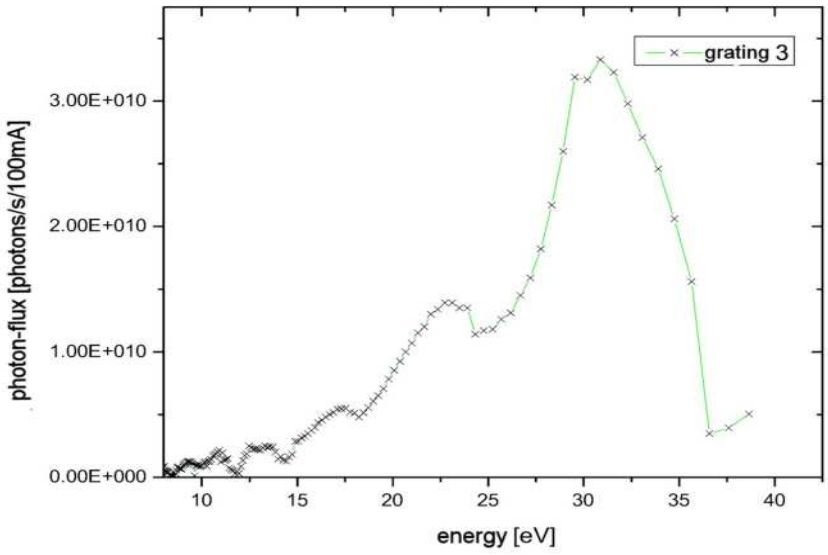

Figure 4: Measured photon flux of grating 3 with 2 mm x 1 mm entrance slit size and 2 mm x 1.5 mm exit slit size.

Acknowledgment

The authors would like to thank the DELTA staff for their support.

[1] Fedoseenko, S. I. ; Vyalikh, D. V. ; Iossifov, I. E. et al.: Commissioning results and performance of the high resolution Russian German Beamline at BESSY II. In: Nuclear Instruments and Methods in Physics Research A 505 (2003), S. 718728

Ultraviolet photoemission spectroscopy at DELTA Development of the New Beamline 12

Christian Taubitz[(a),*], Michael Räkers[(a)] and M. Neumann[(a)]

(a) Fachbereich Physik, Universität Osnabrück, Barbarastrasse 7, D-49069 Osnabrück, Germany

* contact: ctaubitz@uos.de

Introduction

Ultraviolet photoemission spectroscopy (UPS) is a powerful tool to investigate the electronic structure of thin films, adsorbates, single- and polycrystalline solids. Together with a tuneable light source, monochromatised synchrotron radiation and a rotatable electron detector a large variety of different investigations is available. For instance the bandstructure of single crystalline samples and adsorbate layers can be revealed [9,4]. Furthermore small impurities become visible by resonant photoemission [3]. Also radiation damage and surface metallisation can be studied [7]. In the last years we have successfully investigated new oxidic materials with interesting properties (perovskites with colossal magnetoresistance effect [5,8], scandates with high K [6], and multiferroics [in progress]). Their electronic structure can be nicely investigated by ultraviolet photoelectron spectroscopy in combination with theory.

Experimental

Figure 1: The experimental setup

In order to perform experiments on the above mentioned interesting new materials in the UV-regime up to 200eV a TGM-beamline together with an angle resolving photoelectron spectrometer was set up at DELTA during the last year (figure 1).

First experimental tests

The first experiments were carried out in order to test and characterise the experimental setup. In June 2008 gold spectra were measured at different photon energies (figure 2, right), which show a qualitative good agreement with literature [1]. As one can see between 19eV and 23eV a resonant behavior of the valence spectrum at about 6eV binding energy can be observed (colored spectra). This resonance can be explained by a hybridisation of the Au final-state band structure near the Γ-point (figure 2, left). As one can see at about 14 eV the sp-band character of the Au band changes to an f-band character, causing the resonant behavior [2]. These spectra just serve as a demonstration that the apparatus can be used soon for interesting investigations on new materials as mentioned before.

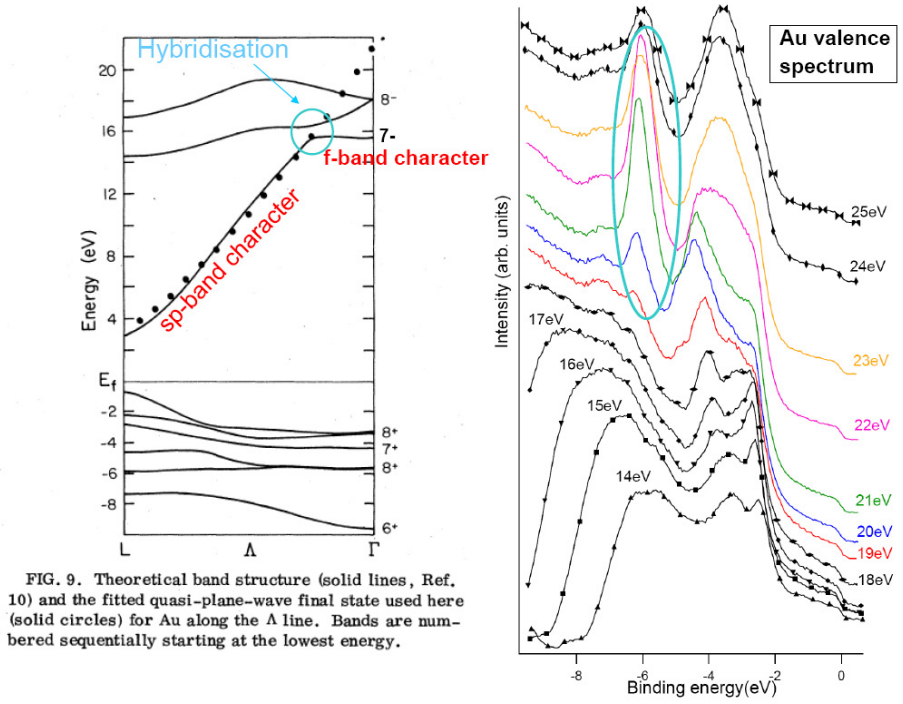

Figure 2: Left: Theoretical band structure of Au (attached from [2]). Right: Au valence spectra measured at DELTA.

References

[1] D.E. Eastman et al., Phys. Rev. Letters, V28, Number 20, (1972)
[2] K.A. Mills et al., Phys. Rev. B, V22, Number 2, (1980)
[3] V.R. Galakhov et al., Solid State Com., Vol.91, No. 4, (1994)
[4] M. Woehlecke et al., Solid State Communication, Vol.49, No.3, (1984)
[5] K. Kuepper et al., Phys. Chem. Letters B, 109, 15667-15670 (2005)
[6] M. Raekers et al., "Electronic and magnetic structure of $RScO_3$ (R=Sm, Gd, Dy)", in progress
[7] M. Reichling et al., Surface Science 402-404, (1998)
[8] K. Kuepper et al., J. appl. Phys. , Vol. 104, (2008)
[9] H. Kuhlenbeck et al., Ber. Bunsenges. Phys. Chem. 96, 15 (1992)